THEORETICAL AND EXPERIMENTAL INVESTIGATION
OF SOLID-STATE MECHANISMS FOR GENERATING
COHERENT RADIATION IN THE ULTRAVIOLET
AND X-RAY REGIONS

Fifth Semiannual Report Under
Grant NGR 45-003-027

For the Period
May 1, 1968 through October 31, 1968

CASE FILE COPY

MICROWAVE DEVICE AND PHYSICAL ELECTRONICS LABORATORY

DEPARTMENT OF ELECTRICAL ENGINEERING

UNIVERSITY OF UTAH

SALT LAKE CITY, UTAH

THEORETICAL AND EXPERIMENTAL INVESTIGATION
OF SOLID-STATE MECHANISMS FOR GENERATING
COHERENT RADIATION IN THE ULTRAVIOLET
AND X-RAY REGIONS

Fifth Semiannual Report Under
Grant NGR 45-003-027

For the Period
May 1, 1968 through October 31, 1968

by

A. Silzars
C. H. Durney
R. W. Grow

Microwave Device and Physical Electronics Laboratory
Electrical Engineering Department
University of Utah
Salt Lake City, Utah

February 15, 1969

Richard W. Grow
Principal Investigator

ABSTRACT

The double-stream interaction in a solid-state plasma is analyzed for a layered structure where the two charge-carrying streams are in adjacent layers, with the stream in one layer assumed to be stationary. The theory has been developed assuming that no external magnetic field is applied.

Starting from an idealized model, the effects of finite temperature, particle collisions, transverse ac velocities, and material losses are considered. Each problem is first investigated separately and then the effect of combining these parameters is discussed.

Analysis of the idealized one-dimensional model with a single drift velocity for all carriers predicts high gain for a frequency of 1 GHz to 10 µm in wavelength, for commercially available semiconductors. The effects of finite temperature, particle collisions, and transverse ac velocities change the results of the idealized model drastically. The velocity spread introduced by the randomizing effects of temperature reduces the gain below useful levels for temperatures above about 35°K in germanium. This limits operation of practical devices to very low temperatures. Particle collisions add severe damping at frequencies below about 300 GHz in most semiconductors, e.g., germanium and indium antimonide. Transverse ac velocities reduce the gain below useful levels unless the conductivity has a large anisotropy. Transverse to longitudinal conductivity ratios of at least 1:100 are required to obtain gain values comparable to the one-dimensional model. The total effect of tem-

perature, collisions, and transverse ac velocities is to impose such stringent requirements on the materials and operating conditions that it is reasonable to conclude that space-charge interactions in solids without an external magnetic field are not likely to result in practical devices.

Gain may not be possible in the submillimeter or shorter wavelength region even with a strong dc magnetic field. If the effect of the magnetic field is only to cause a conductivity anisotropy, i.e., "focusing" as in electron beam devices, then practical devices cannot be built. The fields required become very large (~100 kG) and can only be produced in a well-equipped laboratory.

Finally, additional problems are to be expected with energy coupling from the sample and material fabrication. The space-charge wavelength becomes so short at the submillimeter wavelengths that techniques are presently not available to manufacture efficient output couplers. The very small space-charge wavelength similarly requires very uniform surfaces for the layered structure, and fabrication problems are significant.

In conclusion, it appears that the initially promising result for high-frequency solid-state devices based on space-charge interactions, and in particular the double-stream interaction, is fallacious. A more detailed investigation has shown that the idealized one-dimensional model is not a valid approach to the analysis of space-charge interactions in solids.

TABLE OF CONTENTS

LIST OF ILLUSTRATIONS AND TABLES

I. INTRODUCTION

The purpose of this project is the investigation of gain
mechanisms in solid-state materials for generating coherent radiation
in the ultraviolet and X-ray regions.

This report summarizes the conclusions reached during a major
phase of this study. The initial proposal on space-charge interactions
in solids at ultraviolet and X-ray frequencies was made on the basis
of a simplified plasma model. A more thorough analysis indicated that
serious difficulties were to be expected due to bound electron absorp-
tion and the many possible energy levels in the solid at the higher
frequencies. It was then proposed that the interaction be investigated
in the infrared where electron effects are not important. This would
serve to verify the basic interaction mechanism which could then be
studied in more detail at the higher frequencies. Further study of
the proposed interaction showed, however, that even in this more favor-
able frequency range, a good understanding of space-charge interactions
in solids was not readily obtainable. It was found that there is an
incomplete understanding of space-charge waves in solids even at micro-
wave frequencies; for example, there has been no conclusive experimental
verification of space-charge interactions in solids at any frequency.
For these reasons, it was decided that a thorough analysis of the double-
stream interaction was first necessary in the microwave and infrared
frequencies. This report summarizes the results of this study. Since
it also marks the completion of a major phase of the project, slight

repetition of previously discussed topics has been permitted for the sake of completeness.

Space-charge interactions in solids have received considerable attention over the past several years, and many proposals have appeared in the literature for devices that are essentially analogues of the more familiar electron-beam interactions. Most of these devices have been proposed for use in the microwave region. However, as mentioned previously, very few conclusive experimental results have been obtained. At present, there is considerable uncertainty as to the origin of detected oscillations from solid-state materials. Since the ultimate success of an ultraviolet or X-ray interaction depends on the successful verification of a space-charge interaction in a solid, the more general approach is well justified.

It will, therefore, be the purpose of this report to investigate the feasibility of realizing practical devices from space-charge interactions in solid-state plasmas, and to try to increase the understanding of these interactions. To facilitate the analysis, a particular configuration will be selected which gives good results with the idealized model and which can be experimentally constructed. The analysis will be carried out for the double-stream interaction in a layered structure where the two streams are in the adjacent layers. This configuration permits more flexibility than the hole-electron plasma in a single material. In addition, the effect of layer thickness on each stream can be studied. The theory will be developed assuming that no external magentic field is applied. Large magnetic

fields require bulky electromagnets which limit the useful application
of any proposed device. The analysis has been confined to a frequency
range extending from microwaves up to the infrared, because the space-
charge interaction appears particularly well suited for these frequen-
cies, and material properties are available for use in making numerical
calculations.

A thorough analysis of a solid-state plasma is quite complicated
because several different effects must be included in addition to the
basic interaction mechanism: the temperature of the particles adds a
velocity distribution to the drifting or stationary carriers which tends
to randomize the velocity and decrease the gain, particle collisions
with the lattice and between the particles add loss and must be con-
sidered, and the carriers in the solid are contained by the boundaries
of the material but are otherwise able to move in directions transverse
to the desired drift. One possible method of attacking the problem
would be to try to include all effects at the beginning of the analysis
and arrive at some very general and very complicated equations. This
method has the advantage of being able to "explain" all effects from
one derivation. The disadvantage is that the final result is usually
so complex that it defies interpretation. Because one purpose of this
work is to try to add to the understanding of space-charge interactions,
a more applicable method has been selected. The problems of tempera-
ture, particle collisions, and transverse velocities will be considered
separately and the combined results will be discussed after the effects
of each have been understood. This approach makes it possible to sepa-

rately investigate theoretical methods for analyzing these difficult problems. It is also easier to compare the results to the work of other authors, since very often analyses are presented which completely ignore one or more of these effects.

The general approach of this paper will be to develop the idealized model and then to show how the added physical properties of a semiconducting solid affect the proposed interaction mechanism. First, in Chapter II, some general properties of semiconductors will be discussed which fit the proposed plasma model. Experimental results of other authors will be mentioned which tend to verify the plasma nature of a semiconducting solid. Then, in Chapters III and IV the space-charge interaction mechanisms are described which lead to the configuration to be analyzed. The layered structure is then discussed and results are presented for an idealized model which assumes a uniform drift velocity for all of the carriers.

Chapters V and VI discuss the effects of temperature, particle collisions, and transverse velocities. This is the particularly significant portion of this paper because it is here that the conclusion is reached that space-charge interactions without an external magnetic field are not likely to result in practical devices.

Chapter VII considers the more practical problem of how to couple the energy out of the sample if a space-charge interaction can be found. Material properties and fabrication methods are discussed in Chapters VIII and IX and some of the problems to be expected in experimental work are described.

Although much of the analysis has been done for a particular configuration of two layers, it should be emphasized that this does not restrict all of the topics discussed to this particular problem. The discussions presented on temperature effects, transverse velocities, energy coupling, and material properties have very broad applicability to the analysis of space-charge waves in solids. The approximate computer methods developed for solving problems with a finite velocity distribution due to temperature should prove useful in any analysis involving drifting carriers and space charge. The discussion of losses due to transverse ac velocities would apply to any space-charge interaction. The focusing effect of a dc magnetic field is also briefly mentioned. The coupling of energy out of the sample has been considered assuming that space-charge bunching is present. No particular sample configuration is needed for this discussion. Finally, material properties are described which fit a general plasma behavior that would be of interest for all space-charge interactions.

II. INTRODUCTION TO SOLID STATE PLASMAS

As discussed in the introductory chapter, the analysis to be used in this paper assumes a plasma model for a semiconducting solid. The purpose of this chapter is to discuss, and hopefully to justify, this assumption. First, some very general properties of gas, semiconductor, and metal plasmas will be compared and some of the basic experimental results will be stated which illustrate the plasma properties of these materials. Then in the following sections, a brief review of the pertinent semiconductor theory will be given with emphasis on the particular properties necessary to the analysis of gain mechanisms.

2.1. General Properties of Gas, Semiconductor, and Metal Plasmas

The usual idea of a plasma is a collection of electrons and positively charged ions in the form of a hot gas. However, many effects in solids, both metals and semiconductors, can also be described in terms of a plasma. Table I gives a comparison of some of the pertinent properties of the different kinds of plasmas.

The principal differences between gaseous, semiconductor, and metal plasmas are as follows:

1. In the gaseous plasma the densities are low and the kinetic temperatures are high, so that a Boltzmann distribution law

---

R. Bowers and M. C. Steele, "Plasma Effects in Solids," *Proceedings IEEE*, Vol. 52, October 1964, p. 1106.

Table I

Typical Characteristics of Various Plasmas

	Laboratory Gas Plasma	Plasma in Metal	Plasma in Semiconductor	Ionosphere
Mobile negative charge	Electron	Electron	Electron	Electron
Mobile positive charge	Ionized atom	---	Hole	Ionized atom
Densities	$10^{14}/cm^3$	$10^{22}/cm^3$	$10^{16}/cm^3$	$10^5/cm^3$
Mass -q carrier	m_o	m_o	$0.1\, m_o$	m_o
Mass +q carrier	$10,000\, m_o$	∞ (rigid)	$0.1\, m_o$	$50,000\, m_o$
Magnetic fields encountered (Gauss)	3,000	10,000	10,000	0.2
Plasma frequency $f_p = \dfrac{\omega_p}{2\pi} = \dfrac{1}{2\pi}\sqrt{\dfrac{ne^2}{\varepsilon_o\, m^*}}$	10^{11} Hz	10^{15} Hz	10^{12} Hz	10^6 Hz
Collision time (τ)	10^{-9} to 10^{-10} s	10^{-10} to 10^{-13} s	10^{-10} to 10^{-13} s	≈ 1 second

will give a good description of the particle distributions.

2. In a semiconductor, the electrons and ions are replaced by electrons and holes moving through the stationary lattice. The masses of the particles are now the effective masses, which take into account the effect of the crystal lattice on the particle motion. The particle densities are higher and the temperatures are lower so that often Fermi-Dirac statistics need to be used.

3. Metals have even higher particle densities and here again the kinetic temperatures are very high.

2.2. Experimental Observations of Plasmas in Solids

Since the plasma description of a semiconductor will be of particular interest in the following chapters, we will now take a very brief look at some of the experimentally observed effects which substantiate the plasma model.

Among the first of the plasma-type effects to be observed was the propagation of helicon waves. These waves correspond to the more familiar whistler waves in the ionosphere and have the characteristic helical motion of the electric field vector as the wave propagates. A. Libchaber and R. Veilex[2] demonstrated their propagation at 10 GHz in indium antimonide. Further work has since been done on their observa-

---

[2] A. Libchaber and R. Veilex, "Wave Propagation in a Gyromagnetic Solid Conductor: Helicon Waves," *Physical Review*, Vol. 127, August 1962, pp. 774-776.

tions at different frequencies and also with standing helicon waves.

Another plasma phenomenon which has been observed and studied in solids is the propagation of Alfven waves. G. A. Williams[3] observed the propagation of Alfven waves in bismuth using an interference technique.

Further verification of the plasma nature of semiconductors is the well known "pinch effect." The pinch effect has been studied in gases as a way to contain high temperature plasmas. The effect has also been observed in semiconductors. Self pinching occurs when the magnetic pressure exceeds the kinetic pressure. In indium antimonide at room temperatures, the critical current is about one ampere. Experimentally, the magnetic pinch can be seen either by destructive testing, where the current becomes so high that it locally melts the sample,[4] or by microwave reflection off of select portions of the material.

This has been but a brief survey and there are other types of effects such as spin waves and cyclotron wave resonances, but the results mentioned should be sufficient to show the validity of the plasma model.

2.3. Properties of Semiconductors

With the basic ideas as briefly outlined above, a more detailed description of the semiconductor properties is in order. The intention

---

[3] G. A. Williams, *Bulletin of the American Physical Society*, Vol. 7, 1962, p. 409.

[4] B. Ancker-Johnson and J. E. Drummond, "Thermal Pinching in Electron-Hole Plasma," *Physical Review*, Vol. 131, September 1963, pp. 1961-1965.

here is not to give an all-inclusive discussion, but rather to elucidate some of the more important concepts that have to be used in a plasma description of a semiconducting solid.

The basic principles underlying the physics of semiconducting materials have been achieved through the concept of energy bands. Two fundamentally different approaches may be used, both of which lead to the energy band picture of a solid. The first approach is known as the free-atom or tight binding of electrons, and the second is the free-electron or loose binding method. The free-electron approach is the more appropriate to the plasma model interpretation and, therefore, will be used in the following discussion.

The Drude-Lorentz Free-Electron Model. Even before the energy-band theory was developed, the basic ideas of the free-electron model were first embodied in what is now known as the Drude-Lorentz theory, first proposed for metals. Although the Drude-Lorentz theory does not require the energy band concept, much of its results are still valid and the energy band model can be thought of as an extension to describe additional phenomena. For this reason, it is worthwhile to take a look at the predictions of this theory.

In the Drude-Lorentz plasma model, the ions are considered immobile, and the electrons are considered to be either free or bound to an equilibrium position by a Hooke's law type restoring force. From this model, which is really the combination of the Drude free-electron model

of metals and the Lorentz model of an insulator,[5] a dielectric constant can be obtained which describes the characteristics of wave propagation in solids for a wide frequency range.

For the bound electrons, the dielectric constant is

$$\epsilon_b = \epsilon_o \left[1 - \frac{\omega_{pb}^2}{\omega^2 - j\frac{\omega}{\tau} - \omega_s^2} \right]$$

where ω_s is the "spring constant" frequency, and ω_p is the plasma frequency defined as

$$\omega_p = \sqrt{\frac{-\rho|e|}{\epsilon_o m}}$$

For the free electrons, the dielectric constant is

$$\epsilon_f = \epsilon_o \left[1 - \frac{\omega_{pf}^2}{\omega^2 - j\frac{\omega}{\tau}} \right]$$

In a good insulator where essentially no free electrons are present, ϵ_b is used. In a metal at low frequencies, the polarization is negligible and ϵ_f is used. For intermediate situations the sum of ϵ_b and ϵ_f is used.

This simple approach is surprisingly accurate for a wide range

---

[5] H. Ehrenreich, "The Optical Properties of Metals," *IEEE Spectrum*, Vol. 2, March 1965, pp. 162-170.

of materials and frequencies. For example, H. Ehrenreich[6] discusses the optical properties of metals based on this model. He finds good correlation between theory and experiment.

Although the Drude-Lorentz theory successfully explained many of the properties of metals, it did not agree with experimental evidence in the prediction of a contribution to the molar heat capacity of a metal by the free electrons. The predicted 3R/2 contribution could not be verified. This conclusion was inherent in the theory and was due to the use of Maxwell-Boltzmann statistics.

This problem with the Drude-Lorentz theory was subsequently resolved by the discovery of the Pauli exclusion principle and the application of Fermi-Dirac quantum statistics to the solid as postulated by Sommerfeld. Fermi-Dirac statistics are now the accepted method for general treatment of temperature effects in a semiconductor or metal. However, in many cases it is still possible to make a good approximation and use the Maxwell-Boltzmann results. These cases will be discussed in detail in Chapter V.

Energy Band Theory. The Drude-Lorentz plasma model and the later addition of Fermi-Dirac statistics has given a fairly complete picture of the properties of solids. It would seem at this point that the energy-band concept mentioned at the beginning of Section 2.3 is not needed. However, there is one very important property of materials

---

[6] *Ibid.*

that the Sommerfeld theory still could not explain. Why do some atoms combine to form insulators and others end up being very good conductors? This is a terribly important question because to a large extent it determines whether or not we have a plasma to work with.

A modification of the Drude-Lorentz and Sommerfeld theories is necessary because in a crystal lattice the electron sees the periodic potential of the lattice in addition to any external field. The periodicity of this potential modifies the possible states that an electron may occupy, so that certain energy regions are now forbidden. The electrons in the solid will be found in the permitted regions or energy bands, as they are usually named.

The solid may have some of the energy bands with their states filled and with a large band gap to the next higher states. This will result in an insulator, since the electrons are essentially bound to their positions and energies. However, if the forbidden energy gap is small or a band is only partly filled, a semiconductor or a conductor will result. A quantitative description of this process will be presented in the next section.

2.4. Important Plasma Properties of Semiconductors

The important properties which are needed in a plasma model and which are determined as a consequence of the band theory are the carrier concentration, effective mass, and mobility.

Carrier Concentration in a Semiconductor. For any plasma effects

to occur, there must be a concentration of mobile charged particles within the semiconductor. Furthermore, it is usually necessary to know this concentration with a reasonable degree of accuracy. The total number of mobile carriers in the conduction band (the energy band that results in the normally observed electron conduction) is determined by the number of available states in the conduction band and their probability of occupation. A similar situation holds for the hole concentration in the valence band (the energy band where all electrons are found in the 0°K or unexcited state).

Using Fermi-Dirac statistics and assuming spherical energy bands, the total number of electrons per unit volume in the conduction band is given by[7]

$$n = 2 \int_{E_c}^{\infty} \frac{2\pi \left(\frac{2m_e}{h^2}\right)^{3/2} \left(E - E_c\right)^{1/2} dE}{1 + e^{\left(E - E_f\right)/kT}} \tag{1}$$

where E_c is the lowest energy of the conduction band, and E_f is the Fermi energy.

In order to evaluate the integral of Eq. 1, the approximation is usually made that

$$1 + \exp\left(\frac{E - E_f}{kT}\right) \simeq \exp\left(\frac{E - E_f}{kT}\right) \tag{2}$$

---

[7] C. Kittel, *Introduction to Solid State Physics*, New York, John Wiley & Sons, 1966, p. 304.

The simplification is justified provided that $E - E_f \gtrsim 2kT$, or depending on the desired accuracy of the results. What this simplification means is that we are going to use Maxwell-Boltzmann statistics. Physically, it means that there are many unfilled states at the usual temperatures of interest and the Pauli exclusion principle does not have a significant effect on the occupation probabilities. This, incidentally, is one reason why the Drude-Lorentz model gives an accurate description of many phenomena.

With the approximation of Eq. 2, the integral can be evaluated, and the result is

$$n = 2 \left(\frac{2\pi m_e kT}{h^2} \right)^{3/2} \exp\left(\frac{E_f - E_c}{kT} \right) \tag{3}$$

If we write

$$n = \mathcal{D}_e \exp\left(\frac{E_f - E_c}{kT} \right)$$

then

$$\mathcal{D}_e = 2 \left(\frac{2\pi m_e kT}{h^2} \right)^{3/2} \tag{4}$$

can be thought of as the effective density of states in the conduction band.

The hole concentration can be derived similarly if we recognize that the probability of a hole occupying a state is the same as an elec-

tron not being in that level.

$$g(E) = 1 - f(E)$$

Then writing an equation similar to Eq. 1 and integrating we get

$$p = 2 \left(\frac{2\pi m_h kT}{h^2} \right)^{3/2} \exp\left(\frac{E_v - E_f}{kT} \right) \tag{5}$$

where the limits of integration are now $-\infty$ to E_v, the top of the valence band

$$\mathcal{D}_h = 2 \left(\frac{2\pi m_h kT}{h^2} \right)^{3/2} \tag{6}$$

is the equivalent density of states in the valence band.

For intrinsic materials, the carriers are thermally generated so that $n = p$. Then combining Eqs. 3, 4, 5, and 6

$$n = \left(\mathcal{D}_e \mathcal{D}_h \right)^{1/2} \exp\left(\frac{-E_g}{2kT} \right) \tag{7}$$

where $E_g = E_c - E_v$, i.e., the band gap.

The effective masses m_e and m_h are usually determined from cyclotron resonance experiments, so that for a known value of E_g, we can calculate the carrier concentration as a function of temperature.

For an extrinsic material, impurity atoms can increase the

concentration of either holes or electrons. However, the product

$$np = \mathcal{D}_e\mathcal{D}_h \exp\left(-E_g/kT\right) \qquad (8)$$

is constant at any given temperature, so that if we have an excess of electrons, the holes are correspondingly decreased in number.

One other important difference occurs in doped materials. Impurity doping drastically affects the carrier concentration. As more and more states are made available by the impurity atoms, the Fermi level moves closer to either the conduction band (for n-type) or the valence band (for p-type) materials. This means that the energy difference $\left(E - E_f\right)$ gets smaller and, therefore, closer to kT. For materials of even medium doping concentrations, the Fermi level is sufficiently close to E that there is little change in the carrier concentration with temperature, since all the impurity states are excited. If the doping is made even stronger, the Fermi level finally ends up inside the band and we get what is known as degenerate doping, when the carrier concentration is essentially independent of temperature for all temperatures and the material resembles a metal.

Effective Mass. If we assume that the contribution of the lattice is to modify some external force that is applied to the electron, then it is possible to derive a general relation which results in the effective mass.

For a frequency ν and a wavelength λ, the group velocity v for

an electron wave packet is given by

$$v = \frac{d\nu}{d(1/\lambda)}$$

Using $E = h\nu$ and putting $k = 2\pi/\lambda$, we have

$$v = \frac{2\pi}{h} \cdot \frac{dE}{dk}$$

and

$$\frac{dv}{dt} = \frac{2\pi}{h} \frac{dk}{dt} \frac{d^2E}{dk^2} \qquad (9)$$

If this acceleration is due to a force F, then the work done on an electron in time δt is

$$\delta E = F \cdot v \, \delta t$$

$$= F \, \frac{2\pi}{h} \frac{dE}{dk} \, \delta t$$

But

$$\delta E = \frac{dE}{dk} \, \delta k$$

$$\frac{dE}{dk} \, \delta k = F \, \frac{2\pi}{h} \frac{dE}{dk} \, \delta t$$

which means that

$$\delta k = F \frac{2\pi}{h} \delta t$$

and

$$\frac{\delta k}{\delta t} = \frac{dk}{dt} = F \frac{2\pi}{h} \tag{10}$$

Substituting Eq. 10 into Eq. 9 gives

$$\frac{dv}{dt} = \frac{2\pi}{h} F \frac{2\pi}{h} \frac{d^2E}{dk^2}$$

or finally

$$F = \frac{\hbar^2}{\frac{d^2E}{dk^2}} \frac{dv}{dt} \tag{11}$$

Comparing Eq. 11 to the usual force equation

$$F = m \frac{dv}{dt}$$

we can write a mass term m*

$$m^* = \frac{\hbar^2}{\left(\frac{d^2E}{dk^2}\right)} \tag{12}$$

where the asterisk on "m" is used to denote a possible difference from

the free electron theory. The important point of this deviation is that once we know the relationship of E versus k in any material, then the effect of external forces can be determined.

In a solid, the E versus k curves are in general different in different crystal directions and also may have several energy levels separated by forbidden regions. This leads to an effective mass tensor for any given crystal. In practice, one usually refers to the literature to get a numerical value for the effective mass of a material with the particular crystalographic orientation specified.

Carrier Mobility. The mobility is defined as

$$\mu = \frac{v}{E} \tag{13}$$

and relates the velocity of the carriers to the applied external electric field. This is another important quantity, because interactions involving drifted carriers are strongly dependent on the carrier velocity. Physically, the mobility is determined by the effective mass and by the collision damping. As the carriers are accelerated by the field, their velocity increases until they collide with a lattice point. Then the process is repeated. A steady-state condition is reached where an average drift velocity can be defined. Because the process is essentially collision dominated and the effective mass term has already been discussed, further discussion will be postponed until collisions are considered in detail in Chapter V.

III.   SPACE-CHARGE WAVES AND GAIN MECHANISMS

In Chapter II, the plasma properties of solid-state materials were discussed. Experimental verification of some of these properties leads to the reasonable assumption that other plasma effects may exist. In particular, it may be possible to discover solid-state analogues to electron-beam interactions such as the double-stream amplifier or the traveling-wave tube. In this chapter, we would like to consider in more detail what types of instabilities or gain mechanisms may be possible, what other authors have already analyzed, and what experiments have been performed to verify the theoretical predictions. A detailed analysis of a simple model will then be made to illustrate the fundamental ideas of how the gain arises and what conditions are necessary to have amplification.

3.1.   Growth Mechanisms and Instabilities in Electron Beams

Historically, the first successful practical application of gaseous plasma waves was in the klystron. The klystron operates with a drifting electron stream where an entrance region serves to velocity modulate the beam; the beam is then drifted until the velocity modulation becomes current modulation or space-charge bunching. Some of the dc energy in the beam is thus converted to ac and can be taken as useful power output.

Other possible gain mechanisms were subsequently found and have since been investigated in great detail. The most well-known and practical result of all this effort has been the traveling-wave tube. This

is now a useful microwave amplifier in a frequency region where conventional electron tubes cannot be built. Two other beam-type interactions which were developed in detail are the double-stream amplifier and the admittance wall amplifier.[1] However, they were never put to practical use because a method was needed to couple energy into and out of the beams. The best available method was a helix which sufficiently slowed the propagation in a conductor to synchronize to the slower beam velocity. The traveling-wave tube uses a helix to produce coupling to the beam over the entire interaction length. Therefore, if a helix is needed anyway, why not just make a traveling-wave tube? Another problem with the double-stream amplifier is the difficulty of intermixing two electron streams of slightly different velocities.

Although practical use was not made of all the possible proposed electron-beam interactions, the ideas were well developed, understood, and verified by useful devices. As solid-state materials became further developed and their plasma properties better understood, it was natural to investigate the possibilities of space-charge effects in solids.

3.2. Theoretical Proposals for Solid-State Space-Charge Interactions

The first definitive work in this area was done by D. Pines,[2]

---

[1] C. K. Birdsall and J. R. Whinnery, "Waves in an Electron Stream with General Admittance Walls," *Journal of Applied Physics*, Vol. 24, March 1953, pp. 314-323.

[2] D. Pines, "Coherent Excitation of Plasma Oscillations in Solids," *IRE Transactions on MTT*, Vol. 9, January 1961, pp. 89-92.

and D. Pines and J. R. Schrieffer.[3] They analyzed the double-stream
interaction as it would apply to a semiconductor with holes and elec-
trons comprising the two streams. Their analysis was based on the
Boltzmann equation with a Maxwellian distribution function to include
temperature effects. Collision effects were included by a linear ap-
proximation. In a plasma consisting of holes and electrons, the dif-
ference between the hole and electron effective masses is important as
well as the different effective temperatures. For a practical example
they considered indium antimonide and concluded that gain would be pos-
sible at very low temperatures ($\approx 20°K$) for electric fields of about 100
volts/cm.

Vural and Steele[4] extended the two-stream analysis to include
longitudinal magnetic fields. Their analysis was done to include both
transverse and longitudinal effects instead of the one-dimensional
analysis of Pines and Schrieffer.[5] They concluded that instabilities
in the millimeter-wave region appear possible.

Recently, two other articles have appeared in the literature
which are of particular interest. These articles consider layered
structures such as will be the main topic of this report. B. B.

---

[3] D. Pines and J. R. Schrieffer, "Collective Behavior in Solid-State
Plasmas," *Physical Review*, Vol. 124, December 1961, pp. 1387-1400.

[4] B. Vural and M. C. Steele, "Possible Two-Stream Instabilities of
Drifted Electron-Hole Plasmas in Longitudinal Magnetic Fields,"
Physical Review, Vol. 139, July 1965, pp. A300-A304.

[5] Pines and Schrieffer, *loc. cit.*

Robinson and G. A. Swartz[6] derived a dispersion equation for a configuration of alternate thin layers of p-type and n-type material. They found that, using an analysis similar to that used by Pines and Schrieffer, they could relax some of the conditions to correspond to a more physically realizable situation. In particular, the condition on $\omega_{p+}\,\tau_+$, where ω_{p+} is the hole plasma frequency and τ_+ the hole relaxation time, could be relaxed by about an order of magnitude from ~10 to ~1. However, they concluded that it would still be necessary to have $T_+ \ll T_-$, where T_+ and T_- are hole and electron temperatures. This is a very difficult condition to satisfy experimentally, and would probably require some special thermal contacts to the p-type layers.

A single layer of a thin semiconductor in a magnetic field has been analyzed by B. B. Robinson and B. Vural.[7] They found that the effect of a transverse magnetic field on a thick semiconductor was the same as just having a single infinitely thin layer in a magnetic field.

Some other aspects of the double-stream problem have been analyzed. For example, Kai Fong Lee[8] considered the effects of higher-order modes in bounded and/or inhomogeneous plasmas.

---

[6] B. B. Robinson and G. A. Swartz, "Two-Stream Instability in Semiconductor Plasmas," *Journal of Applied Physics*, Vol. 38, May 1967, pp. 2461-2465.

[7] B. B. Robinson and B. Vural, "Double-Stream Interaction in a Thin Semiconductor Layer," *RCA Review*, Vol. 29, June 1968, pp. 270-280.

[8] K. F. Lee, "Higher-Order Modes of the Two-Stream Instability in Bounded and/or Inhomogeneous Plasmas," *Journal of Applied Physics*, Vol. 38, April 1967, pp. 2172-2178.

A second major area of investigation has been to propose traveling-wave tube analogues for a solid-state plasma. This is a natural outgrowth of the considerable success that traveling-wave tubes have had as beam devices. Unfortunately, the problem becomes much more difficult in a solid, for two reasons:

1. Temperature induced random velocities have much more of a disturbing effect on the gain.

2. Collisions with the lattice and between the particles act as a damping mechanism, once again reducing the gain.

The effects of temperature will be discussed further in this chapter and also in Chapter V, but just to have an idea of how significant the problems are, it is interesting to consider a very crude analogy to electron beams. In an electron beam, the electrons are emitted from a cathode surface at a temperature of about 1000°K, then accelerated to energies on the order of 10^3 to 10^4 electron volts, for typical beam tubes.

For a one-dimensional model, the temperature effect can be approximated as

$$\frac{1}{2} mv_t^2 = \frac{1}{2} kT$$

where v_t is some average thermal velocity. This is a kinetic energy term so that it can just as well be written in terms of electron volts.

$$\text{Energy in electron volts} = \frac{kT}{q}$$

At 1000°K

$$\frac{kT}{q} = .086 \simeq .1 \text{ electron volts} \qquad (14)$$

It is apparent from Eq. 14 that the final electron beam velocity is very much greater than the randomizing effect of temperature. In a solid-state plasma, the highest drift velocities observed are only about two times larger than the v_t thermal velocity term. If this were the case with electron beams, it would mean that at best we could use accelerating voltages of about 1/2 volt instead of 1000 volts. Useful beams would be nearly impossible to produce under these circumstances. The solid, of course, does have well-defined boundaries so that focusing of the beam is not necessary, but the randomizing effect of the kinetic temperature term will cause severe damping of any interaction which depends on well-defined beam velocities, as all of the space-charge interactions do.

In spite of these apparent difficulties, solid-state traveling-wave amplifiers have been proposed by several authors. L. Solymar and E. A. Ash[9] have perhaps made the best analysis to date and concluded that the problem is indeed a difficult one. In addition to the temperature damping discussed above, there are major problems with the transverse losses in a semiconductor and the large difference in natural prop-

---

[9] L. Solymar and E. A. Ash, "Some Traveling-Wave Interactions in Semiconductors: Theory and Design Considerations," *International Journal of Electronics*, Vol. 20, February 1966, pp. 127-148.

agation velocities between the circuit and the beam. The highest attainable drift velocities in semiconductors are about $10^{-3}c$, where c is the speed of light. This means that the slow-wave structure has to slow the wave propagating on it by about this factor. This results in very large ohmic losses and probably requires superconductors or some similar technique. The transverse losses can possibly be overcome by having an anisotropic conductivity tensor. This will be discussed in detail in Chapter VI.

Other essentially similar analyses have been presented, e.g., M. Sumi,[10] and M. Ettenberg and J. Nadan.[11] The conclusions are similar in all these cases. The gain per centimeter is always very high when circuit losses, temperature, and collision effects are ignored. When a realistic model is considered, the results are no longer as encouraging, as one might well expect from the beam analogy discussed above.

The interactions analyzed by the authors cited above by no means exhaust the available literature. An attempt has been made to briefly describe only those references which are very closely connected with the topics to be presented in this report.

3.3. Experimental Observations of Space-Charge Interactions

The wealth of proposed interactions and thoroughness of the

---

[10] M. Sumi, "Traveling-Wave Amplification by Drifting Carriers in Semiconductors," *Applied Physics Letters*, Vol. 9, September 1966, pp. 251-253.

[11] M. Ettenberg and J. Nadan, "Gain in Solid-State Traveling-Wave Amplifiers," *IEEE Proceedings*, Vol. 56, April 1968, pp. 741-742.

analyses should point to a corresponding amount of experimental observation. A survey of the literature shows that this is not the case. A considerable amount of effort has been put into this area, but conclusive results have been meager.

By far the greatest amount of experimental work has been done on indium antimonide. Larrabee and Hicinbothem[12] first observed microwave emission at high fields from InSb. Since the publication of that result, many experimenters have tried various combinations of electric and magnetic fields and sample dimensions. Both low-frequency output in the megahertz range and broadband microwave emission can be found for a wide variety of experimental conditions. Betsy Ancker-Johnson[13] has summarized these results and has proposed a theory to explain some of the experimental observations. The instability is not identified, but the effect of the magnetic field is postulated as being secondary to the electric field. The main effect of the magnetic field is to concentrate the plasma and put it near the radiating surface. If the appropriate surface conditions are met without a magnetic field, the microwave emission is observed in this case also. A measurement of the plasma densities inside InSb should determine the validity of this theory. At this time, it does appear that the experimental data fit this kind of an

[12] R. D. Larrabee and W. A. Hicinbothem, "Observation of Microwave Emission from InSb," *Symposium on Plasma Effects in Solids*, Paris, 1964; Dunod, publisher, 1965.

[13] B. Ancker-Johnson, "Microwave Emission from Nonequilibrium Plasmas in InSb Subject to Magnetic Fields," *Journal of Applied Physics*, Vol. 39, June 1968, pp. 3365-3378.

explanation, in which case the instabilities may be similar to those encountered in gas plasmas at high plasma densities and high fields.

A different approach to the microwave emission from InSb has been taken by G. A. Swartz and B. B. Robinson.[14] They have assumed the double-stream model with a transverse magnetic field to contain the interaction near the surface. By cutting narrow slots in the samples of widths on the order of the space-charge wavelength, they have been able to obtain coherent emission at reasonably well-defined frequencies.

Yet another explanation of the microwave generation has been advanced by M. C. Steele.[15] This paper proposed that the radiation is due to photoconductive mixing of amplified spontaneous radiation. The conditions for this type of amplification are satisfied when the electron-hole density produces the population inversion required for amplification of the band-gap radiation.

Observation of microwave radiation from materials other than InSb has not been successful. One of the few reported results of any kind of oscillations in germanium is by H. Heinrich and D. K. Ferry.[16]

---

[14] G. A. Swartz and B. B. Robinson, *Coherent Microwave Instabilities in a Thin Layer Solid-State Plasma*, Princeton, New Jersey, RCA Laboratories, 1968.

[15] M. C. Steele, "Microwave Generation from Photoconductive Mixing of Amplified Spontaneous Radiation," *RCA Review*, Vol. 27, June 1966, pp. 263-271.

[16] H. Heinrich and D. K. Ferry, "Hot Carrier Current Oscillations in n-Type Germanium," *Applied Physics Letters*, Vol. 11, August 1967, pp. 126-128.

These oscillations are in the megahertz range and at very high electric fields, sufficient to produce current saturation.

It should by now be apparent that a conclusive result has not been obtained to date. The experimental observations neither prove nor disprove the space-charge model. Double-stream interaction does give a suitable explanation for the results of Swartz and Robinson. However, the other proposed theories seem to fit as well. Subsequent chapters of this thesis will bring out some of the many problems with space-charge interactions which would cause the serious experimental difficulties encountered at this laboratory and, apparently, elsewhere.

3.4. Introductory Discussion of the Double-Stream Interaction

From the theories and experiments summarized in Sections 3.2 and 3.3, it should be apparent that a complete or even adequate explanation has yet to be found. Significant contributions can be made in both the theoretical and experimental areas.

As an introduction to a quantitative analysis, a simplified model will now be considered which includes some of the characteristics of a solid-state plasma. We will show how the gain is predicted and then discuss the necessary requirements on the dispersion relation to verify a time and space instability.

Since we have indicated that the plasma model may be a good representation of the actual solid, an analysis based on the hydrodynamic equation for a plasma will be the basis of the subsequent discussion. The hydrodynamic equation is only an approximate approach. For accurate

results, the Boltzmann transport equation should be used instead. This more complicated analysis will be considered in Chapter V.

The effects of thermal velocities and dc drift velocities are very important in solid-state plasmas. To include these effects, we start with the momentum transfer equation for the "ith" component of a multistream plasma, which may be written as[17]

$$\frac{d\vec{v}_i}{dt} = - \frac{1}{n_i m_i} \vec{\nabla} P_i - \frac{Z_i |e|}{m_i} \left(\vec{E} + \vec{v}_i \times \vec{B} \right) - \nu_{ci} \vec{v}_i \tag{15}$$

The symbols in this equation have the usual meaning, i.e., v = velocity, P = pressure, $Z_i |e|$ = total charge, m = mass, and ν_c = collision frequency. Since we have no applied B-field, Eq. 15 can be written in a simpler form.

$$\frac{d\vec{v}}{dt} = - \frac{\vec{\nabla} P}{mn} - |e| \frac{\vec{E}}{m} - \nu_c \vec{v}$$

$$\tag{16}$$

$$- \frac{|e|}{m} \vec{E} = + \frac{\vec{\nabla} P}{mn} + \frac{d\vec{v}}{dt} + \nu_c \vec{v}$$

To facilitate the analysis, we now assume a time and space variation in the z-direction of the usual periodic form, $e^{j(\omega t - \beta z)}$. Then, with the small-signal assumption, i.e., ac velocities much smaller than dc,

$$\frac{d\vec{v}}{dt} = \frac{\partial \vec{v}}{\partial z} \frac{dz}{dt} + \frac{\partial \vec{v}}{\partial t} = - j\beta \vec{v} v_0 + j\omega \vec{v}$$

[17] M. A. Uman, *Introduction to Plasma Physics*, New York, McGraw-Hill, 1964, p. 31.

Therefore,

$$-\frac{|e|}{m}\vec{E}_z = +\frac{\vec{\nabla}P}{mn} + \left(j\omega + \frac{1}{\tau} - j\beta\, v_o\right)\vec{v} \tag{17}$$

However, we can write the pressure term as

$$\frac{\vec{\nabla}P}{m\rho_o} = \frac{\vec{\nabla}\left(\left(\rho + \rho_o\right)kT\right)}{m\rho_o} = \frac{kT\,\vec{\nabla}\rho}{m\rho_o}$$

where $n = \rho_o$ and $n_i = \rho_o + \rho$. Now, if we define a thermal velocity as in Section 3.2

$$\frac{1}{2}\,kT = \frac{1}{2}\,m\,v_t^2$$

then

$$\frac{\vec{\nabla}P}{m\rho_o} = \frac{v_t^2\,\vec{\nabla}\rho}{\rho_o}$$

If ρ has the same periodic variation $e^{j(\omega t - \beta z)}$

$$\frac{\vec{\nabla}P}{m\rho_o} = -\frac{j\beta\,v_t^2\,\rho}{\rho_o}$$

and our force equation becomes

$$-\frac{|e|}{m}E_z = \left(j\omega + \frac{1}{\tau} - j\beta\,v_o\right)v_z - j\,\frac{\beta}{\rho_o}\,v_t^2\,\rho \tag{18}$$

- 32 -

A further simplification can be made if we neglect the $\frac{1}{\tau}$ term. This is the collision relaxation term, and neglecting it will mean device operation at frequencies $\omega \gg \frac{1}{\tau}$. The effect of this term on the gain will be considered in detail in Chapter V.

The determinantal equation for the infinite double-stream case now can be derived as follows:

$$\vec{V} \times \vec{H} = \vec{J}_1 + \vec{J}_2 + j\omega \, \epsilon_o \, \vec{E} = 0 \tag{19}$$

Setting $\vec{V} \times \vec{H} = 0$ implies that there are no transverse variations

$$-\frac{|e|}{m} E_z = \left(j\omega - j\beta v_o\right) v_z - j \frac{\beta}{\rho_o} v_t^2 \rho$$

But

$$J = \rho_o v + v_o \rho$$

for small ac variations. Then, if we define $\beta_e = \frac{\omega}{v_o}$,

$$v = \frac{J - v_o \rho}{\rho_o} = \frac{1}{j\beta_e \rho_o} \left(j\beta_e J + \frac{\partial J}{\partial z}\right)$$

Using this expression for v in the force equation,

$$-\frac{|e|}{m} E_z = \left(j\omega - j\beta v_o\right) \frac{1}{j\beta_e \rho_o} \left(j\beta_e J + \frac{\partial J}{\partial z}\right) + j \frac{\beta}{\rho_o} v_t^2 \frac{1}{j\omega} \frac{\partial J}{\partial z}$$

Now assuming the same periodicity for "J"; i.e.,

$$J = J_1 e^{-j\beta z}$$

The expression for the $\vec{E}$-field in terms of $\vec{J}$ then becomes

$$\frac{-j\beta_e \rho_o |e|}{m} E_z = \left[\left(j\omega - j\beta v_o \right) \left(j\beta_e - j\beta \right) - \frac{j\beta\beta_e v_t^2 j\beta}{\omega} \right] J_z \qquad (20)$$

When this result is substituted in Eq. 19, we arrive at the following result (after a few algebraic manipulations):

$$\frac{\dfrac{\omega_{p1}^2}{v_{o1}^2 - v_{t1}^2}}{\left(\dfrac{\omega}{v_{o1} + v_{t1}} - \beta \right)\left(\dfrac{\omega}{v_{o1} - v_{t1}} - \beta \right)} + \frac{\dfrac{\omega_{p2}^2}{v_{o2}^2 - v_{t2}^2}}{\left(\dfrac{\omega}{v_{o2} + v_{t2}} - \beta \right)\left(\dfrac{\omega}{v_{o2} - v_{t2}} - \beta \right)} = 1 \qquad (21)$$

where

$$\omega_{p1}^2 = \frac{\rho_{o1} e}{\varepsilon_o m}$$

and

$$\omega_{p2}^2 = \frac{\rho_{o2} e}{\varepsilon_o m}$$

The subscripts refer to the carriers as 1 and 2 and the zeros denote dc quantities where they appear before other subscripts.

It is not particularly easy to see from this equation that there is a possibility of getting complex values for ω or β, which would indicate possible growth in space, time, or both. The simplest possible result that still satisfies the requirements of a double-stream interaction is to look at the zero temperature case. Then $v_{t1} = v_{t2} = 0$, and Eq. 21 becomes

$$\frac{\omega_{p1}^2}{\left(\omega - \beta v_{o1}\right)^2} + \frac{\omega_{p2}^2}{\left(\omega - \beta v_{o2}\right)^2} = 1 \qquad (22)$$

It is not absolutely necessary that both streams have a drift velocity, so assume that as a special case $v_{o1} = 0$. This now results in a second-order equation in β which is easy to solve.

$$\frac{\omega_{p2}^2}{\left(\omega - \beta v_{o2}\right)^2} = 1 - \frac{\omega_{p1}^2}{\omega^2} \qquad (23)$$

which simplifies to

$$\beta = \frac{\omega}{v_{o2}} \pm \frac{\omega_{p2}}{v_{o2} \sqrt{1 - \left(\frac{\omega_{p1}}{\omega}\right)^2}} \qquad (24)$$

If $\omega_{p1} > \omega$ in Eq. 24, then β has an imaginary term. One wave will grow spacially and the other will decay.

The more general case where temperature effects are included

is considerably harder to solve. As can be seen from Eq. 21, a fourth-order equation results in ω or β. The simplest method for obtaining solutions is to program the fourth-order equation on a computer. These results will be analyzed in detail in Chapter V.

Another method, which is sometimes useful to see if complex values of β are possible, is to write the dispersion relation in a form that can be analyzed by root-locus techniques. Any equation, such as Eq. 21, which can be rewritten as a ratio of factored polynomials and equated to one, is ideal for a root-locus analysis. The poles and zeros of the equation are plotted in the complex β-plane and the standard rules for positive or negative feedback can then be applied to find the regions of complex β, if any exist. Equation 21 could be analyzed by this technique also. However, the factors are reasonably complicated and many cases would need to be considered for a useful analysis. The infinite plasma is not of sufficient importance to this report to permit this consideration.

3.5. Classification and/or Verification of Instabilities

In Eq. 24, we found that β has complex values for certain values of ω. This implies that a spacial growth or decay exists for a wave propagating, as given by the real part of β. P. A. Sturrock[18] has shown that this is not sufficient to determine whether amplification is pres-

[18] P. A. Sturrock, "Kinematics of Growing Waves," *Physical Review*, Vol. 112, December 1958, pp. 1488-1503.

ent. Additional requirements must be satisfied. Before these requirements can be stated, an understanding of the different possible results is necessary. Sturrock classified waves as either growing or evanescent where these terms have the usual intuitive meaning. The growing waves can be classified further into convective or nonconvective instabilities. A convective instability is one where the wave grows but propagates away from the origin so that the origin may eventually return to its undisturbed state. A nonconvective instability, on the other hand, grows in amplitude and extent but always includes the point of origin. Sturrock[19] was able to make the following general statements: "If ω is real for all real k, then any complex k, for real ω, denotes an evanescent wave. Conversely, if k is real for all real ω, then any complex ω, for real k, denotes nonconvective instability." Sturrock's k corresponds to our β.

From this statement we can see that even though complex β exists, it does not necessarily determine a growing wave in both space and time. If, however, we can find complex ω for real β in addition to complex β for real ω, then at least there is a possibility of finding growing or amplifying waves.

Consider Eq. 23 once more:

$$\frac{\omega_{p2}^2}{\left(\omega - \beta v_{o2}\right)^2} = 1 - \frac{\omega_{p1}^2}{\omega^2} \tag{23}$$

---

[19] *Ibid.*, p. 1488.

If we simplify further and assume that $\omega_{p1}^2 \gg \omega^2$, then

$$\frac{\omega_{p2}^2}{\left(\omega - \beta v_{o2}\right)^2} = - \frac{\omega_{p1}^2}{\omega^2}$$

and

$$\omega = \frac{\beta v_{o2}}{\left(1 \pm j \dfrac{\omega_{p2}}{\omega_{p1}}\right)} \tag{25}$$

Complex ω will exist for real β, and growing waves are a possibility. Unfortunately, this does not guarantee a convective instability. The general rules are only for the evanescent waves and nonconvective instabilities. Sturrock discusses the case of a double-stream amplifier and concludes that when the stream velocities are in the same direction, two of the waves carried by the streams represent a convective instability. When the streams are in opposite directions a nonconvective instability results, so that complex ω and real β must be used for the analysis. Therefore, by knowing the physical process involved, Sturrock is able to identify the type of instability occurring. This is all we need to know for the present work, since all the cases to be considered fit well into this framework. It is interesting to note, however, that given a dispersion relation with more than two waves and of unknown origin, in some cases we would not be able to completely determine the type of instability or whether growing waves really did exist.

R. N. Sudan[20] has investigated this problem further and has been able to arrive at a set of conditions which are helpful in resolving problems of the type just mentioned. These conditions can be simply stated, using the notation of this report, as follows:

For a propagating wave that can be written as

$$\exp j(\omega t - \beta(\omega)z)$$

where

$$\omega = \omega_r + j\omega_i$$

$$\beta = \beta_r + j\beta_i$$

a. $\lim_{\omega_i \to -\infty} \operatorname{Re}\left\{j\beta(\omega)\right\}$ must approach $+\infty$ for $-\infty < \omega_r < +\infty$, for causality to be satisfied. Causality means that there is an initial disturbance at $z = 0$, and the observed effects are due to this disturbance.

b. A convective instability is assured if

$$\operatorname{Re}\left\{j\beta(\omega)\right\} < 0, \quad \omega_i = 0$$

for any value of ω on the real axis, if criterion a is also satisfied.

c. $d\omega/d\beta$ must vanish for some values of $\omega_i < 0$ if a nonconvective instability exists.

---

[20] R. N. Sudan, "Classification of Instabilities from their Dispersion Relations," *Physics of Fluids*, Vol. 8, October 1965, pp. 1899-1904.

Let us now apply these rules to the simple result of Eq. 23

$$\beta v_{o2} = \omega \pm \frac{\omega_{p2}}{\sqrt{1 - \dfrac{\omega_{p1}^2}{\omega^2}}} \qquad (26)$$

As $\omega_i \to -\infty$

$$\beta v_{o2} \to -j\infty \pm \omega_{p2}$$

then Re $(j\beta) \to +\infty$ so that both signs of Eq. 26 satisfy condition a.
If $\omega_i = 0$, and $\omega_{p1} > \omega$, then Re $\left\{ j\left(j\beta_i\right) \right\} < 0$, and by condition b, a
convective instability exists for $\omega_{p1} > \omega$. Finally, calculate $d\omega/d\beta$

$$v_{o2} \frac{d\beta}{d\omega} = 1 \pm \frac{\omega_{p2}\omega_{p1}^2}{\left(\omega^2 - \omega_{p1}^2\right)^{3/2}}$$

Then $d\omega/d\beta$ is zero only when $\omega = \pm \omega_{p1}$.

Both of these values are on the real axis, so there is no possibility
of nonconvective instability.

3.6. Summary of Chapter III

This chapter has introduced the fundamental ideas of space-
charge interactions and has presented some of the possible explana-
tions for the experimental observations. The short review of what has
been accomplished in this field should serve as a very persuasive argu-
ment that further investigation is necessary.

An idealized problem has been discussed in detail to illustrate the basic interaction mechanism. A set of rules for determining instabilities from their dispersion relations has been presented, and applied to the idealized model.

IV. ANALYSIS OF PERIODIC LAYERED STRUCTURE

The one-dimensional double-stream analysis considered in Chapter III provides understanding because of its simplicity, but it is not a physically realizable situation. The two electron streams of different drift velocities were assumed to be perfectly intermixed, and a one-dimensional model was used which presumed infinite transverse geometry.

This chapter will consider some of the more practical cases. First, the infinite periodic array of drifting plasma layers will be analyzed. This avoids the problem of intermixing the streams but still requires infinite geometry. An infinite array is useful for mathematical convenience to illustrate the transition to the more complicated finite structures. Then we will consider two physically realizable configurations $\left(\text{with } v_t = 0, \nu_c = 0\right)$, analyze some numerical results, and compare these to the simple idealized model of Chapter III.

4.1. Analysis of an Infinite Periodic Array of Drifting Plasma Layers

Consider an infinite array of electron streams or drifting plasmas as shown in Fig. 1. We will assume that the electrons have
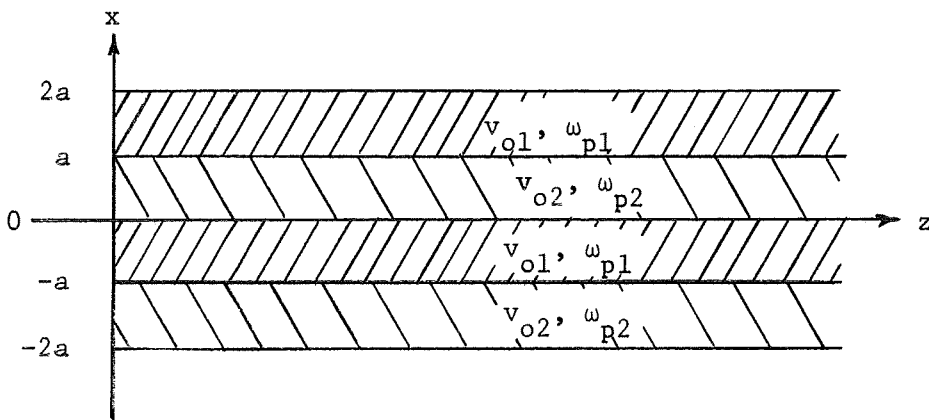
Fig. 1. Infinite array of plasmas drifting in the z-direction.

dc and ac velocities only in the z direction, that all quantities vary as $e^{j(\omega t - \beta z)}$, and that the usual small-signal approximations hold.

We can begin our discussion very generally by starting with the coupled-wave equation for the vector potential and then using the usual Lorentz condition as follows:

$$\vec{\nabla}(\vec{\nabla} \cdot \vec{A}) - \nabla^2 \vec{A} = \mu \vec{J} - \mu\epsilon \frac{\partial^2 \vec{A}}{\partial t^2} - \vec{\nabla}\left(\mu\epsilon \frac{\partial \Phi}{\partial t}\right) \tag{27}$$

$$\vec{\nabla} \cdot \vec{A} + \mu\epsilon \frac{\partial \Phi}{\partial t} = 0 \tag{28}$$

then

$$-\nabla^2 \vec{A} = \mu \vec{J} - \mu\epsilon \frac{\partial^2 \vec{A}}{\partial t^2} \tag{29}$$

For velocities in the z direction only and small-signal propagation of $e^{j(\omega t - \beta z)}$, J has already been derived in Chapter III as

$$J_z = \frac{-j \dfrac{\beta_e \rho_o |e|}{m} E_z}{\left[\left(j\omega - j\beta v_o\right)\left(j\beta_e - j\beta\right) - j \dfrac{\beta\beta_e v_t^2 j\beta}{\omega}\right]} \tag{20}$$

Since $\vec{J}$ and $\vec{E}$ have z components only, the vector potential $\vec{A}$ will likewise have only a z component.

$$- \nabla^2 A_z - \frac{\mu\epsilon_o j \frac{\omega}{v_o} \omega_p^2 E_z}{\left[\left(j\omega - j\beta v_o\right)\left(j\beta_e - j\beta\right) + \beta^2 \frac{v_t^2}{v_o}\right]} + \mu\epsilon \frac{\partial^2 A_z}{\partial t^2} = 0$$

(30)

$$- \nabla^2 A_z + \frac{\mu\epsilon_o j \omega \omega_p^2 E_z}{\left(\omega - \beta v_o\right)^2 - \beta^2 v_t^2} + \mu\epsilon \frac{\partial^2 A_z}{\partial t^2} = 0$$

But the $\vec{E}$ field can be written as

$$\vec{E} = -j\omega\left[\vec{A} + \frac{1}{k^2}\vec{\nabla}(\vec{\nabla} \cdot \vec{A})\right]$$

(31)

If we let A_z have the periodic variation $e^{-j\beta z}$, then

$$\vec{\nabla}\left(\vec{\nabla} \cdot A_z\right) = -\beta^2 A_z$$

(32)

$$- \nabla^2 A_z + \frac{\mu\epsilon_o \omega^2 \omega_p^2 \left(A_z - \frac{1}{k^2}\beta^2 A_z\right)}{\left(\omega - \beta v_o\right)^2 - \beta^2 v_t^2} + \mu\epsilon \frac{\partial^2 A_z}{\partial t^2} = 0$$

(33)

But

$$\frac{\partial^2 A_z}{\partial t^2} = -\omega^2 A_z \qquad , \qquad \mu\epsilon \omega^2 = k^2$$

and

$$\nabla^2 A_z = \nabla_T^2 A_z - \beta^2 A_z$$

This then gives us the final wave equation for the vector potential A_z

$$\nabla_T^2 A_z - \left(\beta^2 - k^2\right)\left[1 - \frac{\omega_p^2}{\left(\omega - \beta v_o\right)^2 - \beta^2 v_t^2}\right] A_z = 0 \qquad (34)$$

Equation 34 can be put into a more convenient form by defining

$$T_1^2 = \left(\beta^2 - k^2\right)\left[1 - \frac{\omega_{p1}^2}{\left(\omega - \beta v_{o1}\right)^2 - \beta^2 v_{t1}^2}\right] \qquad (35)$$

where the subscripts define the stream for which the wave equation is written. Then for stream No. 1, the equation reduces to

$$\left(\nabla_T^2 - T_1^2\right) A_{z1} = 0 \qquad (36)$$

and similarly for stream No. 2.

Assuming that there is no variation in the y direction, the boundary conditions on the electric and magnetic fields require that A_z and $\partial A_z/\partial x$ be continuous at the boundaries between the streams. Matching the vector potential $\vec{A}$ and its derivative at the boundary assumes that ε and μ have the same values in both materials. A more general condition will be considered shortly. It may be noted that the boundary conditions are identical for the $\vec{E}$ field and that the

same equation results if an analysis is made in terms of the $\vec{E}$ fields.

For no y variation, the wave equation will have solutions of the form

$$A_z = Ae^{Tx} + Be^{-Tx} \tag{37}$$

where A and B are constants which will have to be evaluated.

We can now write the solutions in two adjacent layers as

$$A_{z1} = Ae^{T_1 x} + Be^{-T_1 x}$$

$$\tag{38}$$

$$A_{z2} = Ce^{T_2 x} + De^{-T_2 x}$$

Let this boundary be at $x = 0$; then we must match the solutions smoothly.

$$A + B = C + D$$

$$T_1 A - T_1 B = T_2 C - T_2 D$$

Since the alternate layers extend to infinity, a periodicity condition must be included. This may be done in the following way

$$A_z e^{-igx} = \Pi_g(x)$$

$$\Pi_g(-a) = \Pi_g(+a)$$

Therefore,

$$e^{+iqa}\left(Ae^{-T_1a} + Be^{+T_1a}\right) = e^{-iqa}\left(Ce^{+T_2a} + De^{-T_2a}\right)$$

$$e^{iqa}\left[A\left(iq - T_1\right)e^{-T_1a} + B\left(iq + T_1\right)e^{T_1a}\right]$$

$$= e^{-iqa}\left[C\left(T_2 - iq\right)e^{T_2a} - D\left(iq + T_2\right)e^{-T_2a}\right]$$

In order to have nonzero solutions for A, B, C, and D the determinant of coefficients is set equal to zero.

$$\begin{vmatrix} 1 & 1 & 1 & 1 \\ T_1 & -T_1 & T_2 & -T_2 \\ e^{+iqa}e^{-T_1a} & e^{+iqa}e^{T_1a} & e^{-iqa}e^{T_2a} & e^{-iqa}e^{-T_2a} \\ \left(iq-T_1\right)e^{iqa}e^{-T_1a} & \left(iq+T_1\right)e^{iqa}e^{T_1a} & \left(T_2-iq\right)e^{-iqa}e^{T_2a} & -\left(iq+T_2\right)e^{-T_2a}e^{-iqa} \end{vmatrix} = 0$$

If the determinant is expanded by minors and simplified, the resulting

equation is

$$\frac{T_1^2 + T_2^2}{T_1 T_2} \sinh\left(T_1 a\right) \sinh\left(T_2 a\right) - 2 \cosh\left(T_1 a\right) \cosh\left(T_2 a\right)$$

$$= 2 \cos\left(2\, qa\right) \qquad\qquad (39)$$

where $qa = \frac{2\pi\ell}{N}$, N is any integer, and ℓ ranges in integral steps from $-N/2$ to $N/2$.

Suppose now that "a" is small enough so that

$$\left(T_1 a\right) \ll 1 \qquad ; \qquad \left(T_2 a\right) \ll 1$$

In this case

$$\sinh\left(T_1 a\right) \to T_1 a$$

$$\cosh\left(T_1 a\right) \to 1$$

and the determinantal equation reduces to

$$\left(T_1 a\right)^2 + \left(T_2 a\right)^2 = 2 \cos\left(2qa\right) - 2 \qquad\qquad (40)$$

$$a^2\left(\beta^2 - k^2\right)\left[2 + \frac{\dfrac{\omega_{p1}^2}{v_{t1}^2}}{\left(\beta - \dfrac{\omega}{v_{t1}}\right)\left(\beta + \dfrac{\omega}{v_{t1}}\right)} - \frac{\dfrac{\omega_{p2}^2}{v_{o2}^2 - v_{t2}^2}}{\left(\beta - \dfrac{\omega}{v_{o2} + v_{t2}}\right)\left(\beta - \dfrac{\omega}{v_{o2} - v_{t2}}\right)}\right]$$

$$= 2\cos(2qa) - 2 \qquad (41)$$

where, as in the previous chapter, we have assumed that $v_{o1} = 0$. This equation shows the coupling between the plane waves, represented by $\beta^2 - k^2$, and the space-charge waves, represented by the terms involving ω_{p1} and ω_{p2}. The infinite number of values $\cos(2qa)$ can have represents harmonics due to the infinite, periodic nature of the electron streams.

The easiest case to consider is $\cos(2qa) = 1$. Then, in addition to the plane waves $\beta = \pm k$, there are space-charge waves given by the solution of

$$\frac{-\dfrac{\omega_{p1}^2}{2v_{t1}^2}}{\left(\beta - \dfrac{\omega}{v_{t1}}\right)\left(\beta + \dfrac{\omega}{v_{t1}}\right)} + \frac{\dfrac{\omega_{p2}^2}{2\left(v_{o2}^2 - v_{t2}^2\right)}}{\left(\beta - \dfrac{\omega}{v_{o2} + v_{t2}}\right)\left(\beta - \dfrac{\omega}{v_{o2} - v_{t2}}\right)} = 1 \qquad (42)$$

Since this is the same equation as that obtained in Chapter III for the infinite double streams if ω_{p1}^2 and ω_{p2}^2 are replaced by $\omega_{p1}^2/2$ and

$\omega_{p2}^2/2$, we can conclude that there is a growing wave present in this periodic array having the same gain factor as the growing wave in the previous case, only at a lower frequency.

4.2. Dispersion Relations for Finite Layered Structures

Since the purpose of this report is to investigate the possible space-charge interactions that could result in useful devices, we would now like to consider two configurations which could be realized in the laboratory. Two finite layers of a semiconducting material can be placed in intimate contact if the surfaces are polished. If one of the layers must be very thin, then vacuum deposition techniques could be used. Unless special conditions were satisfied, vacuum coating would result in polycrystalline material of low mobility. This would fit well into an analysis which considers one of the streams as stationary.

The two possibilities which will be considered are:

1. Two adjacent plasma layers with metallic outer boundaries, as in Fig. 2.

2. Two adjacent plasma layers with free space at the outer boundaries, as in Fig. 3.

The configuration with metallic boundaries is useful because of the simpler equations that result. The configuration which does not have this restriction, on the other hand, is easier to build. In any case, both possibilities should be considered and the results compared.

Adjacent Plasma Layers with Metallic Outer Boundaries. Figure 2

- 50 -

x = +a   Metallic boundary

Region 1 ε_1, ω_{p1}

Region 2 ε_2, ω_{p2}

x = -b   Metallic boundary
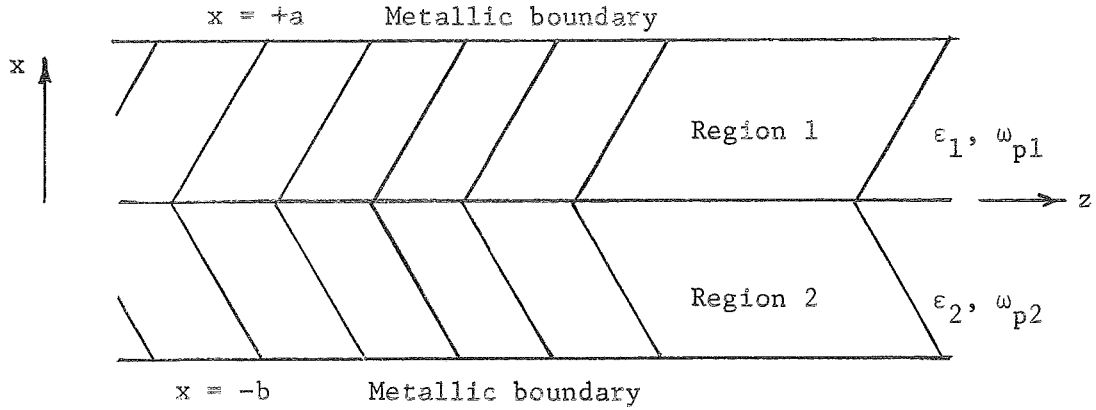
Fig. 2. Adjacent semiconducting layers with perfectly
conducting outer boundaries.

illustrates the configuration for which we will now derive the dis-
persion relation. In Section 4.1 we derived the general wave equation
for a plasma with propagation in the z direction.

$$\left(\nabla_T^2 - T^2 \right) A_z = 0 \tag{36}$$

where, in the zero temperature case

$$T^2 = \left(\beta^2 - k^2 \right) \left[1 - \frac{\omega_p^2}{\left(\omega - \beta v_o \right)^2} \right] \tag{43}$$

For the infinite layered structure of Section 4.1, we matched ampli-
tudes and derivatives across the boundary. A more general treatment
is to match longitudinal $\vec{E}$ and $\vec{H}$ fields across the boundary.

- 51 -

In terms of A_z, the electric and magnetic fields are given by

$$E_z = \frac{-j\omega}{k^2}\left(k^2 - \beta^2\right) A_z \tag{44}$$

$$E_x = \frac{\omega\beta}{k^2} \frac{\partial A_z}{\partial x} \tag{45}$$

$$H_y = -\frac{1}{\mu} \frac{\partial A_z}{\partial x} \tag{46}$$

assuming no variation in y.

The solutions for A_z tailored for boundary conditions in Regions 1 and 2, respectively, are

$$A_{z1} = B_1 \sinh T_1 (a - x)$$

$$A_{z2} = B_2 \sinh T_2 (b + x)$$

and E_z and H_y are

$$E_{z1} = \frac{-j\omega}{k_1^2}\left(k_1^2 - \beta^2\right) B_1 \sinh T_1 (a - x)$$

$$E_{z2} = \frac{-j\omega}{k_2^2}\left(k_2^2 - \beta^2\right) B_2 \sinh T_2 (b + x)$$

$$H_{y1} = +\frac{T_1}{\mu} B_1 \cosh T_1 (a - x)$$

$$H_{y2} = -\frac{T_2}{\mu} B_2 \cosh T_2 (b + x)$$

These expressions satisfy the boundary conditions at x = +a and x = -b respectively.

The boundary conditions at x = 0 are that E_z and H_y are continuous. Therefore,

$$\frac{\left(k_1^2 - \beta^2\right)}{k_1^2} B_1 \sinh\left(T_1 a\right) = \frac{\left(k_2^2 - \beta^2\right)}{k_2^2} B_2 \sinh\left(T_2 b\right)$$

$$T_1 B_1 \cosh\left(T_1 a\right) = - T_2 B_2 \cosh\left(T_2 b\right)$$

The determinantal equation obtained by combining these two equations is

$$\frac{\left(k_1^2 - \beta^2\right)}{k_1^2 T_1} \tanh\left(T_1 a\right) = - \frac{\left(k_2^2 - \beta^2\right)}{k_2^2 T_2} \tanh\left(T_2 b\right) \tag{47}$$

Equation 47 is the general dispersion relation which will determine the regions where gain exists and what material properties are required. Before looking at this equation in more detail, however, let us derive a similar expression for the case without metallic boundaries, as illustrated in Fig. 3.

Adjacent Plasma Layers with Free Space at the Outer Boundaries.
Consider the case of two finite layers in free space or on an insulating
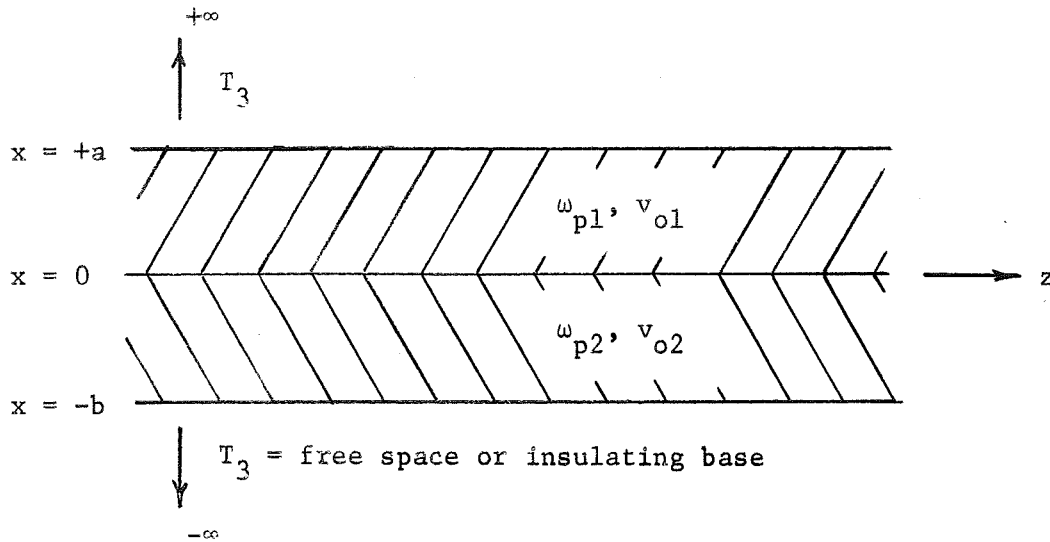
Fig. 3. Two finite solid-state plasma layers in free space.

base as shown in Fig. 3. The general form of the solutions will be given as

$$A_{z1} = A e^{T_1 x} + B e^{-T_1 x}$$

$$A_{z2} = C e^{T_2 x} + D e^{-T_2 x}$$

$$A_{z+} = E e^{-T_3 x}$$

(48)

$$A_{z-} = F e^{T_3 x}$$

Using Eqs. 44 and 46, we can write the E_z and H_y fields as follows:

$$E_{z1} = -\frac{j\omega}{k_1^2}\left(k_1^2 - \beta^2\right)\left(A\,e^{T_1 x} + B\,e^{-T_1 x}\right)$$

$$E_{z2} = -\frac{j\omega}{k_2^2}\left(k_2^2 - \beta^2\right)\left(C\,e^{T_2 x} + D\,e^{-T_2 x}\right)$$

$$E_{z+} = -\frac{j\omega}{k^2}\left(k^2 - \beta^2\right)E\,e^{-T_3 x}$$

$$E_{z-} = -\frac{j\omega}{k^2}\left(k^2 - \beta^2\right)F\,e^{T_3 x}$$

$$(49)$$

$$H_{y1} = -\frac{1}{\mu}\left(A\,T_1\,e^{T_1 x} - B\,T_1\,e^{-T_1 x}\right)$$

$$H_{y2} = -\frac{1}{\mu}\left(C\,T_2\,e^{T_2 x} - D\,T_2\,e^{-T_2 x}\right)$$

$$H_{y+} = +\frac{1}{\mu}\,E\,T_3\,e^{-T_3 x}$$

$$H_{y-} = -\frac{1}{\mu}\,F\,T_3\,e^{T_3 x}$$

We now match boundary conditions on E_z and H_y at $x = 0$, $x = a$, and $x = -b$ to get the six equations following.

At $x = 0$,

$$\frac{k_1^2 - \beta^2}{k_1^2} (A + B) = \frac{k_2^2 - \beta^2}{k_2^2} (C + D)$$

$$T_1 (A - B) = T_2 (C - D)$$

at x = a,

$$\frac{k_1^2 - \beta^2}{k_1^2} \left(A e^{T_1 a} + B e^{-T_1 a} \right) = \frac{k^2 - \beta^2}{k^2} E e^{-T_3 a}$$

$$T_1 \left(A e^{T_1 a} - B e^{-T_1 a} \right) = -E T_3 e^{-T_3 a}$$

(50)

at x = -b,

$$\frac{k_2^2 - \beta^2}{k_2^2} \left(C e^{-T_2 b} + D e^{T_2 b} \right) = \frac{k^2 - \beta^2}{k^2} F e^{-T_3 b}$$

$$T_2 \left(C e^{-T_2 b} - D e^{T_2 b} \right) = F T_3 e^{-T_3 b}$$

Following the same procedure as in the previous subsection, we can now write Eqs. 50 as a determinant of coefficients and equate to zero. First, simplify the notation by defining

$$n_i = \frac{k_i^2 - \beta^2}{k_i^2} \tag{51}$$

Then the determinant of coefficients is given as

$$
\begin{vmatrix}
n_1 & n_1 & -n_2 & -n_2 & 0 & 0 \\
n_1 e^{T_1 a} & n_1 e^{-T_1 a} & 0 & 0 & -n\, e^{-T_3 a} & 0 \\
0 & 0 & n_2 e^{-T_2 b} & n_2 e^{T_2 b} & 0 & -n\, e^{-T_3 b} \\
T_1 & -T_1 & -T_2 & +T_2 & 0 & 0 \\
T_1 e^{T_1 a} & -T_1 e^{-T_1 a} & 0 & 0 & T_3 e^{-T_3 a} & 0 \\
0 & 0 & T_2 e^{-T_2 b} & -T_2 e^{T_2 b} & 0 & -T_3 e^{-T_3 b}
\end{vmatrix} = 0
$$

When this determinant is expanded and simplified, we arrive at the dispersion relation for the configuration of Fig. 3.

$$\left(\frac{nT_2}{n_2T_3} + \frac{n_2T_3}{nT_2}\right)\tanh\left(T_2b\right) + \left(\frac{nT_1}{n_1T_3} + \frac{n_1T_3}{nT_1}\right)\tanh\left(T_1a\right) +$$

$$\text{(52)}$$

$$+\left(\frac{n_1T_2}{n_2T_1} + \frac{n_2T_1}{n_1T_2}\right)\tanh\left(T_1a\right)\tanh\left(T_2b\right) + 2 = 0$$

Equation 52 for free space at the outer boundary is equivalent to Eq. 47 for the metallic boundary. It is now easy to see why the metal boundaries were included as a way to simplify the dispersion relation.

Other configurations of three or four layers could similarly be analyzed. However, the two-layer structure includes all of the significant characteristics so there would be no particular purpose in looking at the ever more complicated expressions.

4.3. Properties of the tanh(z) and tanh(z)/(z) Functions

Both Eqs. 47 and 52 contain tanh(z) functions in various combinations. In this section, we will consider a simplified form of Eq. 47 and show what conditions are required of the tanh(z)/z function, and consequently of the semiconducting materials, to result in complex β or ω.

Once again, we make some approximations to make the analysis more manageable. If Region 2 is assumed to be a thick layer, then

$$\tanh\left(T_2b\right) \simeq 1$$

In addition, we assume that $k_1^2 = k_2^2$ and that $\beta^2 >> k_1^2$. The assumption that β^2 is large is known as the slow-wave approximation. It means that the beam is much slower than the speed of light in the material and that the space-charge waves are propagating at near the beam velocity. Calculations done on a digital computer, which will be discussed in the next section, show that these approximations give quite accurate results. With these approximations, we now rewrite Eq. 47 as

$$\frac{\tanh\left(T_1 a\right)}{\left(T_1 a\right)} = -\frac{1}{T_2 a} \tag{53}$$

The important observation to make from Eq. 53 is that in order to have solutions, $\tanh\left(T_1 a\right)/\left(T_1 a\right)$ will have to be the negative of $1/\left(T_2 a\right)$. The key to the problem is to find regions of $\tanh(z)/z$ where sign changes are possible. With this in mind, the $\tanh(z)/z$ function was plotted on the computer with the results as shown in Fig. 4. Only the first quadrant needs to be plotted because the magnitudes and signs of the $\tanh(z)/z$ function are related as follows:

$$\frac{\tanh(\pm z)}{\pm z} = x + jy$$

$$\frac{\tanh(\pm z^*)}{\pm z^*} = x - jy$$

where z^* means the complex conjugate of z.

- 59 -

Figure 4 shows that there are periodic regions of sign changes in Re(tanh(z)/z) for values of Re(z) less than Im(z). This is an important observation because

$$T_1 = \sqrt{\left(\beta^2 - k_1^2\right)\left(1 - \frac{\omega_{p1}^2}{\omega^2}\right)}$$

and in the slow-wave approximation

$$T_1 = \beta\sqrt{1 - \frac{\omega_{p1}^2}{\omega^2}} \tag{54}$$

where $\beta = \beta_r + j\beta_i$.

Reasonable gain values are on the order of 1 percent to 10 percent per wavelength, so that β_i should be considerably smaller than β_r. Then if $\omega_{p1}^2 \leq \omega^2$, it would never be possible to get the necessary sign changes, and growing wave solutions would not exist. In Chapter III, we concluded that $\omega_{p1} > \omega$ would give gain in the infinite plasma. This turns out to be exactly the condition that must be satisfied in this case also. If, for example, $\omega_{p1}^2 >> \omega^2$ then

$$T_1 = \beta j \frac{\omega_p}{\omega}$$

and $\tag{55}$

$$T_1 a = -\beta_i \frac{\omega_p}{\omega} a + j\left(\beta_r \frac{\omega_p}{\omega} a\right)$$
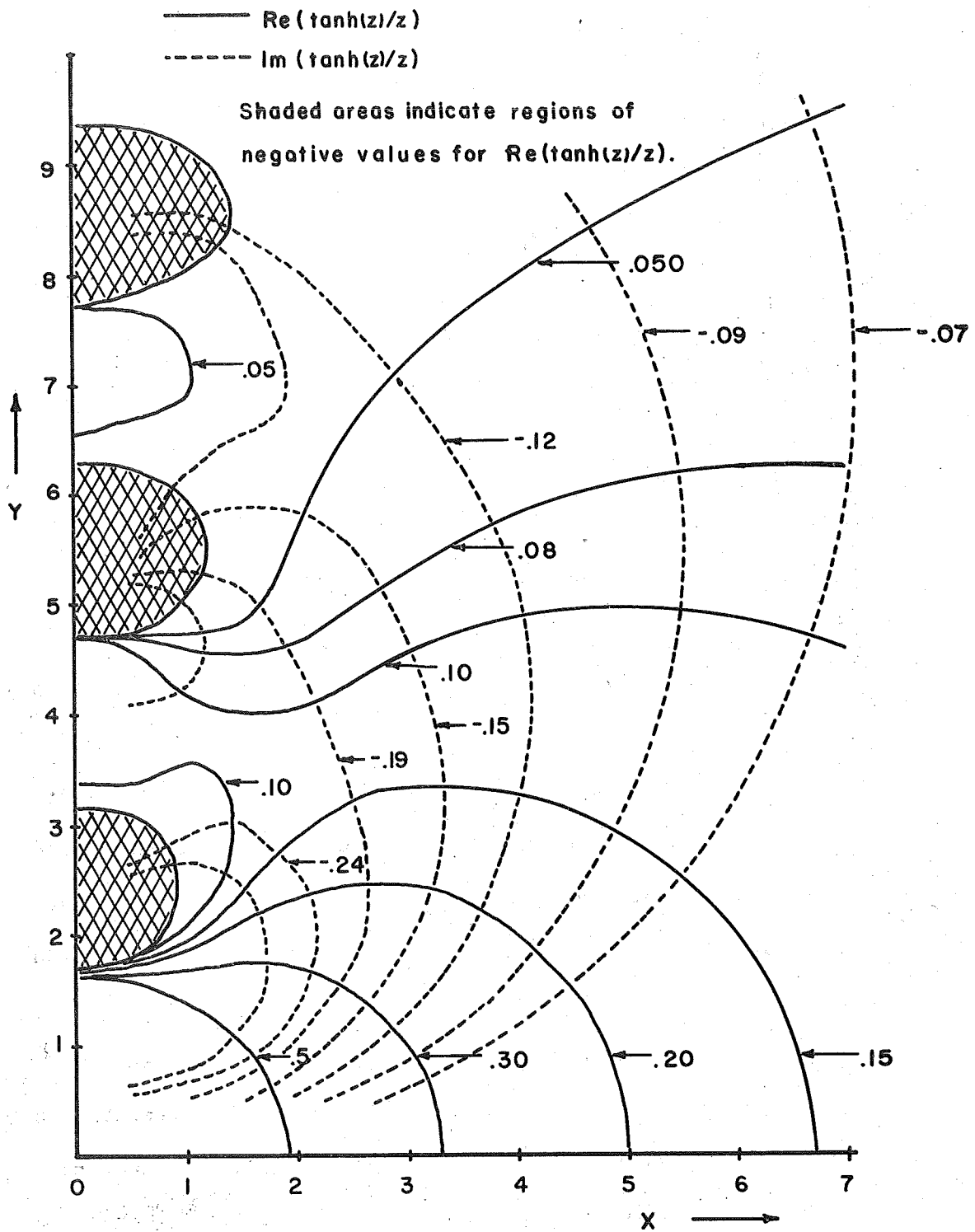
Fig. 4. Numerical plot of the tanh(z̄)/z function, where z = x + jy.

Define λ such that

$$\beta_r = \frac{2\pi}{\lambda}$$

From Fig. 4 and Eq. 55, we can now see that solutions will be possible in the ranges of

$$\frac{2\pi}{\lambda} \frac{\omega_{p1}}{\omega} a = \frac{\pi}{2} \to \pi, \frac{3}{2}\pi \to 2\pi, \frac{5}{2}\pi \to 3\pi, \text{ etc.} \qquad (56)$$

or solving Eq. 56 for "a" (the thickness of Region 1)

$$a = \frac{\omega}{\omega_{p1}} \lambda \left[1/4 \to 1/2, \ 3/4 \to 1, \ 5/4 \to 3/2, \ . \ . \ . \right] \qquad (57)$$

One immediate observation that can be made from Eq. 57 is that as ω_{p1} gets larger, "a" will have to be correspondingly smaller to result in gain. Furthermore, all the dispersion relations will now have to be investigated for the thickness "a" before gain vs. frequency can be plotted.

The type of analysis that has been presented in this section results only in some very broad conclusions as to the requirements necessary to get growing waves. However, the more specific computer results are also more difficult to obtain and not nearly as easy to interpret.

4.4   Computer Investigation of the Metal Boundary Configuration

Equation 47 was programmed, without making any approximations,

on a digital computer, and results have been obtained for both complex β as a function of the thickness a, and ω vs. β for a particular thickness. To make the problem manageable, only "a" was varied and "b" was taken to be a large value as proposed in Section 4.3. Figure 5 shows the results of β vs. a. The shaded areas indicate the previously predicted gain regions. As can be seen, Re(β) always lies within these areas. The numerical values chosen are

$$\omega = 1.88 \times 10^{12} = 2\pi (300 \text{ GHz})$$

$$\omega_{p1} = 9.5 \times 10^{12}$$

$$\omega_{p2} = 1.5 \times 10^{12}$$

$$v_2 = 3 \times 10^5 \text{ m/s}$$

The choice of these values may seem rather arbitrary at this time, but they are based on reasonable semiconductor properties that will be discussed in detail in subsequent chapters. The prime consideration here is to see what relative effect each factor has on the overall dispersion relation.

Throughout this report ω-β diagrams will be used as the indicators of what effects temperature, collisions, etc. have on the gain. The general method would be to always show the entire ω-β plane for the interaction. However, since we are interested in frequencies greater than zero and in the conditions that result in gain, it is appropriate to consider only a portion of the first quadrant. To clarify this statement, a general ω-β diagram for the double-stream interaction is illus-

$\omega = 1.88 \times 10^{12}$

$\omega_{p1} = 9.5 \times 10^{12}$

$\omega_{p2} = 1.5 \times 10^{12}$

$v_2 = 3. \times 10^5$ m/s

$\varepsilon_1 = \varepsilon_2 = 16.0$

Shaded areas indicate possible regions of β_{real} where growing waves can exist.

—— $= \beta_{real}$

--x-- $= \beta_{imag.}$

$\times 10^5$ for β_{im}

$\times 10^6$ for β_r

10.

β_e

5.

$\times 10^{-6}$ m

a

Fig. 5. Complex β as a function of the thickness of Region 1 for the two-layer structure with metallic boundaries.

trated in Fig. 6. If the two plasmas are taken separately, we get

plasma waves of frequencies $\pm\omega_{p1}$ and $\pm\omega_{p2}$ "propagating" at the drift

velocity (shown by the dotted lines in Fig. 6). When the streams are

intermixed, the waves are all coupled together; and while we still get

four propagating waves, they are quite different from the individual

plasma waves. The fast waves of streams 1 and 2 couple to produce an

evanescent wave as do the slow waves of streams 1 and 2. For $\omega > 0$,

the slow wave of the fast beam couples to the fast wave of the slow

beam in such a way that complex β results. This is the portion of the

diagram where $\text{Re}(\beta)$ vs. ω is essentially a straight line. Equation 24,

for $\omega_{p1} > \omega$, gives the mathematical expression (for the infinite case)

for this portion of the curve. Because this is the region where the

significant gain is found, it will be the region that is plotted in all

the computer work. The curves will always be plotted from the origin

at $\omega = 0$, $\beta = 0$ and terminated when $\text{Im}(\beta)$ shows that significant gain

no longer exists.

Figure 7 compares the computer results for the two-layer struc-

ture with metal boundaries to the infinite case of Section 3.4. The

general propagation and gain characteristics are obviously similar. The

gain for the layered structure terminates sooner due to the additional

effect of the thickness "a."

In Section 3.5, we discussed the necessary requirements to show

that a growing wave exists. Figure 7 shows that the basic interaction

is still the same. However, it is interesting to verify this by repeat-

ing the calculations for complex ω and real β instead of complex β and
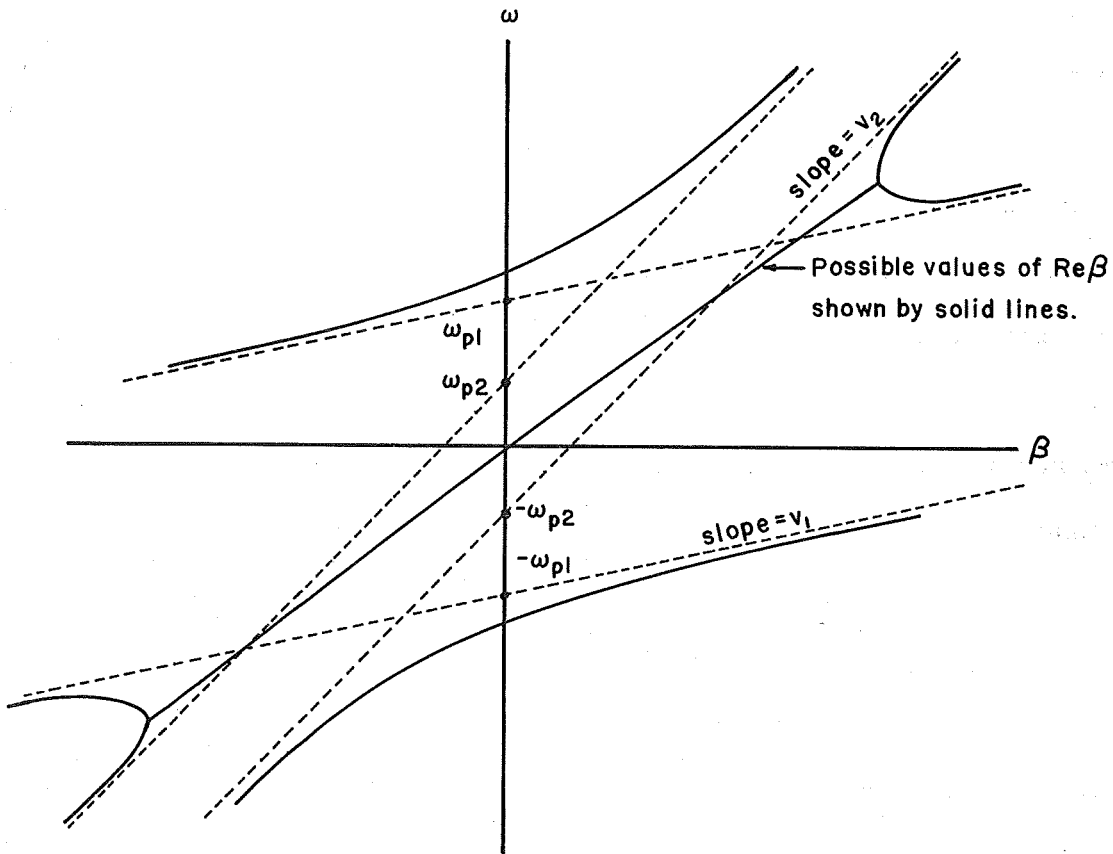
Fig. 6.   General ω-β diagram for the double-stream
          interaction with streams in the same direction.
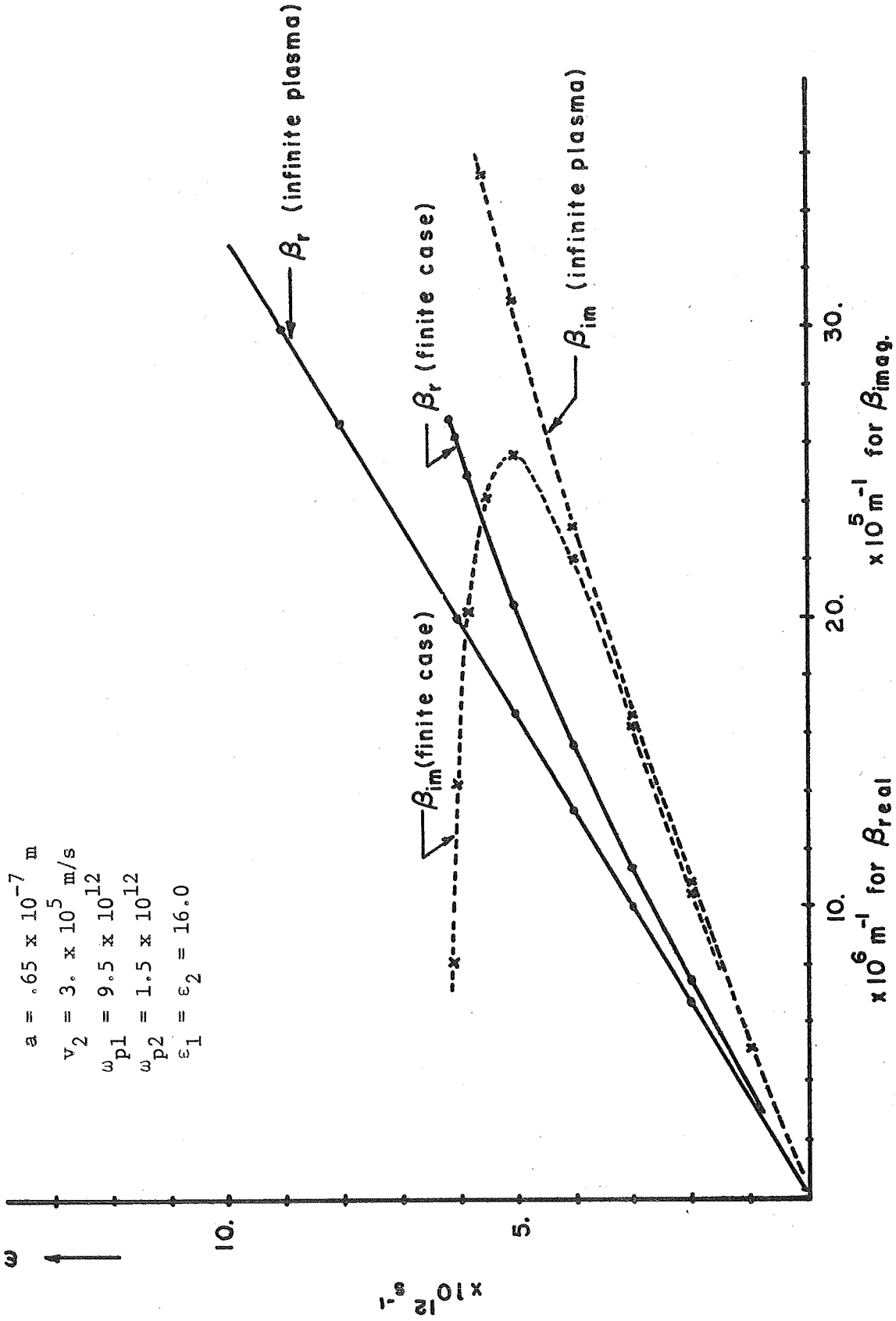
Fig. 7. $\omega-\beta$ diagram comparing the layered structure with metallic boundaries to an infinite plasma.

$a = .65 \times 10^{-7}$ m

$v_2 = 3. \times 10^{5}$ m/s

$\omega_{p1} = 9.5 \times 10^{12}$

$\omega_{p2} = 1.5 \times 10^{12}$

$\varepsilon_1 = \varepsilon_2 = 16.0$

β_r (infinite plasma)

β_r (finite case)

β_{im} (infinite plasma)

β_{im} (finite case)

$x10^6$ m^{-1} for β_{real}

$x10^5$ m $^{-1}$ for $\beta_{imag.}$

10.

20.

30.

5.

10.

ω

$x10^{12}$ s^{-1}

real ω. Since there is no particular difficulty in identifying the interacting waves for this case, solutions with $Im(\omega) < 0$ will prove the existence of a convective instability. Figures 8 and 9 show the results for the metal boundary configuration solved in terms of complex ω. Figure 8 shows a few of the gain regions as a function of the thickness "a" and Fig. 9 is the $\omega-\beta$ diagram that compares to Fig. 7 for complex β and real ω. There should be no further questions regarding the validity of the basic interaction mechanism for either the infinite plasma or discrete finite layered structures.

4.5. Computer Results for a Layered Structure with Free Space at the Outer Boundaries

The results for this configuration are obtained by solving Eq. 52 on the digital computer. Figures 10 and 11 give the results for complex β and real ω that correspond to Figs. 5 and 7 for the metal boundary configuration. The basic similarity of the results is to be expected and is obviously verified. Once again, we get regions of gain for $Re(\beta)$ as a function of the thickness "a." The regions of gain are exactly where the "forbidden regions" were for the metal boundary case. Physically, this can be interpreted as an interference effect, similar to a thin dielectric film in optics. In that case, we also get alternate bands of $\lambda/4$ for reflection and absorption, and the bands are determined by the reflection properties of the material behind the film.

A somewhat arbitrary choice was initially made for ω_{p2}, since its effect on the interaction is a little harder to predict. Figure 12 shows that the choice of ω_{p2} is not critical as long as it is suffi-

$$\beta = 6.27 \times 10^6 \ \text{m}^{-1}$$
$$v_2 = 3. \times 10^5 \ \text{m/s}$$
$$\omega_{p1} = 9.5 \times 10^{12}$$
$$\omega_{p2} = 1.5 \times 10^{12}$$
$$\varepsilon_1 = \varepsilon_2 = 16.0$$

Only some of the possible solutions for ω are shown.

ω_{real}

ω_{im}

$\beta_e v_2$

ω_{im}

ω_{real}

$d \quad \times 10^{-6} \ \text{m}$

$\times 10^{12} = \omega_{real}$

$\times 10^{11} = -\omega_{im}$
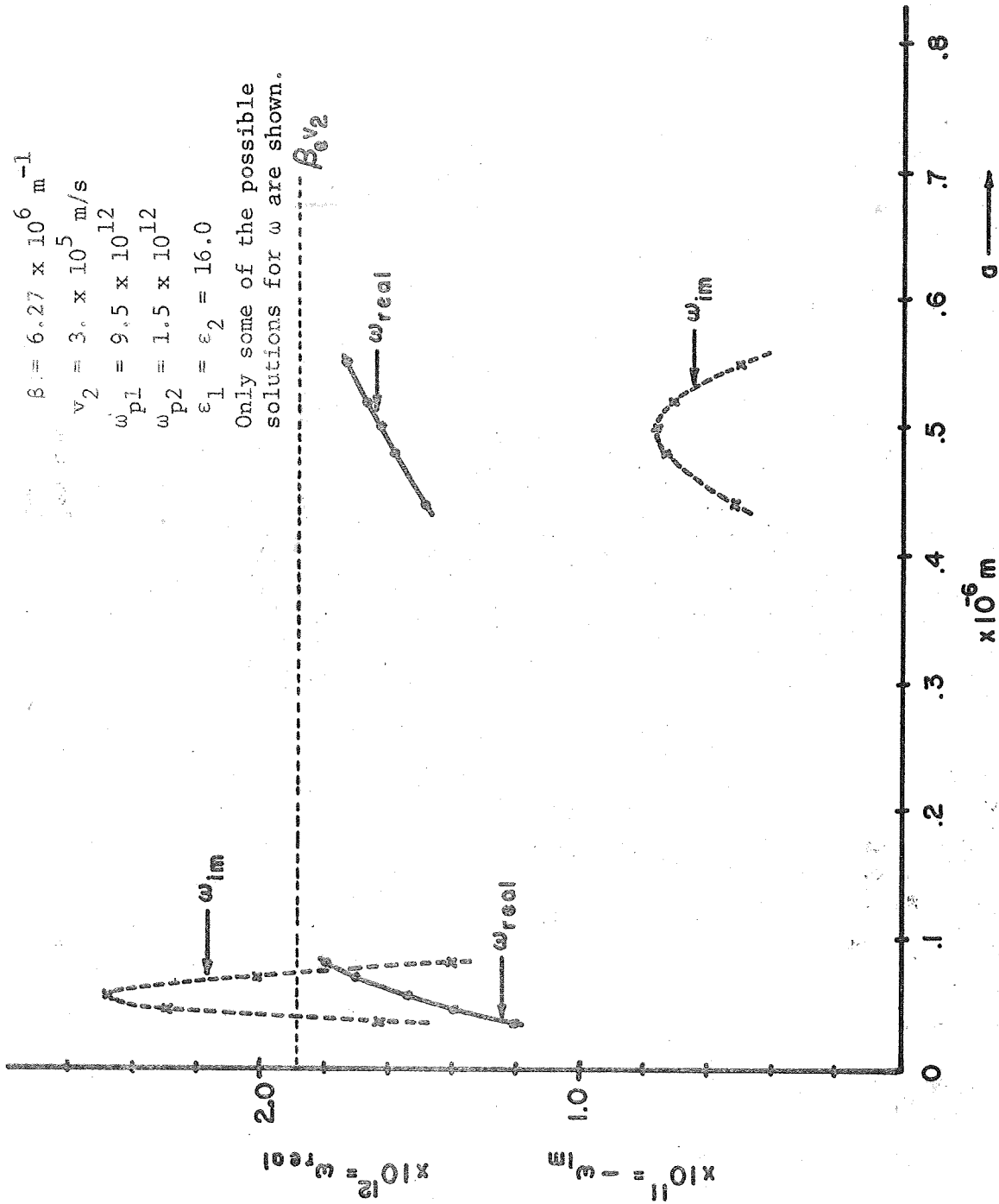
Fig. 8. Complex ω as a function of the thickness of Region 1, for the layered structure with metallic boundaries.

Fig. 9. ω-β diagram for ω complex and β real for the layered structure with metallic boundaries.

$a = .7 \times 10^{-7}$ m

$v_2 = 3. \times 10^5$ m/s

$\omega_{p1} = 9.5 \times 10^{12}$

$\omega_{p2} = 1.5 \times 10^{12}$

$\varepsilon_1 = \varepsilon_2 = 16.0$

Fig. 10. Complex β as a function of the thickness of Region 1 for the two-layer structure.

$\omega = 1.88 \times 10^{12}$
$\omega_{p1} = 9.5 \times 10^{12}$
$\omega_{p2} = 1.5 \times 10^{12}$
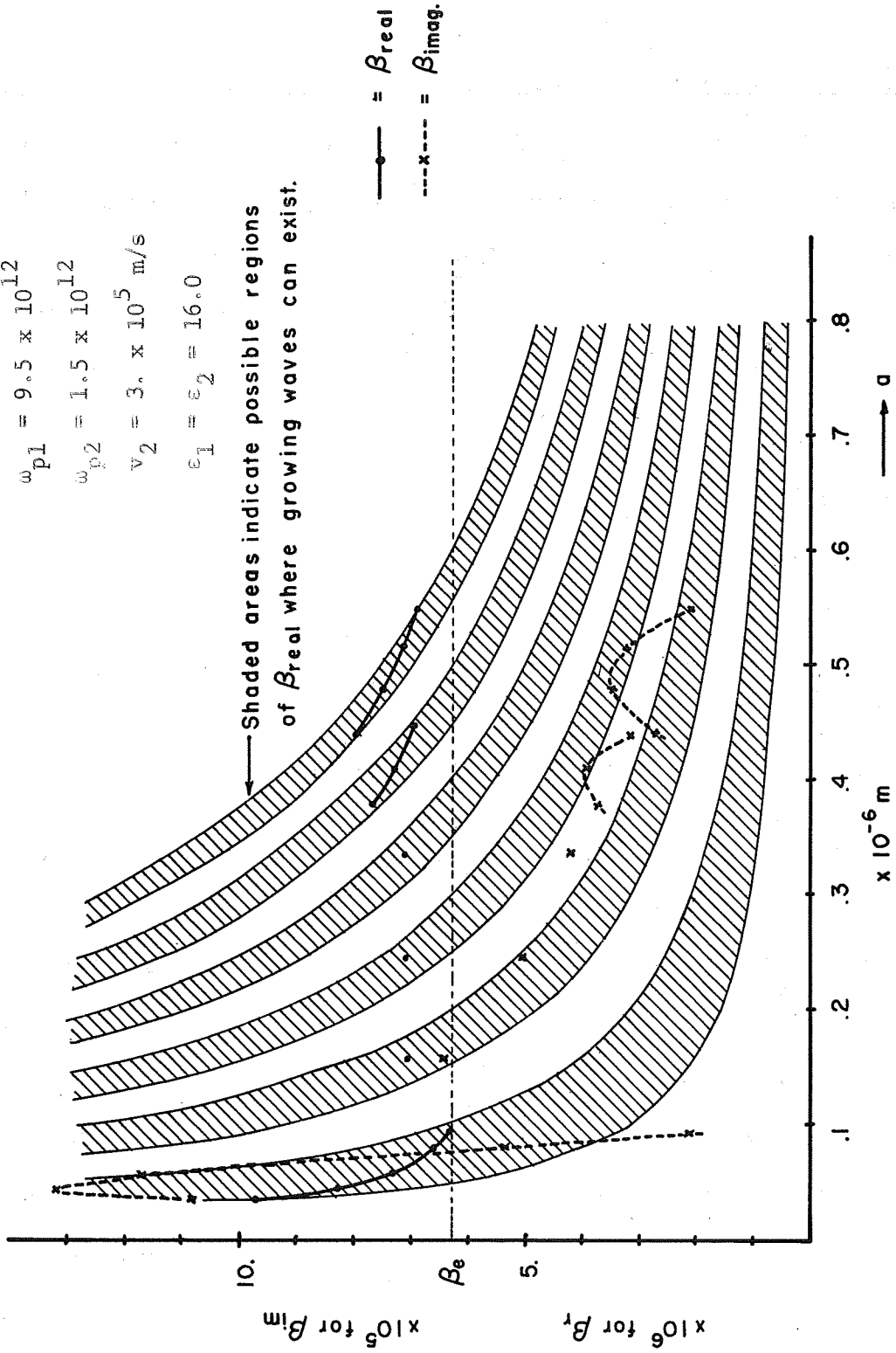$v_2 = 3. \times 10^5$ m/s
$\varepsilon_1 = \varepsilon_2 = 16.0$

$\underline{\quad\bullet\quad} = \beta_{real}$
$\text{---x---} = \beta_{imag.}$

Unshaded areas indicate possible regions of β_{real} where growing waves can exist.

$a = 1.1 \times 10^{-7}$ m

$\omega_{p1} = 9.5 \times 10^{12}$

$\omega_{p2} = 1.5 \times 10^{12}$

$v_2 = 3. \times 10^5$ m/s

$\epsilon_1 = \epsilon_2 = 16.0$

ω_{p1}

β_{real}

β_{im}

ω_{p2}

ω

$\times 10^{12}$

10.

5.

1.

$\times 10^6$ for β_{real}

$\times 10^5$ for β_{im}

10.

20.

30.
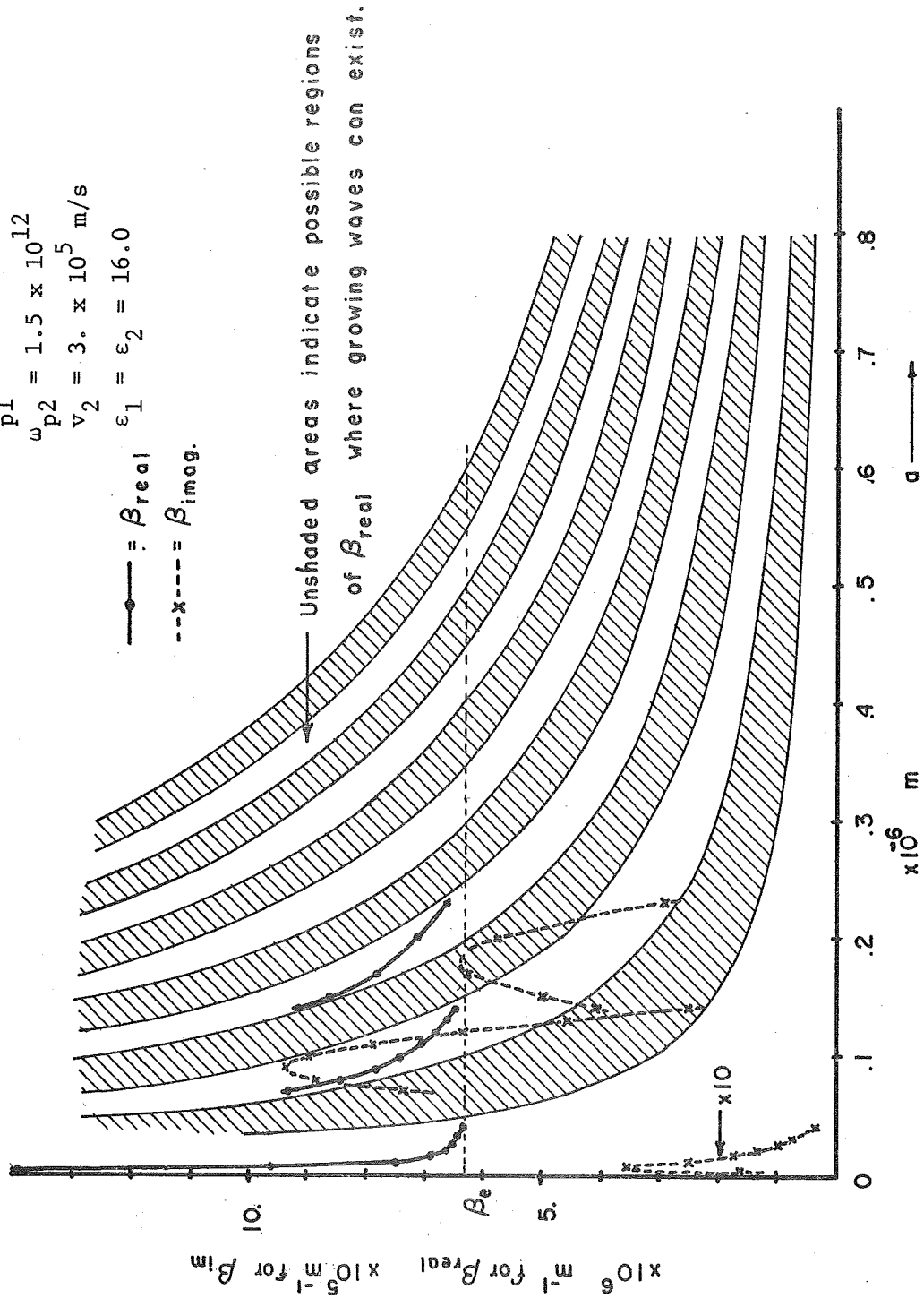
Fig. 11. ω–β diagram for the two-layer structure with free space at the outer boundaries.

$a = 1.1 \times 10^{-7}$ m

$\omega = 2. \times 10^{12}$

$\omega_{p1} = 9.5 \times 10^{12}$

$v_2 = 3. \times 10^5$ m/s

$\varepsilon_1 = \varepsilon_2 = 16.0$

β_{im}

β_{real}

ω_{p2} of previous programs.

ω_{p2}

$\times 10^{12}$

$\times 10^6$ for β_{real} $\times 10^5$ for β_{im}
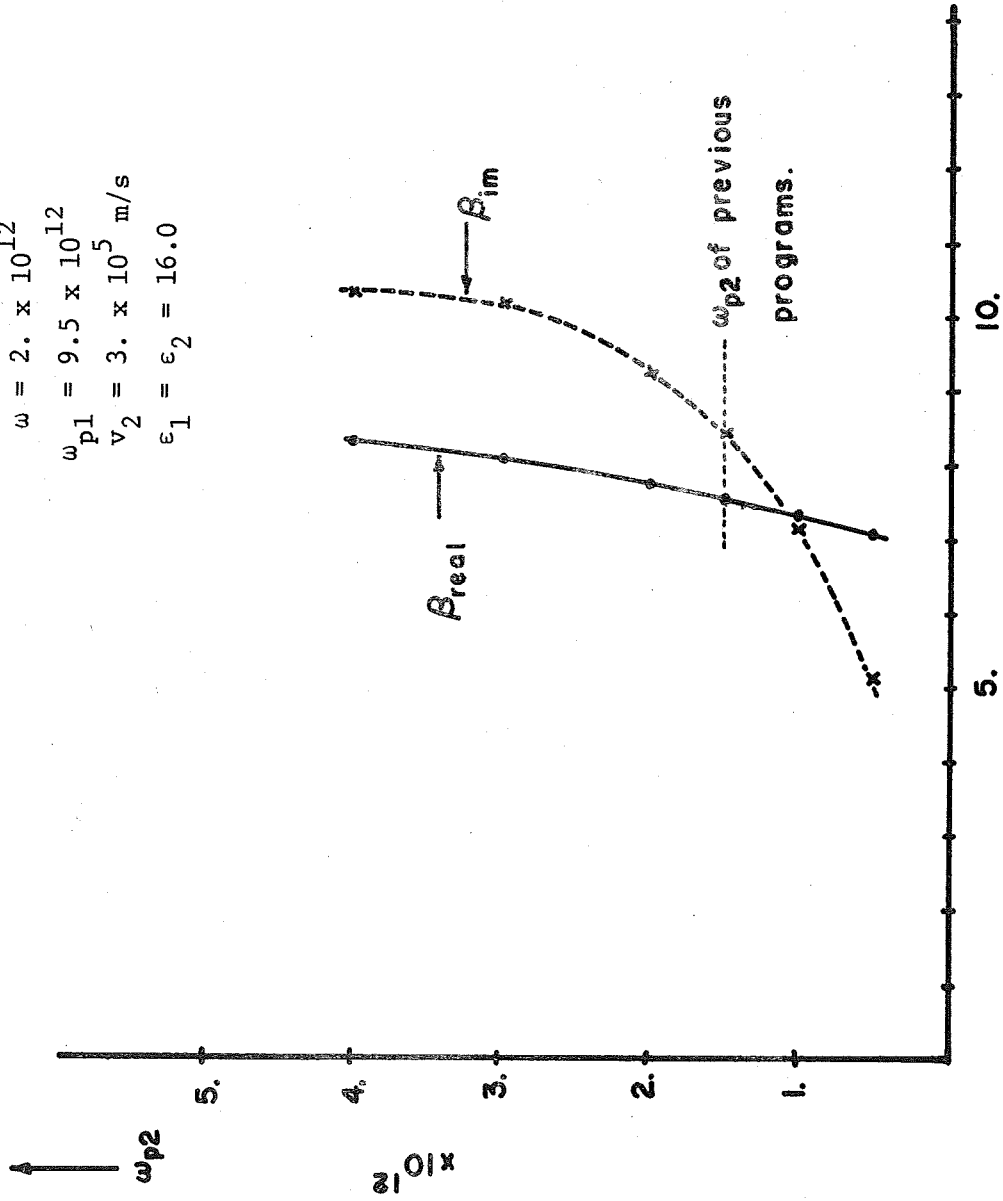
Fig. 12. Complex β as a function of ω_{p2} for the two-layer structure.

ciently large. If $\omega_{p2} \geq \omega$, then the gain will be near the optimum value.

4.6. Summary of Chapter IV

This chapter presented a detailed analysis of layered structures where the plasma streams are not intermixed but flow in adjacent materials. To investigate the basic interaction mechanism, temperature effects and particle collisions were neglected, and space-charge bunching was assumed to be in the direction of the dc drift. The dispersion relations were derived for a configuration with metallic outer boundaries and a configuration with free space at the outer boundaries. Useful gain regions were found in both cases and the results were presented in terms of ω-β diagrams. The basic interaction mechanism has now been verified and numerical results obtained for a practical case. The next chapter will consider the limitations of the present model and what changes are necessary to arrive at a theory that is suitable for predicting experimental results.

V. THE EFFECTS OF TEMPERATURE AND PARTICLE COLLISIONS

The previous chapters concentrated on showing that the space-charge interaction appears very promising in a solid under some idealized (but unachievable) conditions. With this chapter we begin the discussion of how to theoretically analyze solid-state plasmas that would be found in the laboratory. In any type of plasma, it is usually important to include the randomizing effects of temperature and particle collisions. In solids, we shall see that this turns out to be a particularly serious problem.

As is usually the case, more accurate models also become more complicated, and a variety of approximate techniques become possible and necessary. This case is no exception. The theory for nonequilibrium temperature and collision effects in solids is not well developed. Even if the theory were available, it would in all probability be hopelessly difficult to use.

In the following sections, the thermal and collision effects will be considered in some detail. Several approximate techniques have been investigated and will be compared. A simple computer technique for obtaining reasonably good results will be discussed. A simple model for particle collisions will then be analyzed and both the thermal and collision effects will be included in a physically realizable model.

5.1. Analyzing Temperature Kinetics

Two techniques are standard in plasma physics for including thermal effects. The Boltzmann equation is used for all problems where

the slope of the velocity distribution is important. When approximate

results are desired, however, often the hydrodynamic equation is used

to include temperature effects. This equation was utilized in the deriva-

tion presented in Chapter III (Eqs. 15 to 21). In this report, we will

use a somewhat different technique, in addition to the hydrodynamic

model, which is particularly suitable for analysis of streaming charge

carriers. This technique assumes a superposition of velocity streams

which in the limit can be taken as an integral over a distribution func-

tion.[1]

First, let us derive the new dispersion relation using the super-

position technique and then compare this to the Boltzmann equation re-

sult and the hydrodynamic model. We will begin by considering a super-

position of an infinite number of electron streams having velocities

corresponding to some velocity distribution $f(v)$.

If, for one of the electron streams, we let v_{oi} be the velocity

including the thermal velocity and v_i be the ac small signal velocity

and assume there are velocities in the z direction only,

$$J_i = \rho_{oi} v_i + \rho_i v_{oi}$$
(58)

By using the previously assumed periodic time variation and

the continuity equation for ρ and J,

---

[1] C. C. Johnson, *Field and Wave Electrodynamics*, New York, McGraw-Hill, 1965, p. 379.

$$-j\beta\, J_i = -j\omega\, \rho_i$$

$$J_i = \rho_{oi}\, v_i + v_{oi}\, \frac{\beta}{\omega}\, J_i$$

$$J_i = \frac{\rho_{oi}\, v_i}{1 - v_{oi}\, \beta/\omega} \qquad (59)$$

And, from the force equation

$$j\left(\omega - \beta v_{oi}\right) v_i = \eta_i\, E_z$$

$$\qquad (60)$$

$$v_i = \frac{\eta_i\, E_z}{j\left(\omega - \beta v_{oi}\right)}$$

Therefore,

$$J_i = \frac{\rho_{oi}\, \eta_i\, \omega\, E_z}{j\left(\omega - \beta v_{oi}\right)^2} \qquad (61)$$

The total current density will be a superposition of these currents.

$$J = \sum_i J_i \qquad (62)$$

Define the particle density as $n_{oi} = \dfrac{\rho_{oi}}{e}$ and then

$$\eta_i \rho_{oi} = \frac{n_{oi} e^2}{m} = \frac{n_o e^2}{m} f\left(v_{oi}\right) \Delta v_{oi} \tag{63}$$

$$J = -\sum_i \frac{j\omega n_o e^2}{m} \frac{f\left(v_{oi}\right) \Delta v_{oi}}{\left(\omega - \beta v_{oi}\right)^2} E_z$$

In the limit, J can be expressed as an integral

$$J = -\frac{j\omega n_o e^2}{m} E_z \int_{-\infty}^{\infty} \frac{f\left(v_o\right) dv_o}{\left(\omega - \beta v_o\right)^2}$$

Using the previous definition of the plasma frequency,

$$J = -j\omega\varepsilon \, E_z \, \omega_{po}^2 \int_{-\infty}^{\infty} \frac{f\left(v_o\right) dv_o}{\left(\omega - \beta v_o\right)^2} \tag{64}$$

This is now in a form that can be used in the wave equation for the vector potential, as derived in Section 4.1.

$$\left(\nabla_T^2 + k^2 - \beta^2\right) A_z = -\mu J_z$$

$$= j\omega\mu\varepsilon \, \omega_{po}^2 \int_{-\infty}^{\infty} \frac{f\left(v_o\right) dv_o}{\left(\omega - \beta v_o\right)^2} E_z \tag{65}$$

But,

$$E_z = \frac{j\left(\beta^2 - k^2\right)}{\omega\mu\epsilon} A_z$$

so that

$$\left(\nabla_T^2 + k^2 - \beta^2\right)A_z = -\left(\beta^2 - k^2\right)\omega_{po}^2 \int_{-\infty}^{\infty} \frac{f\left(v_o\right)dv_o}{\left(\omega - \beta v_o\right)^2} A_z$$

This can now be written in the familiar form of Eq. 34

$$\left\{\nabla_T^2 - \left(\beta^2 - k^2\right)\left[1 - \omega_{po}^2 \int_{-\infty}^{\infty} \frac{f\left(v_o\right)dv_o}{\left(\omega - \beta v_o\right)^2}\right]\right\} A_z = 0 \qquad (66)$$

As in Eq. 35, we define a "T" such that

$$\left(\nabla_T^2 - T^2\right) A_z = 0 \qquad (67)$$

Then we have a new definition for the T's given by

$$T^2 = \left(\beta^2 - k^2\right)\left[1 - \omega_{po}^2 \int_{-\infty}^{\infty} \frac{f\left(v_o\right)dv_o}{\left(\omega - \beta v_o\right)^2}\right] \qquad (68)$$

This expression for T is valid for any one-dimensional distribution function that we wish to use. Its usefulness is limited only by

the difficulties usually encountered in evaluating the integral.

Now, as promised earlier, let us compare this result to a derivation from the Boltzmann equation. Neglecting collision effects and assuming a one-dimensional analysis, the Boltzmann equation is given as[2]

$$\frac{\partial f}{\partial t} - \frac{|e|}{m} E \cdot \frac{\partial f}{\partial v} + v \frac{\partial f}{\partial z} = 0$$

Assume that f can be written as an equilibrium term plus a small perturbation due to the interaction.

$$f = n_o f_o(v) + f_1(v,z,t) \tag{69}$$

The $f_o(v)$ term in Eq. 69 has been normalized to correspond to the $f_o(v)$ of Eq. 63. Then, neglecting second-order terms, the Boltzmann equation becomes

$$\frac{\partial f_1}{\partial t} - \frac{\partial f_o}{\partial v} E \frac{|e|n_o}{m} + v \frac{\partial f_1}{\partial z} = 0 \tag{70}$$

Equation 70 can be simplified further if f_1 is assumed to have the usual plane wave dependence $e^{j(\omega t - \beta z)}$

$$j(\omega - \beta v) f_1 = \frac{|e|n_o}{m} E \frac{\partial f_o}{\partial v}$$

---

[2] M. A. Uman, *Introduction to Plasma Physics*, New York, McGraw-Hill, 1964, p. 34.

and

$$f_1 = \frac{\dfrac{|e|n_o}{m} E \dfrac{\partial f_o}{\partial v}}{j(\omega - \beta v)} \qquad (71)$$

The charge density ρ is defined in terms of f_1 as

$$\rho = q \int f_1 dv$$

Since f_1 has been written in terms of the E field, we can write ρ the same way

$$\nabla \cdot \vec{E} = \frac{\rho}{\varepsilon}$$

and for one dimension

$$\frac{\partial E}{\partial z} = \frac{\rho}{\varepsilon}$$

or simply

$$-j\beta E = \frac{\rho}{\varepsilon} = \frac{-|e|}{\varepsilon} \int f_1 dv$$

Substituting for f_1 from Eq. 71 and using the previous definition for plasma frequency ω_p gives

$$1 = \frac{-\omega_p^2}{\beta} \int_{-\infty}^{\infty} \frac{\dfrac{\partial f_o}{\partial v}}{(\omega - \beta v)} dv \qquad (72)$$

- 81 -

Equation 72 is the one-dimensional dispersion relation for an infinite plasma derived from the Boltzmann equation approach. The comparable equation by the superposition technique is obtained by setting $\nabla_T = 0$ in Eq. 67. Then it follows that $T^2 = 0$ and

$$1 = \omega_{po}^2 \int_{-\infty}^{\infty} \frac{f(v_o) dv_o}{(\omega - \beta v_o)^2} \tag{73}$$

The integrals of Eqs. 72 and 73 contain a denominator term which can be equal to zero for ω and β real. If the equality occurs in a region where $f(v_o) \neq 0$, then the integrals do not exist. This difficulty can be avoided simply by specifying that β will always be complex for acceptable solutions. Physically, this means that there will be either gain or loss for all cases of interest. All the subsequent numerical calculations will be done for the gain region. With this restriction, Eq. 73 can be shown to be the same as Eq. 72 if we integrate Eq. 73 by parts.

$$\int_{-\infty}^{\infty} \frac{f(v_o) dv_o}{(\omega - \beta v_o)^2} = f(v_o) \frac{1}{\beta(\omega - \beta v_o)} \Bigg|_{-\infty}^{\infty} - \int_{-\infty}^{\infty} \frac{dv_o}{\beta(\omega - \beta v_o)} \left(\frac{\partial f}{\partial v_o} \right)$$

To have a physically realizable situation, $f(v_o) = 0$ at $-\infty$ and $+\infty$ which eliminates the first term. Then,

$$\int_{-\infty}^{\infty} \frac{f(v_o) dv_o}{(\omega - \beta v_o)^2} = - \int_{-\infty}^{\infty} \frac{\left(\frac{\partial f}{\partial v_o} \right) dv_o}{\beta(\omega - \beta v_o)} \tag{74}$$

Comparing Eqs. 72, 73, and 74 leads to the obvious conclusion that the Boltzmann equation approach and the superposition technique give identical results for analysis of the temperature problem. Because the superposition technique is easier to understand in terms of streaming particle interactions, it will be used in all subsequent discussions.

The remaining problem now is to fit the hydrodynamic model into the distribution function approach. The derivation in Chapter III (Eqs. 15 to 21) of the dispersion relation based on the hydrodynamic model was very straightforward and gave an algebraic expression for the result which, although complicated, is not too difficult to solve. Once again, to compare the results, consider the one-dimensional dispersion relation of a single stream. For a single stream, Eq. 21 of Chapter III becomes

$$\frac{\omega_p^2}{\left(\omega - \beta v_o\right)^2 - \beta^2 v_t^2} = 1 \tag{75}$$

In the zero temperature case where $v_t = 0$ and $f\left(v_o\right)$ is a delta function in v_o, Eqs. 75 and 73 give identical results. What then is the reason that the hydrodynamic approach gives a simple algebraic result while the Boltzmann equation or a superposition technique results in an integral equation? Is there any way to relate the two results mathematically? The first question can be answered simply by recognizing that the hydrodynamic equation is the result of averaging the velocity distribution to obtain an effective thermal velocity v_t. The

averaging is done without regard to any possible interaction between the particle streams. The derivation is based on the assumption that some average kinetic pressure can be defined for the system of thermally excited particles. The net effect of using this theory is that instead of having a single drift velocity, the temperature spreads the velocity over a range $v_d - v_t$ to $v_d + v_t$. The hydrodynamic result can be mathematically obtained from the distribution function integral by assuming a rectangular distribution as in Fig. 13a of Section 5.3. Normalizing $f(v_o)$ so that

$$\int_{v_d - v_t}^{v_d + v_t} f(v_o) \, dv_o = 1$$

and since $f(v_o)$ is assumed to be constant over the range of integration

$$f(v_o) = \frac{1}{2v_t}$$

Consequently,

$$\frac{\omega_{po}^2}{2v_t} \int_{v_d - v_t}^{v_d + v_t} \frac{dv_o}{\left(\omega - \beta v_o\right)^2} = \frac{\omega_{po}^2}{\left(\omega - \beta v_o\right)^2 - \beta^2 v_t^2} \tag{76}$$

which is the same as the hydrodynamic equation result.

It is interesting to note that if the integral of Eq. 76 is

done in terms of the Boltzmann equation integral as in Eq. 72, then we need to evaluate $\partial f / \partial v_o$, and for a rectangular distribution this just gives two delta functions at $v_d - v_t$ and $v_d + v_t$. The final result is the same as in Eq. 76. The interesting conclusion is that the *slope* of the distribution function is very important and will have to be carefully examined in subsequent work. One would expect, therefore, that because of the above-stated reasons the distribution function model should be used for best results. In the following sections, both the hydrodynamic model and the distribution function method will be applied to practical problems and compared in detail.

5.2. Statistical Methods for Semiconductors

The dispersion relations of Section 5.1 are given in terms of some velocity distribution function $f(v_o)$. This distribution function must be a good physical representation of the particle behavior within the semiconductor, but also it should be mathematically manageable. Neither of these requirements is easy to satisfy. In order to have space-charge interactions between drifting carriers, large electric fields must be applied to the semiconductor to get high drift velocities. It is experimentally found that at a certain point, velocity saturation occurs so that there is no longer a linear relationship between the E field and v_{drift}. (This will be discussed further in Chapter VIII.) The velocity distribution $f(v_o)$ will be affected by the applied field. For small applied fields, much below velocity saturation, the distribution function will be shifted by v_{drift} so that it is symmetrically

centered about v_{drift}. However, at fields near the saturation level,

a symmetric distribution function is no longer appropriate. To date

there has not been sufficient experimental work in this area to permit

any definitive statements. Therefore, one of the purposes of this chap-

ter will be to investigate several possible distribution functions to

see what particular properties are most important and what approximate

methods give consistent results.

For semiconductors, Fermi-Dirac statistics give the most com-

plete description. The basis for postulating Fermi-Dirac statistics

and some fundamental results were described in Section 2.3. There it

was also suggested that for many situations Fermi-Dirac statistics

could conveniently be replaced by a Maxwell-Boltzmann description. The

Fermi-Dirac distribution function is given as

$$f(E) = \frac{A}{e^{\left(E - E_f\right)/kT} + 1} \tag{77}$$

The explicit normalization constants of Eq. 77 have been included in

the factor A. This is sufficient for the subsequent discussion.

It was stated in Section 2.3 that in most cases $\left|E_f - E\right| \gg kT$,

so that the result can be approximated by a Maxwell-Boltzmann distribu-

tion. It is easy to see that this is indeed true for all temperatures

near or below room temperature and for almost any doping level normally

encountered. The energy E is equal to E_g, the band gap, plus the kinetic

energy of the particles. Experimentally, the kinetic energy is never

much larger than kT. The Fermi energy E_f is usually near the middle of

the band gap. The approximation that $|E_f - E| \gg kT$ will be acceptable for all cases where $|E_f - E_g| \gg kT$. E_f will approach E_g only for very heavily doped materials. Use of such materials is not anticipated.

Then, taking $|E_f - E| \gg kT$, Eq. 77 becomes

$$f(E) \simeq e^{\left(E_f - E\right)/kT}$$

$$f(E) \simeq e^{\left(E_f - E_g\right)/kT} e^{-mv^2/2kT} \tag{78}$$

The $f(E)$ of Eq. 78 is obviously proportional to the Maxwell-Boltzmann distribution function which is given as[3]

$$f\left(v_o\right) = \left(\frac{m}{2\pi kT}\right)^{1/2} e^{-\frac{m\left(v_o - v_d\right)^2}{2kT}} \tag{79}$$

where v_d = drift velocity about which the distribution is centered. The only differences between Eqs. 78 and 79 are that the Fermi-Dirac distribution is not normalized, whereas the Maxwell-Boltzmann result is given in a form such that

$$\int_{-\infty}^{\infty} f\left(v_o\right)dv_o = 1 \tag{80}$$

[3] T. H. Stix, *The Theory of Plasma Waves*, New York, McGraw-Hill, 1962, p. 177.

and the Maxwell-Boltzmann distribution has been shifted by v_d.

From the above discussion, we can now conclude that at low dc electric fields a shifted Maxwell-Boltzmann velocity distribution is an accurate representation of the temperature effects in a semiconductor under experimentally expected conditions. When strong electric fields are applied, however, the distribution may no longer be symmetrical about v_{drift} and some correction may be necessary.

5.3. Approximate Techniques for Evaluation of the Distribution Function

From the above discussion it appears that all that remains to be done is to replace $f(v_o)$ in Eq. 68 by the Maxwell-Boltzmann distribution function, perform the integration, and analyze the answer. Unfortunately, the integral of Eq. 68 with a Maxwell-Boltzmann distribution in place of $f(v_o)$ cannot be evaluated explicitly. At best, it can be expressed in terms of the complex error function which has been tabulated by B. D. Fried and S. D. Conte.[4] This is not a particularly satisfying situation, and has consequently been one reason why other approximate techniques have been investigated. The need to understand what effect the distribution function has on the integration is further emphasized by the uncertainty of what shape it has in an actual solid, as discussed in the previous section. If the results critically depend on the distribution function, then accurate theoretical prediction of a practical result cannot be expected. If, on the other hand, the dispersion relation is

---

[4] B. D. Fried and S. D. Conte, *The Plasma Dispersion Function*, New York, Academic Press, 1961.

- 88 -

not particularly sensitive to the shape of the velocity distribution, then theoretical results will be valuable in predicting space-charge interactions in semiconductors.

In the course of this work, many possible distribution functions were considered to approximate the Maxwell-Boltzmann distribution. There are basically two methods which were found to be useful:

1. Straight line approximations.

2. Algebraic functions involving powers of v and a temperature term.

The simplest functions which illustrate these two methods are a triangle-shape distribution and the Lorentzian distribution function as given by Eq. 81

$$f\left(v_o\right) = \frac{b/\pi}{\left(v_o - v_d\right)^2 + b^2} \tag{81}$$

where b is the effective temperature term. The Lorentzian and triangle distributions are sketched in Fig. 13, parts b and c. Also shown for comparison is the hydrodynamic model (part a) and the Maxwell-Boltzmann distribution (part d).

Other distribution functions could also be tried. For example, the triangle distribution could probably be improved by taking additional straight line segments near the peak of the distribution and also adding a "tail" at the velocities further from v_d. The Lorentzian could be improved by taking higher powers in v such as Eq. 82.

$$v_t - v_d \qquad\qquad v_t + v_d$$
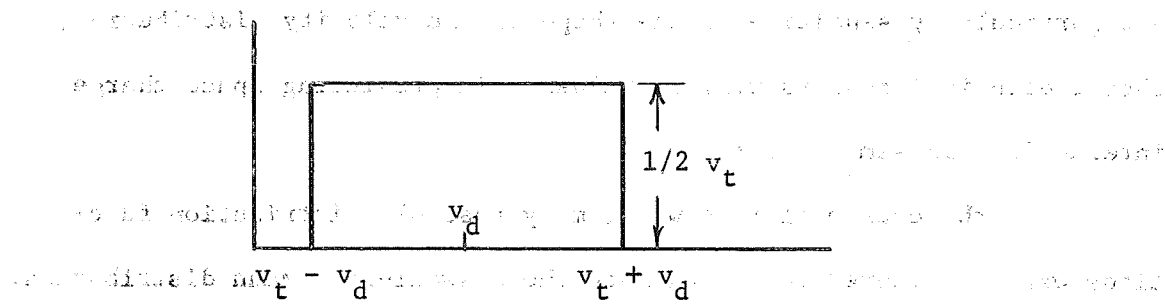
a. Model with an average thermal velocity v_t, from the hydrodynamic equation.
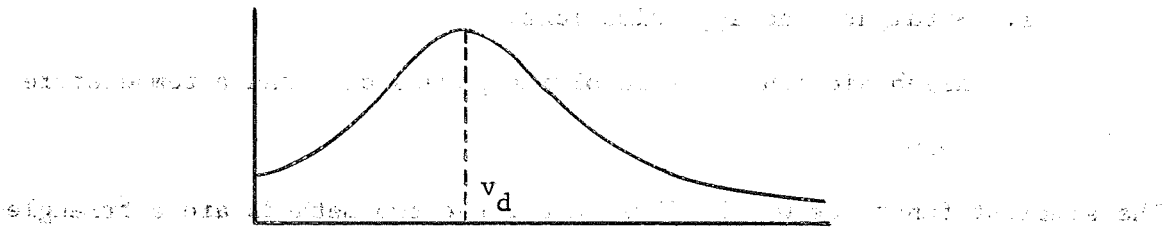
b. Lorentzian thermal velocity distribution.
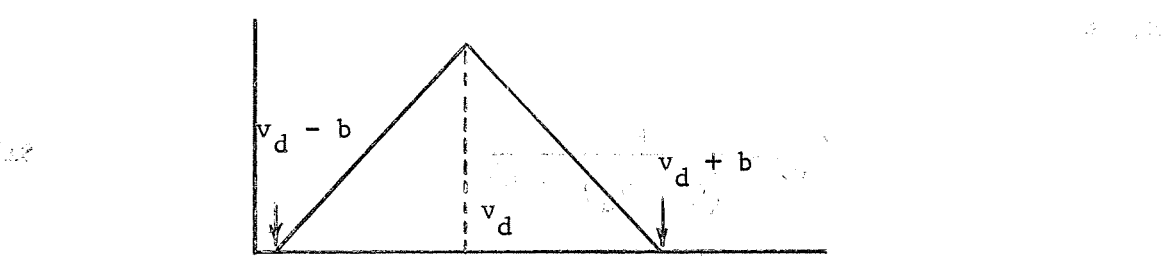
c. Triangle distribution.
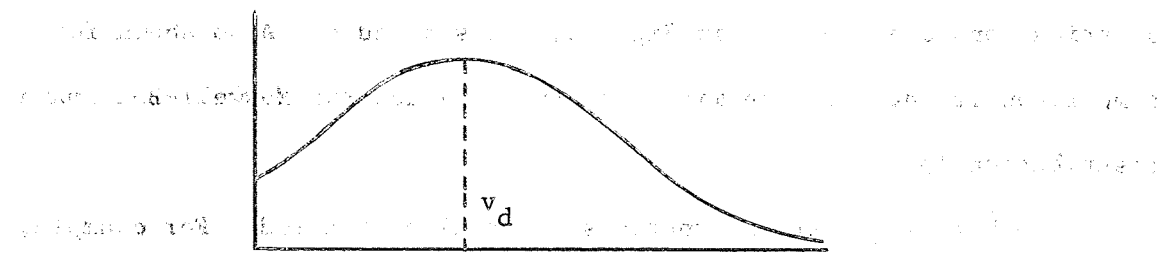
d. Boltzmann distribution.

Fig. 13. A comparison of some possible thermal velocity distribution functions.

$$f\left(v_o\right) = \frac{1}{\left(v_o^2 + b^2\right)^2} \qquad (82)$$

or also

$$f\left(v_o\right) = \frac{1}{v_o^4 + b^4} \qquad (83)$$

Both Eqs. 82 and 83 give graphical results that are closer to the Maxwell-Boltzmann distribution. It was found, however, that these refinements greatly add to the complexity of evaluating the integral, and very good results can be obtained without recourse to such functions.

In this report, we will make a detailed analysis of the four cases illustrated in Fig. 13: the hydrodynamic model, the Lorentzian distribution, the triangle distribution, and the Maxwell-Boltzmann velocity distribution. The hydrodynamic model and the Maxwell-Boltzmann distribution will be used to check the overall results, the hydrodynamic model because of its simplicity and historical value, and the Maxwell-Boltzmann distribution as the closest estimate of actual material behavior.

All the proposed distribution functions, except for the hydrodynamic model, are used in the integral appearing in Eq. 68. It is convenient to evaluate and discuss this integral for all three functions at this point before analyzing the dispersion relations for particular numerical results. Since the distributions are of somewhat different shapes, it is necessary to decide on a common basis for comparison so that numer-

ical solutions will give meaningful results. First, we will normalize all distributions so that

$$\int_{-\infty}^{\infty} f\left(v_o\right) dv_o = 1$$

The Maxwell-Boltzmann distribution can be normalized in terms of physical properties of the materials as previously given in Eq. 79.

$$f\left(v_o\right) = \left(\frac{m}{2\pi kT}\right)^{1/2} \exp\left(\frac{-m\left(v_o - v_d\right)^2}{2kT}\right) \tag{79}$$

Using the Maxwell-Boltzmann distribution as a reference, a somewhat arbitrary choice was made to equate the peak values of the distributions at v_d. The normalized Lorentzian distribution is then given as

$$f\left(v_o\right) = \frac{b/\pi}{\left(v_o - v_d\right)^2 + b^2} \tag{81}$$

Then at $v_o = v_d$

$$f\left(v_o\right) = \frac{1}{b\pi}$$

and in terms of the Maxwell-Boltzmann result of Eq. 79

$$b = \frac{1}{\pi^{1/2}} \left(\frac{2kT}{m}\right)^{1/2} \tag{84}$$

The integral which must be evaluated for the Lorentzian distribution is

$$\int_{-\infty}^{\infty} \frac{b/\pi \; dv_o}{\left(v_o - \frac{\omega}{\beta}\right)^2 \left[\left(v_o - v_d\right)^2 + b^2\right]}$$

Since ω/β may be complex, the appropriate method to use is contour integration.

$$\int_{-\infty}^{\infty} \frac{b/\pi \; dv_o}{\left(v_o - \frac{\omega}{\beta}\right)^2 \left[\left(v_o - v_d\right)^2 + b^2\right]} = \int_{-\infty}^{\infty} \frac{b/\pi \; dv}{\left(\frac{\omega}{\beta} - v\right)^2 \left[\left(v - v_d\right) + jb\right]\left[\left(v - v_d\right) - jb\right]}$$

$$= 2\pi jb/\pi \sum \text{residues}$$

The residues are evaluated by using well known theorems of complex algebra. The final result is

$$\int_{-\infty}^{\infty} \frac{b/\pi \; dv_o}{\left(v_o - \frac{\omega}{\beta}\right)^2 \left[\left(v_o - v_d\right)^2 + b^2\right]} = \frac{1}{\left(v_d + jSb - \frac{\omega}{\beta}\right)^2} \tag{85}$$

where

$$S = \begin{cases} + 1 \text{ if } \text{Im}\left(\frac{\omega}{\beta}\right) < 0 \\ \\ - 1 \text{ if } \text{Im}\left(\frac{\omega}{\beta}\right) > 0 \end{cases}$$

The significant observation that can be made from Eq. 85 is that the integral has resulted in a reasonably manageable algebraic expression. In fact, the result is not so very different from the hydrodynamic model of Eq. 76. Comparing the Lorentzian distribution to the Maxwell-Boltzmann distribution in Fig. 13, we see that the Lorentzian is narrower in the region near v_d, and for values of $v \gg v_d$ it does not fall off nearly as rapidly as the Maxwell-Boltzmann distribution. Also, the slope of the Lorentzian distribution is significantly different in the region near v_d.

The triangle distribution is sketched in Fig. 13c. Mathematically it can be written as

$$f\left(v_o\right) = \frac{1}{b^2}\left[\left(b - v_d\right) + v_o\right] \quad \text{for the region of } v_d - b \text{ to } v_d \tag{86}$$

$$f\left(v_o\right) = -\frac{1}{b^2} v_o + \frac{1}{b^2}\left(v_d + b\right) \quad \text{for the region } v_d \text{ to } v_d + b \tag{87}$$

$$f\left(v_o\right) = 0 \quad \text{for } -\infty \rightarrow v_d - b \text{ and } v_d + b \rightarrow \infty$$

Equations 86 and 87 have been written assuming a velocity distribution that is symmetrical about v_d. It would be very easy, however, to change the slope of either side of the triangle to consider unsymmetrical distributions such as may be encountered at high electric fields (see Section 5.2).

Equations 86 and 87 can now be used in the integral of Eq. 68

$$\int_{-\infty}^{\infty} \frac{f\left(v_o\right)dv_o}{\left(\frac{\omega}{\beta} - v_o\right)^2} = \int_{v_d - b}^{v_d} \frac{\left[\frac{1}{b^2} v_o + \frac{1}{b^2}\left(b - v_d\right)\right] dv_o}{\left(\frac{\omega}{\beta} - v_o\right)^2}$$

$$+ \int_{v_d}^{v_d + b} \frac{\left[- \frac{1}{b^2} v_o + \frac{1}{b^2}\left(v_d + b\right)\right] dv_o}{\left(\frac{\omega}{\beta} - v_o\right)^2}$$

(88)

Assuming that β is complex, as discussed in Section 5.1, the integrals appearing on the right side of Eq. 88 can be evaluated either from tables or by straightforward integration

$$\int_{-\infty}^{\infty} \frac{f\left(v_o\right)dv_o}{\left(\frac{\omega}{\beta} - v_o\right)^2} = \frac{1}{b^2} \left\{ \left[\log\left(\frac{\omega}{\beta} - v_o\right) + \frac{\frac{\omega}{\beta}}{\left(\frac{\omega}{\beta} - v_o\right)} \right]_{v_d - b}^{v_d} \right.$$

$$- \left[\log\left(\frac{\omega}{\beta} - v_o\right) + \frac{\frac{\omega}{\beta}}{\left(\frac{\omega}{\beta} - v_o\right)} \right]_{v_d}^{v_d + b}$$

(89)

$$+ \left(b - v_d\right) \left[\frac{1}{\left(\frac{\omega}{\beta} - v_o\right)} \right]_{v_d - b}^{v_d}$$

$$\left. + \left(v_d + b\right) \left[\frac{1}{\left(\frac{\omega}{\beta} - v_o\right)} \right]_{v_d}^{v_d + b} \right\}$$

Substitution of the limits indicated in Eq. 89 and algebraic manipulation results in a much simpler result for the integral

$$\int_{-\infty}^{\infty} \frac{f\left(v_o\right)dv_o}{\left(\frac{\omega}{\beta} - v_o\right)^2} = \frac{1}{b^2} \log \left[\frac{\left(\frac{\omega}{\beta} - v_d\right)^2}{\left(\frac{\omega}{\beta} - v_d\right)^2 - b^2} \right] \tag{90}$$

Equation 90 is written in terms of the temperature-dependent quantity "b" just as was done for the Lorentzian distribution. Using the same normalization procedure in this case as was used for the Lorentzian distribution results in

$$b = \left(\frac{2\pi kT}{m}\right)^{1/2} \tag{91}$$

Comparing Eqs. 91 and 84, we see that

$$b_{triangle} = \pi b_{Lorentz} \tag{92}$$

The evaluation of the integral has resulted in an expression which is in terms of a log function. This results in a transcendental equation when substituted back into the dispersion relation. Because of this, an analytic solution would be extremely difficult and may not even be possible. This case can best be treated by computer techniques and will be discussed further in Section 5.4.

The Maxwell-Boltzmann distribution was given in its normalized form in Eq. 79

$$f\left(v_o\right) = \left(\frac{m}{2\pi kT}\right)^{1/2} \exp\left(\frac{-m\left(v_o - v_d\right)^2}{2kT}\right) \qquad (79)$$

As mentioned in the introductory paragraph to this section, this distribution cannot be integrated explicitly. Integrals involving this type of a term are usually manipulated into a form that gives them in terms of the complex error function or complex plasma dispersion function. Then, either numerical tables are used or approximate computer methods are employed to evaluate the remaining integrals. However, if numerical integration has to be done on the computer anyway, why not just do it on the integral as it stands? There is no particular advantage in converting over to the plasma dispersion function. In fact, the results are harder to evaluate because of their complexity and the consequent difficulty of estimating the computer integration errors. For these reasons, direct numerical integration was used. The specific method will be discussed in Section 5.4.

Figure 14 compares the normalized Lorentzian, triangle, and Maxwell-Boltzmann distribution functions for a particular temperature. It is interesting to note how well the simple triangle distribution matches the Maxwell-Boltzmann distribution in both magnitude and slope.

With the results of this section, we are now ready to consider numerical calculations and make a detailed investigation of the effect of temperature.

5.4. <u>Numerical Comparison of the Distribution Functions</u>

In Sections 5.2 and 5.3, the usefulness of several different

- 97 -
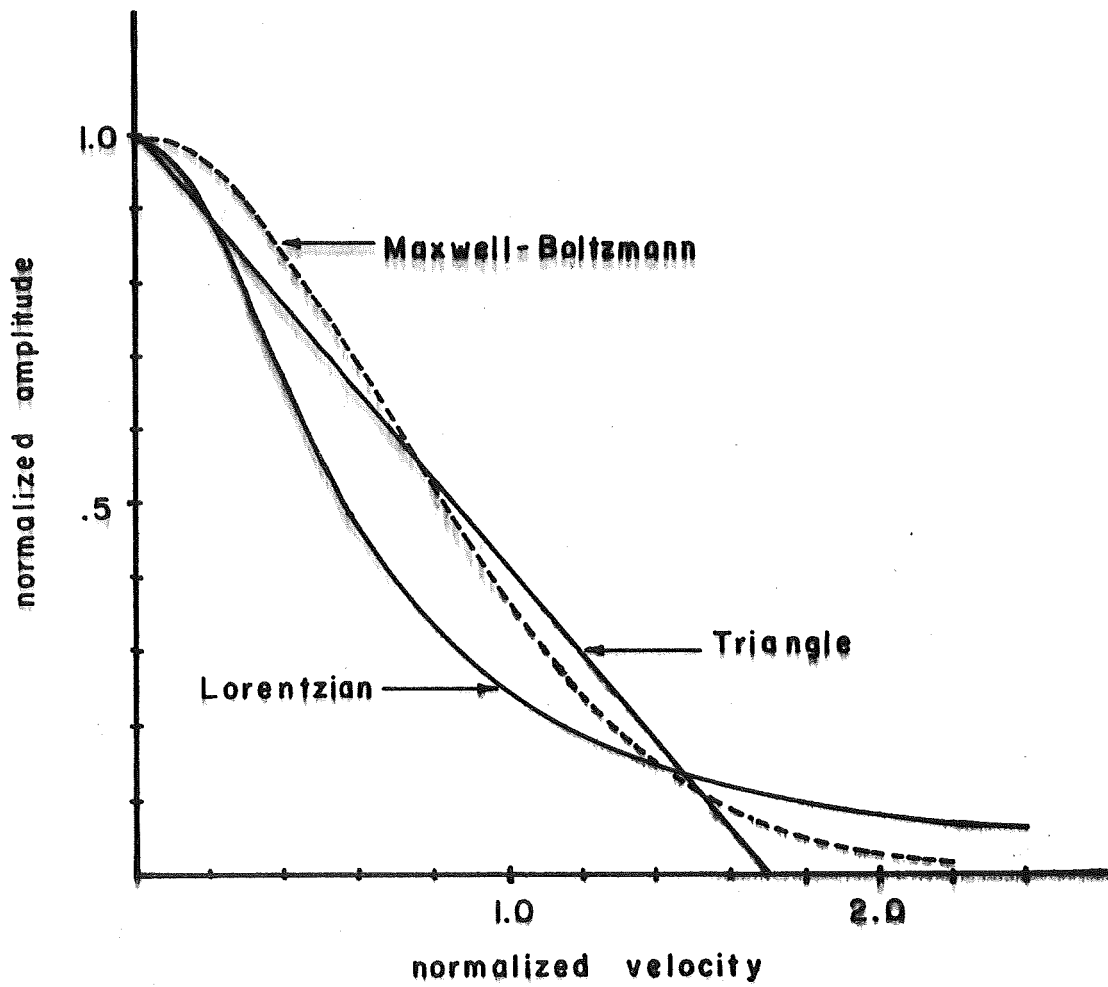
Fig. 14. The Maxwell-Boltzmann, triangle, and Lorentzian
distributions at a particular temperature.

velocity distribution models was discussed and the integrals were evaluated for the cases of interest. All these cases have been investigated on the Univac 1108 digital computer. Before presenting these results, a few comments need to be made concerning specific numerical values used and the general methods of programming.

For programming on a digital computer it was of course necessary to choose numerical values for all parameters. The choice was made partly on available data. Indium antimonide, germanium, and silicon are the three semiconductors for which reasonably good data are currently available. Any one of these materials could be used.

Most of the experimental and theoretical work has been done with InSb. However, there is nothing unique about InSb for space-charge interactions. The lack of observed emission from other materials may, in fact, indicate that the oscillations in InSb are being generated by some other process. The theoretical investigation of a different material can, therefore, add significantly to the understanding of this problem. If oscillations are predicted for other materials under similar conditions but are not observed experimentally, then this should be a good indication of the lack of correlation between experiment and theory.

Germanium was chosen for the computer investigation because there is sufficient numerical information available, and because thin layers are easier to make with germanium than with a compound semiconductor such as lead sulfide. The material properties that need to be known for the computer work are the plasma frequencies, drift velocities, dielectric constants, and electron temperatures. Detailed discussions of the mate-

rial properties will be left for Chapter VIII, but we do need to indicate briefly how the various parameters were chosen. The plasma frequencies are determined from commercially available doping concentrations. The drift velocity of the thin layer (Region 1) was taken to be zero. Layers of the necessary thinness will probably have to be made by vacuum deposition and this usually results in polycrystalline material of very low mobility. The drift velocity of the other region was determined from experimental data of D. M. Chang and J. G. Ruch.[5] The lattice dielectric constant was assumed the same for Region 1 and Region 2 and was taken to be 16.0 (see Chapter VIII). Electron temperatures were varied in the computer program so that no predetermined value was necessary. It was, however, assumed that Region 1 and Region 2 were at the same temperature. Because Region 1 is very thin, this is a good assumption and greatly reduces the number of curves that have to be plotted.

The actual methods of programming the various dispersion relations varied somewhat, depending on the difficulty of the solution. All of the solutions were done for the free space model discussed in Sections 4.2 and 4.5, using the dispersion relation of Eq. 52. The only change was in T_1 and T_2 as given in general by Eq. 68. For the hydrodynamic, Lorentz, and triangle distributions, $Re(\beta)$ and $Im(\beta)$ were incremented and the values then tested for minimum error in the deter-

---

[5] D. M. Chang and J. G. Ruch, "Measurements of the Velocity Field Characteristic of Electrons in Germanium," *Applied Physics Letters*, Vol. 12, February 1968, pp. 111-112.

minantal equation. A search routine was developed which automatically searched a given region of the complex β-plane for a root. It was only necessary to know the general area of the β-plane where a solution exists for Re(β) and Im(β). The search routine was then able to find the solution to about 0.01 percent accuracy in ten to thirty tries.

The Maxwell-Boltzmann distribution was treated similarly with one additional step for numerical integration. First, the Maxwell-Boltzmann distribution function itself was programmed so that it could be integrated numerically. Since it is normalized to one, the results will approach this value for a proper choice of increments and limits. When accuracy of the numerical integration was acceptable, the integration routine was inserted into the program to evaluate the integral of Eq. 68. Equation 68 for the Maxwell-Boltzmann distribution becomes

$$ T^2 = \left(\beta^2 - k^2 \right) \left[1 - \omega_{po}^2 \int_{-\infty}^{\infty} \frac{\left(\frac{m}{2\pi kT} \right)^{1/2} \exp \frac{\left(-m\left(v_o - v_d \right)^2 \right)}{2kT} \, dv_o}{\left(\omega - \beta v_o \right)^2} \right] \tag{93} $$

The exponential numerator of the integral in Eq. 93 assures convergence for Im(β) ≠ 0. If β is purely real then the integral does not converge. However, this is a physically unlikely case, since for all cases of interest we will find loss or gain and hence complex β.

5.5. Discussion of Computer Results for Distribution Functions

Figures 15 to 23 give the results obtained from the computer investigation. Much of the information is self-evident from an examina-

$\omega = 1.88 \times 10^{12}$

$\omega_{p1} = 9.5 \times 10^{12}$

$\omega_{p2} = 1.5 \times 10^{12}$

$v_2 = 1.2 \times 10^5$ m/s

$\varepsilon_1 = \varepsilon_2 = 16.0$

$\bullet\!-\!\bullet = \beta_{real}$

$-\!-x\!-\!- = \beta_{imag.}$

43°K

19.2°K

0°K

0°K

β_e

19.2°K

43°K

$\times 10^6$ for β_{im}

$\times 10^7$ for β_{real}

3.

2.

1.

0   .1   .2   .3   .4   .5

$\times 10^{-7}$ m

a ⟶
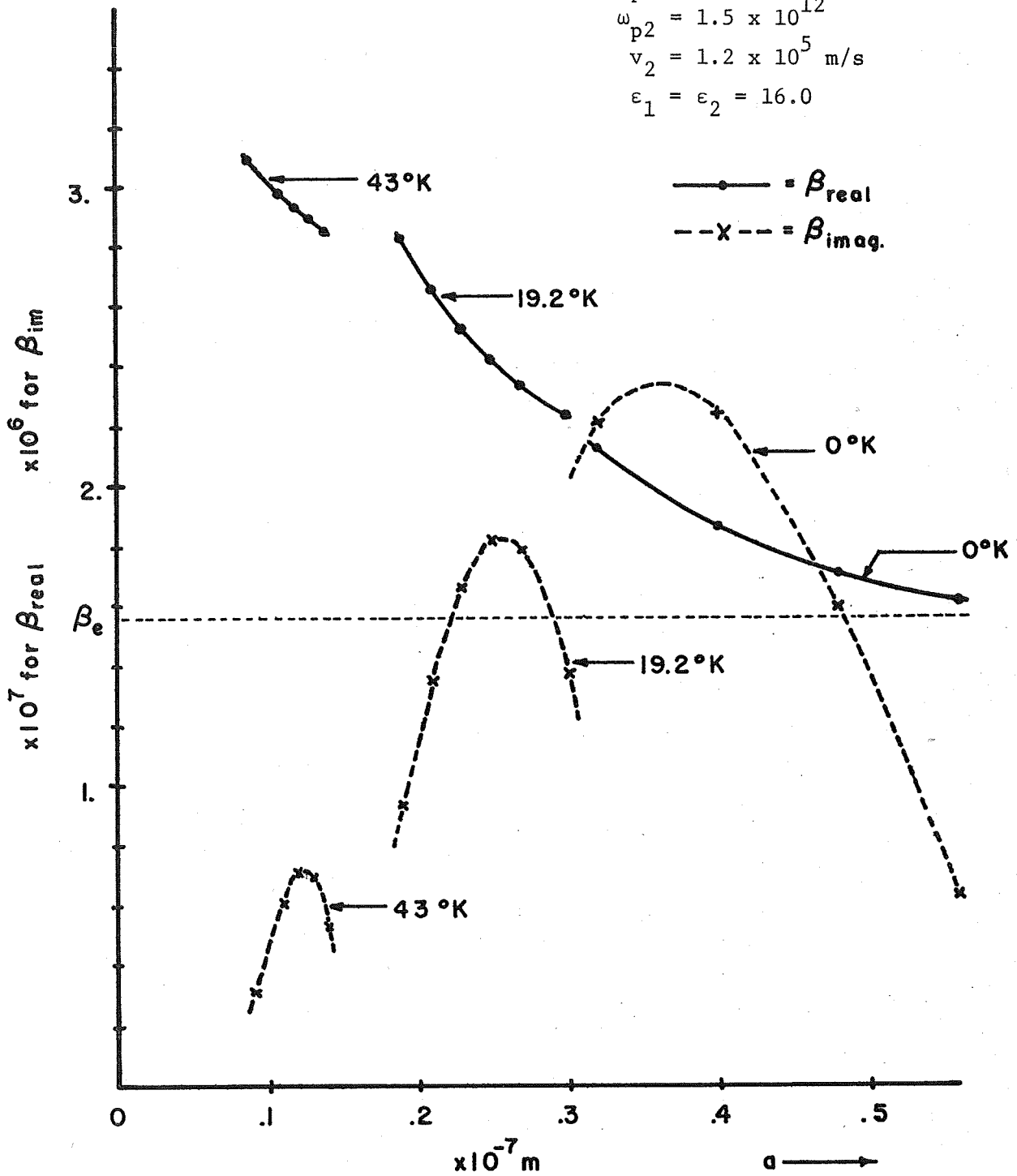
Fig. 15.   Complex β as a function of "a" and
temperature for the hydrodynamic model.
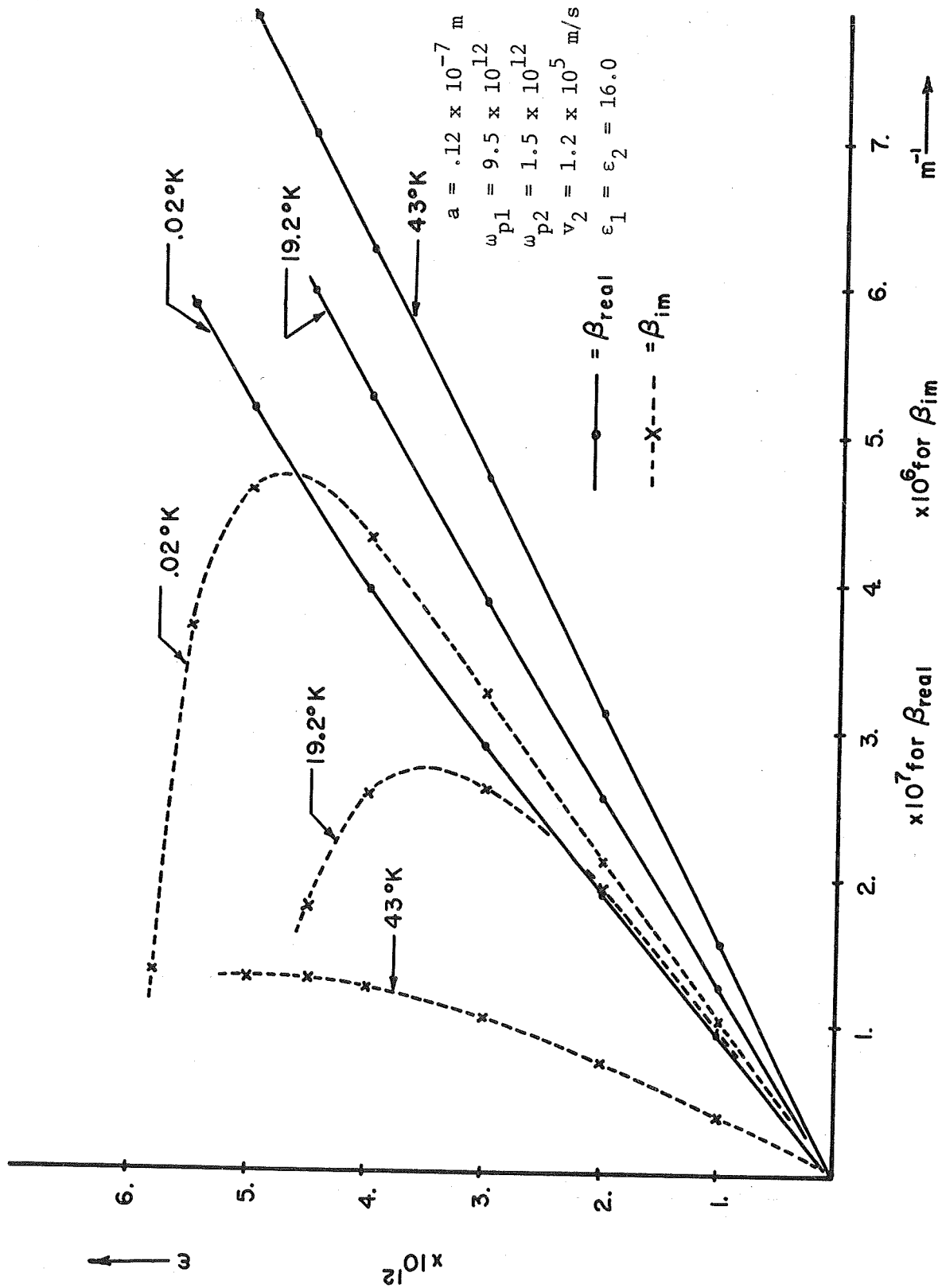
Fig. 16. ω–β diagram for the hydrodynamic model with the two-layer configuration.

$a = .12 \times 10^{-7}$ m

$\omega_{p1} = 9.5 \times 10^{12}$

$\omega_{p2} = 1.5 \times 10^{12}$

$v_2 = 1.2 \times 10^{5}$ m/s

$\varepsilon_1 = \varepsilon_2 = 16.0$

——— $= \beta_{real}$

– – –X– – – $= \beta_{im}$

x10⁷for β_{real} x10⁶for β_{im} m⁻¹

x10¹²

ω

.02°K

19.2°K

43°K

.02°K

19.2°K

43°K

$$\omega = 1.88 \times 10^{12}$$
$$\omega_{p1} = 9.5 \times 10^{12}$$
$$\omega_{p2} = 1.5 \times 10^{12}$$
$$v_2 = 1.2 \times 10^5 \text{ m/s}$$
$$\varepsilon_1 = \varepsilon_2 = 16.0$$
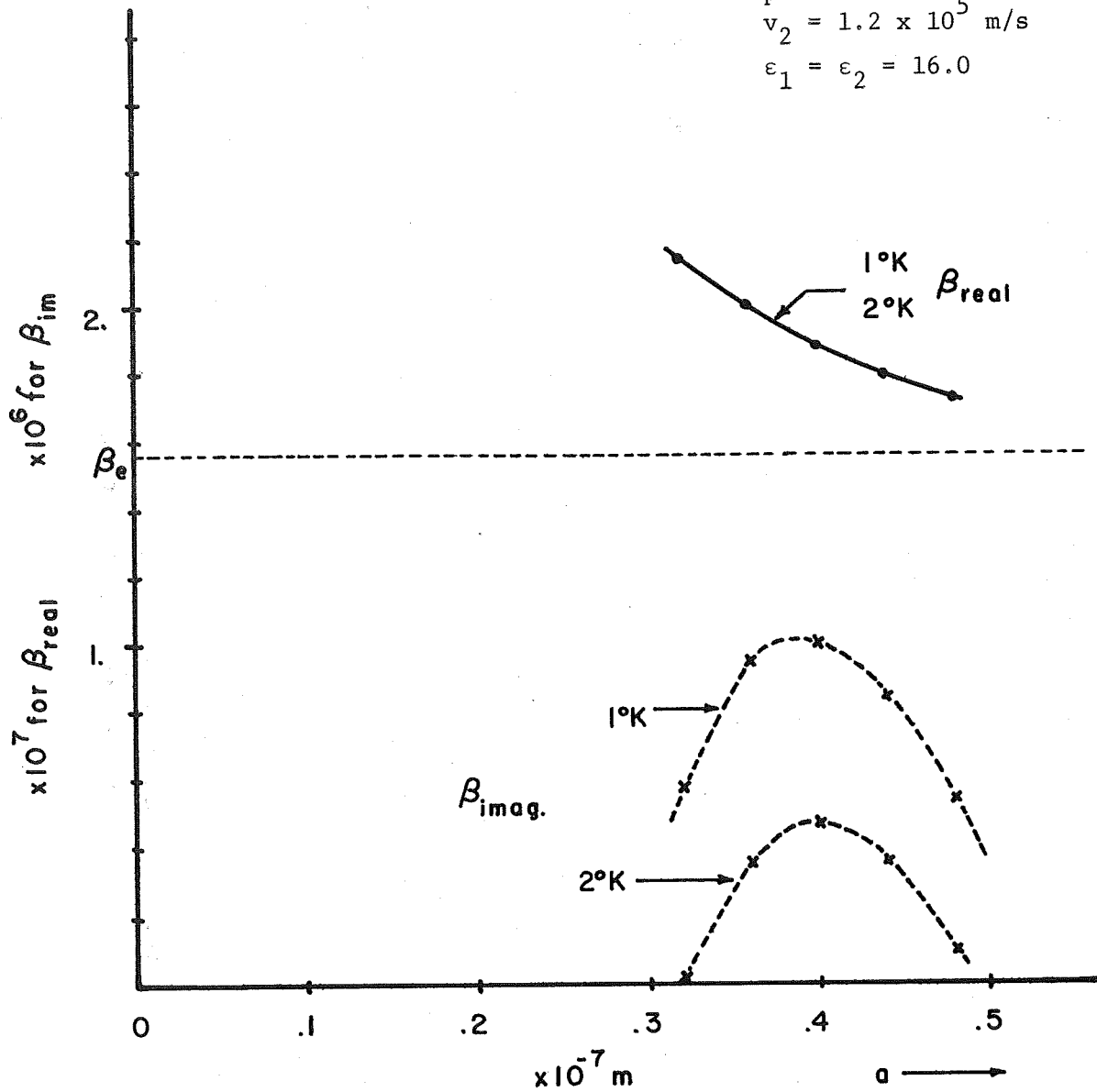
Fig. 17.   Complex β as a function of "a" and temperature
for the Lorentzian distribution function.

$$\omega = 1.88 \times 10^{12}$$
$$\omega_{p1} = 9.5 \times 10^{12}$$
$$\omega_{p2} = 1.5 \times 10^{12}$$
$$v_2 = 1.2 \times 10^5 \ m/s$$
$$\varepsilon_1 = \varepsilon_2 = 16.0$$
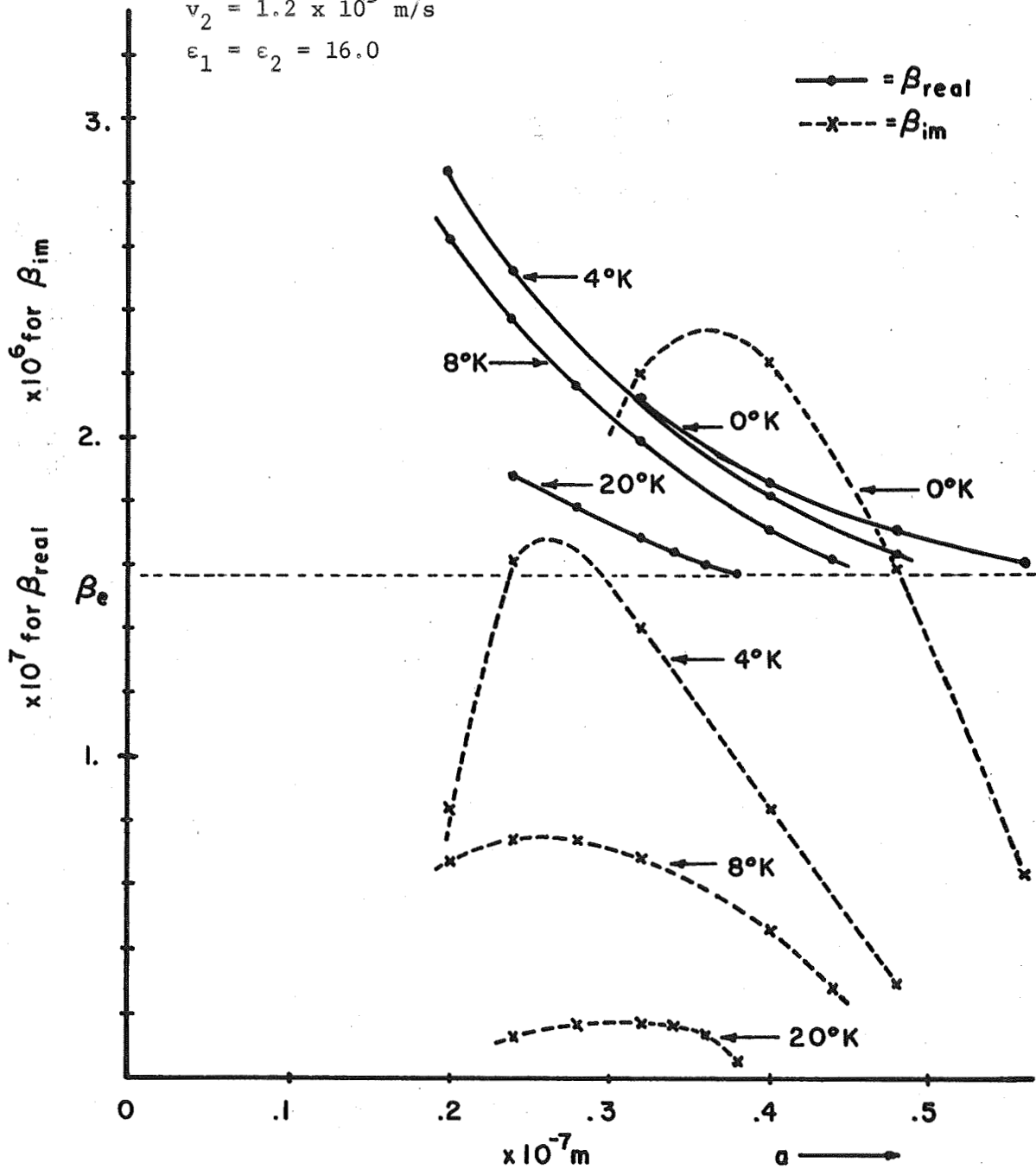
Fig. 18. Complex β as a function of "a" and temperature for the triangular velocity distribution.

- 105 -
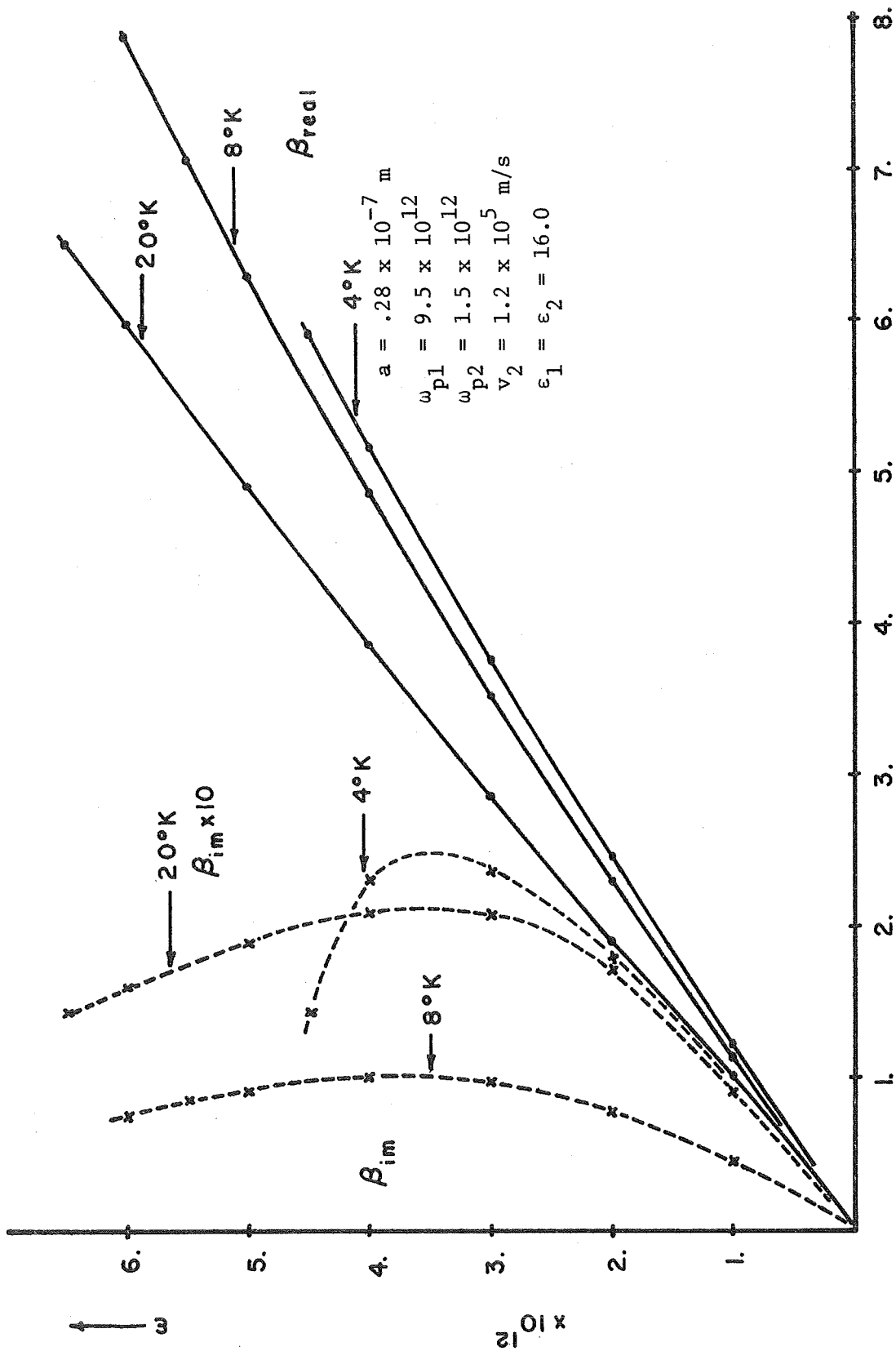
Fig. 19. $\omega-\beta$ diagram for the triangle velocity distribution with the two-layer configuration.

$x10^7$ for β_{real} $x10^6$ for β_{im}

β_{real}

$a = .28 \times 10^{-7}$ m
$\omega_{p1} = 9.5 \times 10^{12}$
$\omega_{p2} = 1.5 \times 10^{12}$
$v_2 = 1.2 \times 10^5$ m/s
$\varepsilon_1 = \varepsilon_2 = 16.0$

$\beta_{im} \times 10$

β_{im}

ω

$x10^{12}$
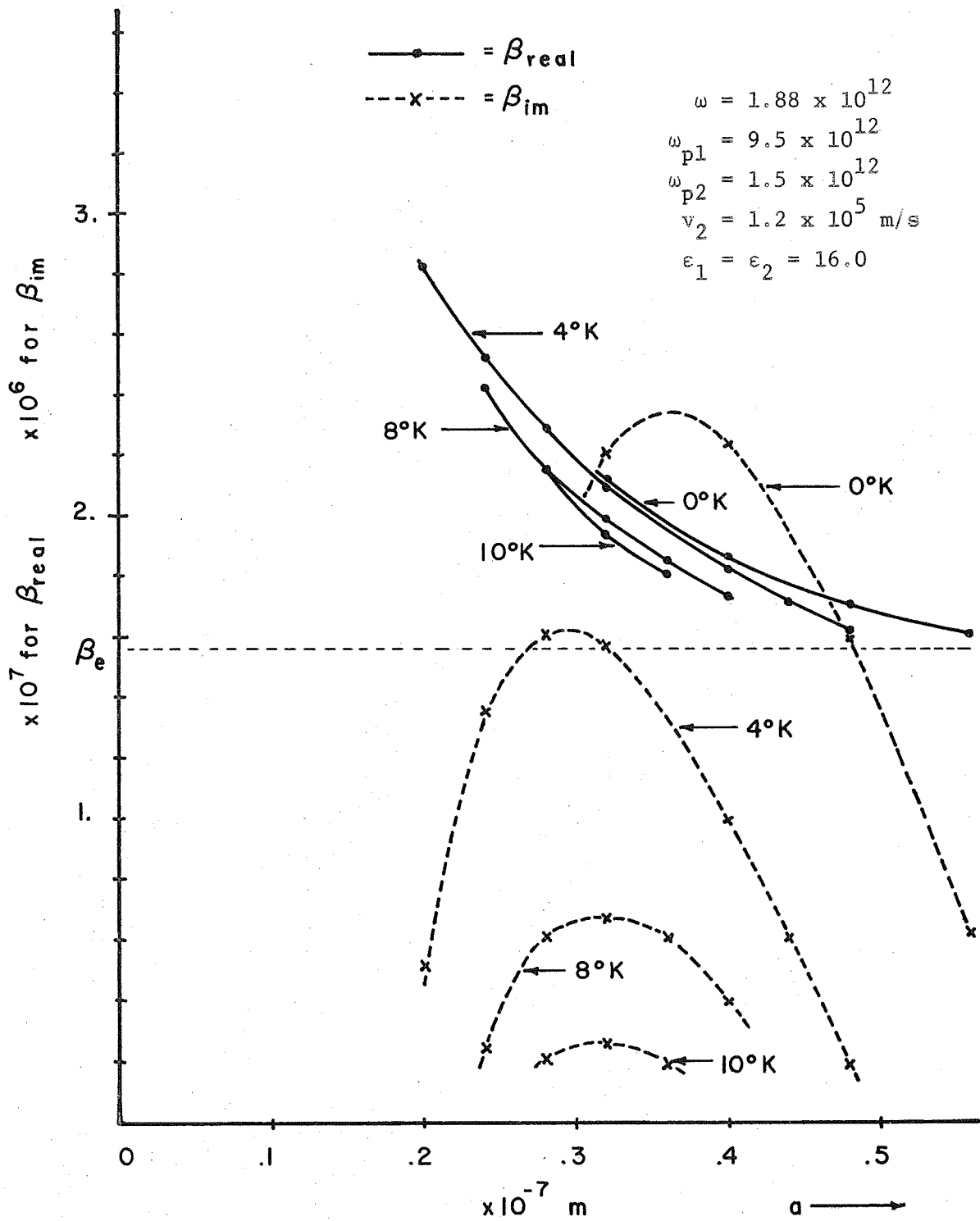
Fig. 20. Complex β as a function of "a" and temperature for the Maxwell-Boltzmann velocity distribution.
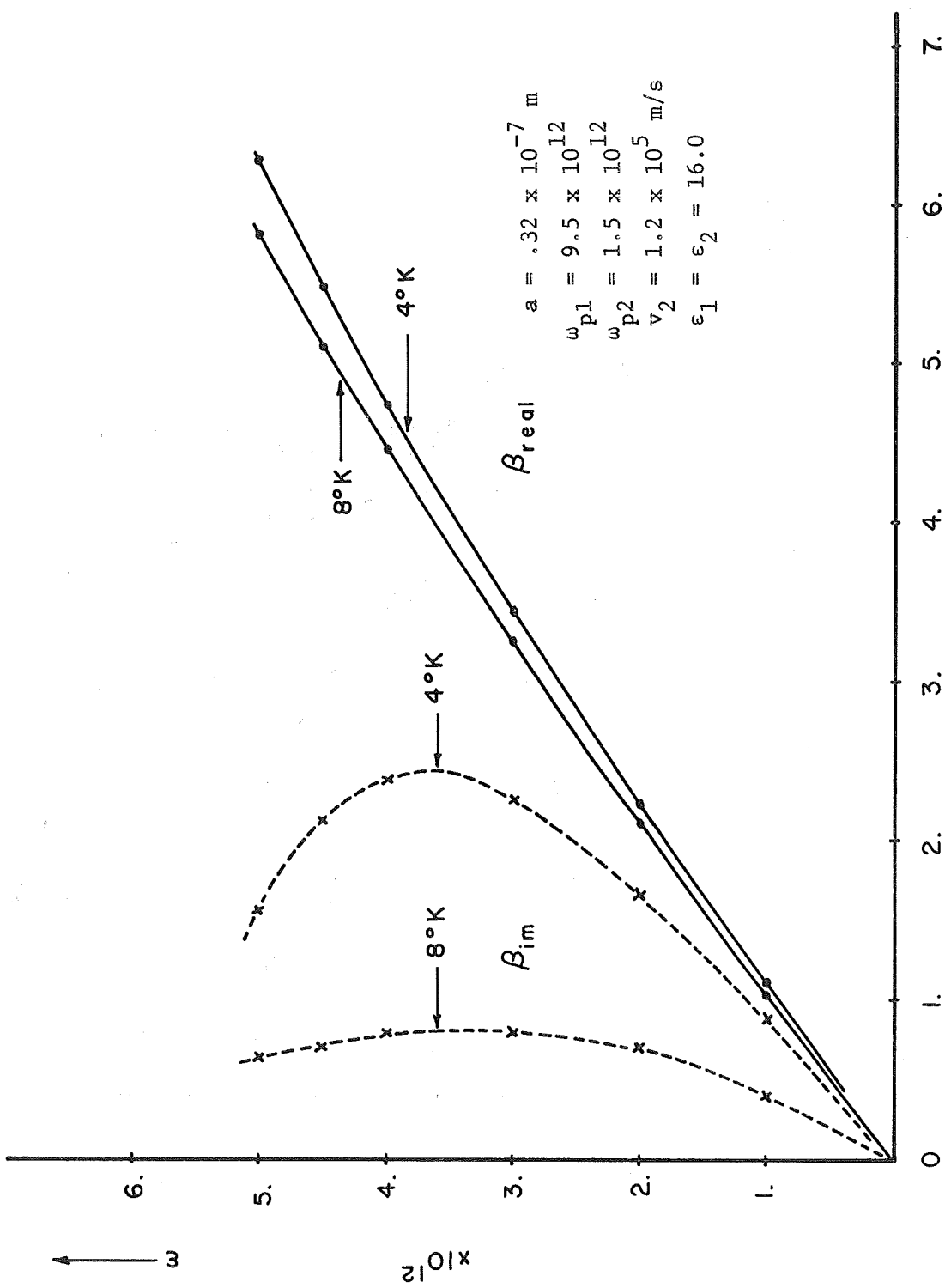
Fig. 21. ω–β diagram for the Maxwell–Boltzmann velocity distribution with the two-layer configuration.
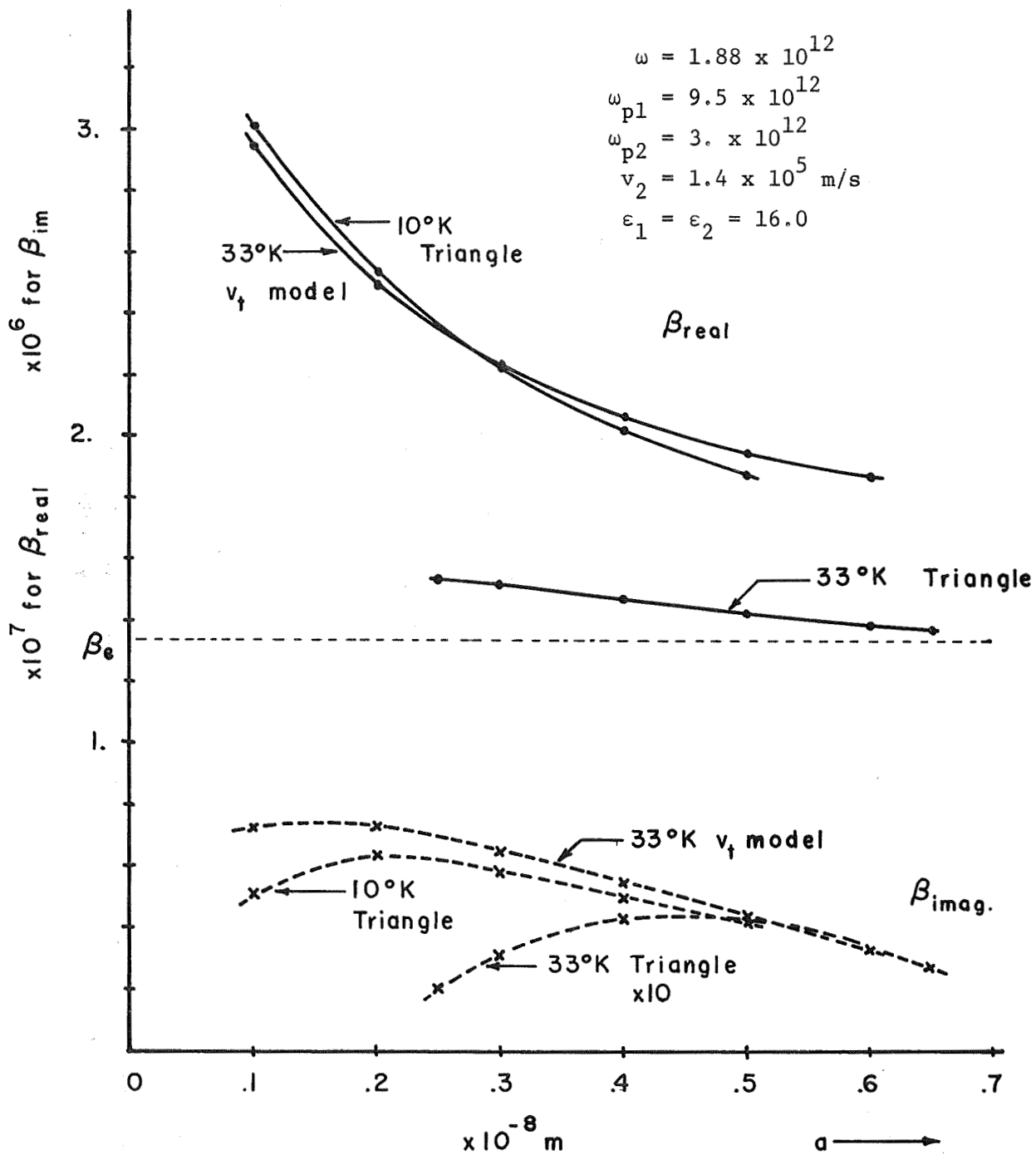
Fig. 22. Complex β as a function of "a" and temperature for optimized parameters with the hydrodynamic (v_t) model and triangle distribution.
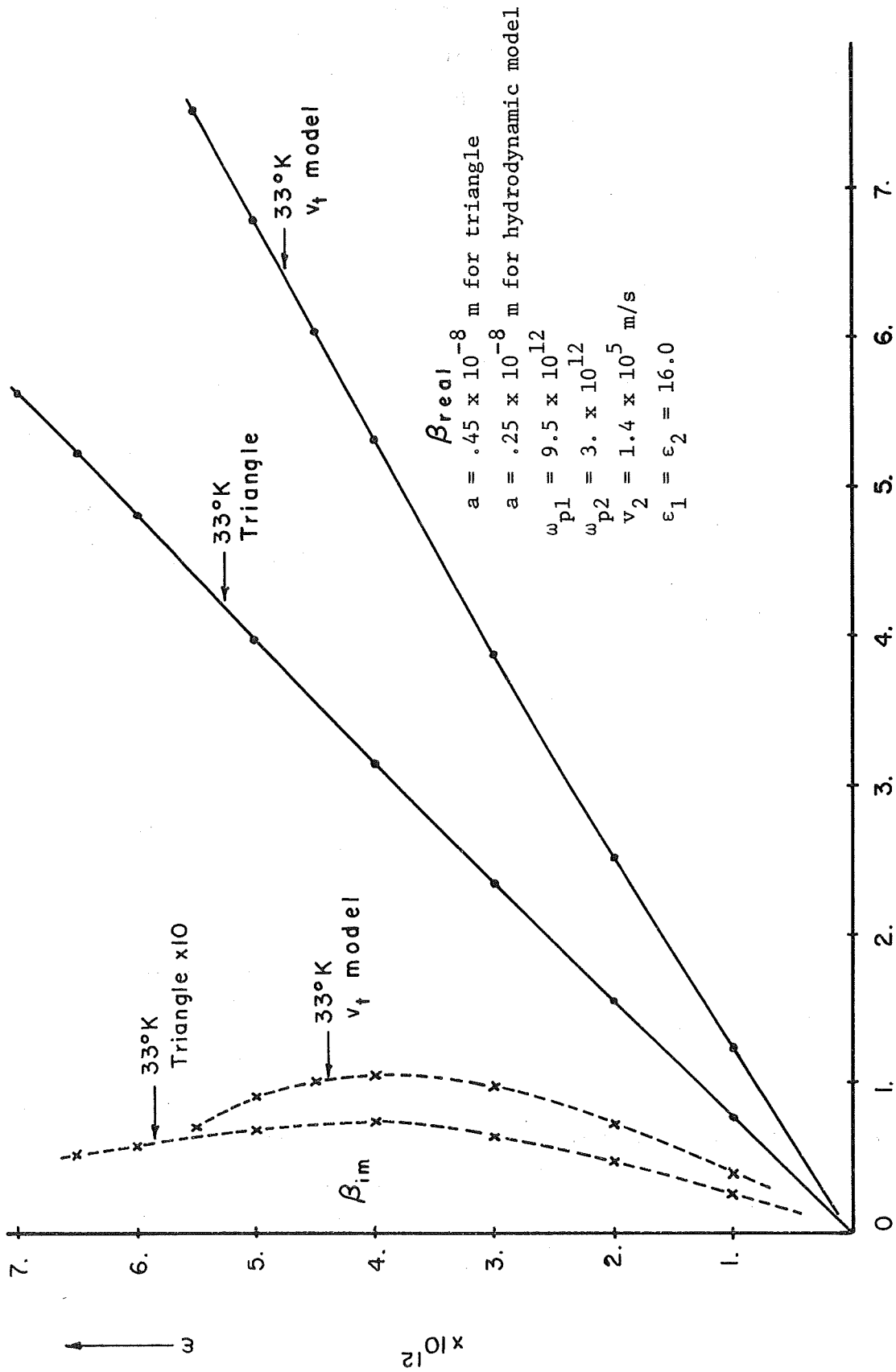
Fig. 23. ω-β diagram for optimized parameters for the hydrodynamic (v_t) model and the triangle velocity distribution.

β_{real}

$a = .45 \times 10^{-8}$ m for triangle

$a = .25 \times 10^{-8}$ m for hydrodynamic model

$\omega_{p1} = 9.5 \times 10^{12}$

$\omega_{p2} = 3. \times 10^{12}$

$v_2 = 1.4 \times 10^5$ m/s

$\varepsilon_1 = \varepsilon_2 = 16.0$

33°K v_t model

33°K Triangle

33°K v_t model

33°K Triangle x10

β_{im}

$x10^7$ for β_{real}

$x10^6$ for β_{im}

ω

$x10^{12}$

tion of these figures. It will be the purpose of this section to describe the more important results.

All the calculations have been made for the configuration illustrated in Fig. 3 and with the material properties for germanium as discussed in Section 5.4. As was shown in Chapter IV, the gain is critically dependent on the thickness of Region 1. It is therefore necessary to first find the propagation characteristics as a function of this thickness "a" before an ω-β diagram can be made. For the figures where β is plotted as a function of "a," the frequency of operation is chosen as 300 GHz. This choice is based on the available plasma frequencies for germanium, but also this is a range where new devices such as oscillators and amplifiers are badly needed.

In Figs. 15 and 16, the results are given for the hydrodynamic model. The important observation to make here is that the gain drops very rapidly with increasing temperature. At 77°K, gain no longer exists. The .02°K curves are given for comparison and are essentially the same as those found in Figs. 10 and 11 for the zero temperature case $\left(\text{except for a scale factor due to a different } v_{drift}\right)$.

Figure 17 gives the results for the Lorentzian distribution. The unbelievably low temperature at which gain disappears is a result that was checked with a great deal of care. A careful hand calculation of the dispersion relation, which will not be given here, verifies the computer results. This result is so bad that an ω-β diagram was not made. It is fortunate that the other distribution functions do not give such a hopeless result.

Figures 18 and 19 give the results for the triangle distribution. Here again the important point to note is that the gain is a strong function of temperature. Although not nearly as bad as the Lorentzian distribution, the gain drops rapidly for temperatures in the 20°K range.

Figures 20 and 21 give the results for the Maxwell-Boltzmann distribution. This is physically the distribution we would expect in the solid, so particular emphasis is to be placed on this result. The most striking observation is made by comparing Figs. 18 to 20 and Figs. 19 to 21. It is evident that the results are very similar. Over most of the range for both β_{real} and $\beta_{imaginary}$, there is agreement to within ± 20 percent. This is a very important result because it indicates that the triangle distribution is a very good approximation to the Maxwell-Boltzmann result. The numerical integration that has to be done for the Maxwell-Boltzmann distribution is time consuming, even on a high speed computer. There is also some loss of accuracy in the numerical integration when $\beta_{imaginary}$ becomes small. Then the denominator term $\left(\omega - \beta v_o \right)^2$ has very large fluctuations with sharp peaks necessitating many more increments in the integration. This further adds to the computer time requirements. The triangle distribution avoids these problems and is, therefore, a very useful approximate technique for finding growing wave solutions.

Some general statements can be made about the effect of the distribution function shape by comparing the results of the Lorentzian, triangle, Maxwell-Boltzmann, and hydrodynamic models:

1. The slope of the distribution function is very important
   and should match the experimental model as closely as pos-
   sible.

2. The velocities that are large compared to v_d, i.e., the
   "tails" of the distribution, are not particularly important
   because they are small in the Maxwell-Boltzmann distribu-
   tion. The approximate distribution function, however, can-
   not have large "tails" as does the Lorentz distribution.
   This reduces the gain severely.

3. The best results will be obtained by straight-line approxi-
   mations. Algebraic equations in powers of v_o will not be
   able to match the slope significantly better, and will
   always have larger values for velocities much greater than
   v_d.

Unsymmetric distributions, such as would be expected at large
electric fields (see Section 5.2), have not been analyzed numerically.
There would be no experimental basis for such an analysis. Data are
not available on what shape the distribution function should have. If
such data do become available, then the simplest method would be to take
the triangle and make the slopes different for the two sides. This would
be a very easy modification in the equations and would probably give some
very interesting results.

The final two figures (22 and 23) represent the theoretical cal-
culations based on an optimized model. The drift velocity, temperature,
thickness of Region 1, and plasma frequency have been adjusted to give

the highest expected gain compatible with experimentally measured material properties. The data for temperature and drift velocity were taken from D. M. Chang and J. G. Ruch.[6] The figures show the results at 33°K for both the hydrodynamic model and the triangle distribution. In Fig. 27, the triangle distribution is also shown for 10°K, assuming the same drift velocity as for 33°K. It is interesting to note how well the hydrodynamic model at 33°K compares to the triangle distribution at 10°K. Evidently the hydrodynamic model is too optimistic in predicting gain at higher temperatures.

5.6. The Effect of Particle Collisions

The subject of charge-carrier collisions in a semiconductor is a difficult one to discuss and is filled with all kinds of conjectures and uncertainties. The basic idea is very simple. An electric field is applied to a semiconductor and a steady current results. The particle acceleration is evidently limited by some process. If particle collisions are postulated which cause the particles periodically to lose their momentum in the direction of the field, then an average collision frequency is the natural result. Postulating such a collision time $\tau = 1/\nu_c$, where ν_c is the collision frequency, the simple steady-state force equation is

$$- |e| \, E = \frac{m^* v}{\tau} \tag{94}$$

---

[6] *Ibid.*

The conductivity for electrons is given as

$$\sigma_e = nq\mu_e$$

where μ_e is the mobility defined by

$$\mu_e = \frac{v}{E}$$

Then

$$\sigma_e = \frac{nqv}{E}$$

and from Eq. 94, for electrons

$$\sigma_e = \frac{nq^2 \tau_e}{m_e^*}$$

Experimentally, we usually know μ, q, and m^*, so it is more convenient to write

$$\tau_e = \frac{\mu_e m_e^*}{q}$$

or if $\tau_e = \frac{1}{\nu_e}$

$$\nu_e = \frac{q}{\mu_e m_e^*} \tag{95}$$

Equation 95 can be calculated for a variety of materials, since

μ and m^* can usually be found in the literature.

For example, consider InSb at 77°K where $m^* \simeq 0.013 \, m_e$ and $\mu_e \simeq 500,000 \, \frac{cm^2}{v \, sec}$. For this case

$$\nu_e \simeq 250 \text{ GHz}$$

This is the simplest possible assumption, but it does accurately predict Ohm's law for a steady-state field. The computer results to be presented in this section were calculated on the basis of this model. However, it cannot be emphasized too strongly that this is only a brief introduction to this subject. The reason why it is done at all is to indicate the lower frequency limit for the proposed device. Collisions will limit the gain in a similar way as the temperature did in Section 5.5. The preferred operating range will be at the higher frequencies, where collision effects do not reduce the gain below useful levels.

An accurate description of the collision problem is really formidable. First, there will certainly be some frequency distribution for the collisions; the particles have a velocity distribution due to temperature and do not travel the same distance between successive collisions. Second, it is a very difficult problem to identify the types of collisions. Are they elastic or not? What is the effective collision cross section? What fraction of the collisions are between the particles themselves and what fraction between particles and the lattice? Does a doped semiconductor behave the same as an intrinsic material or a perfect crystal? Some of these questions have been discussed in the

literature, and with a very complicated model could probably be included in the analysis of the double-stream interaction. It was felt, however, that the complexity of the theory and the uncertainty of obtaining accurate results did not justify the time and effort required. Physically, we expect the gain to decrease at frequencies where the collisions become important. The simple theory should indicate the region of the frequency spectrum where this occurs.

The simple collision model has been numerically analyzed for the hydrodynamic model and the triangle velocity distribution. It is interesting to note that the collision term as derived above is similar to the hydrodynamic equation for thermal velocities. In both cases, the effect is represented by a simple average term. It is, therefore, consistent to use the simple collision theory in the hydrodynamic equation.

Before presenting the results obtained from the computer analysis, it is necessary to show how the collision frequency term modifies the dispersion relations. This will be done for the hydrodynamic model and for the triangle velocity distribution.

To modify the hydrodynamic model and its dispersion relation, consider Eq. 18 in Section 3.4

$$- \frac{|e|}{m} E_z = \left(j\omega + \frac{1}{\tau} - j\beta v_o \right) v_z - j \frac{\beta}{\rho_o} v_t^2 \rho \tag{18}$$

Then following the derivation of Section 3.4 but without omitting $1/\tau$

$$J = \rho_o v + \rho v_o$$

For small ac variations

$$v = \frac{1}{j\beta_e \rho_o}\left(j\beta_e J + \frac{\partial J}{\partial z}\right)$$ (96)

Combining Eq. 18 and Eq. 96 with the ac continuity equation gives the result of Eq. 97 for the current density J

$$J = \frac{\varepsilon_o j\omega \, \omega_p^2 \, E_z}{\left(\omega - \beta v_o - j\nu_c\right)\left(\omega - \beta v_o\right) - \beta^2 v_t^2}$$ (97)

This current density term can now be combined with the wave equation derived in Section 4.1 (Eq. 29)

$$\nabla^2 A + \mu J - \mu\varepsilon \frac{\partial^2 A}{\partial t^2} = 0$$

Following the derivation given in Section 4.1, it is easy to see that the new T^2 for the hydrodynamic model will be given as

$$T^2 = \left(\beta^2 - k^2\right)\left[1 - \frac{\omega_p^2}{\left(\omega - j\nu_c - \beta v_o\right)\left(\omega - \beta v_o\right) - \beta^2 v_t^2}\right]$$ (98)

The collision term is similarly included in the distribution function theory by starting with Eq. 60 of Section 5.1, adding the collision term, and following the derivation step by step.

The new force equation is

$$\left(j\omega + \nu_c - j\, v_{oi} \right) v_i = \frac{-|e|}{m} E_z$$

then

$$v_i = \frac{\eta_i E_z}{\left(j\omega + \nu_c - j\beta v_{oi} \right)}$$

and

$$J_i = \frac{\rho_{oi}\,\eta_i\,E_z}{\left(1 - v_{oi}\frac{\beta}{\omega} \right)\left(j\omega + \nu_c - j\beta v_{oi} \right)} \tag{99}$$

Summing J_i, as was done in Section 5.1, and converting to an integral gives

$$J = -j\omega\epsilon\, E_z\, \omega_{po}^2 \int_{-\infty}^{\infty} \frac{f\!\left(v_o\right) dv_o}{\left(\omega - \beta v_o \right)\left(\omega - j\nu_c - \beta v_o \right)} \tag{100}$$

This will follow through the derivation exactly the same as the integral of Eq. 64, and we will get the new expression for T^2 as

$$T^2 = \left(\beta^2 - k^2 \right)\left[1 - \omega_{po}^2 \int_{-\infty}^{\infty} \frac{f\!\left(v_o\right) dv_o}{\left(\omega - \beta v_o \right)\left(\omega - j\nu_c - \beta v_o \right)} \right] \tag{101}$$

For the hydrodynamic model, the T^2 term is in suitable form for use in the computer program. The distribution function model, however, must be evaluated explicitly for a particular case. As

stated previously, this will be done for a triangle distribution. To evaluate the integral for this case, we once again use Eqs. 86 and 87 for $f\left(v_o\right)$. The method is the same as that used in Section 5.3 immediately following Eq. 86 and 87. The only difference is that, with the collision term included, the terms do not combine as nicely and the final result is more complicated.

Letting

$$\left(v_d - \frac{\omega}{\beta}\right) = A$$

and

$$\left(v_d - \frac{\omega}{\beta} + j\frac{\nu_c}{\beta}\right) = C$$

the final result is

$$\int_{-\infty}^{\infty} \frac{f\left(v_o\right) dv_o}{\left(\frac{\omega}{\beta} - v_o\right)\left(\frac{\omega}{\beta} - j\frac{\nu_c}{\beta} - v_o\right)} = \frac{1}{j\nu_c b^2}\left\{ \left(\omega - v_d\beta\right)\log\left|\frac{A^2\left(C^2 - b^2\right)}{C^2\left(A^2 - b^2\right)}\right|\right.$$

$$\left. + j\nu_c \log\left|\frac{c^2}{c^2 - b^2}\right| - b\beta \log\left|\frac{(A - b)(C + b)}{(C - b)(A + b)}\right|\right\}$$

(102)

Equation 102 can now be easily combined with Eq. 101 and the result is then suitable for use with the computer.

Figures 24 through 28 give the results obtained for the hydrodynamic model and the triangle velocity distribution function. The com-
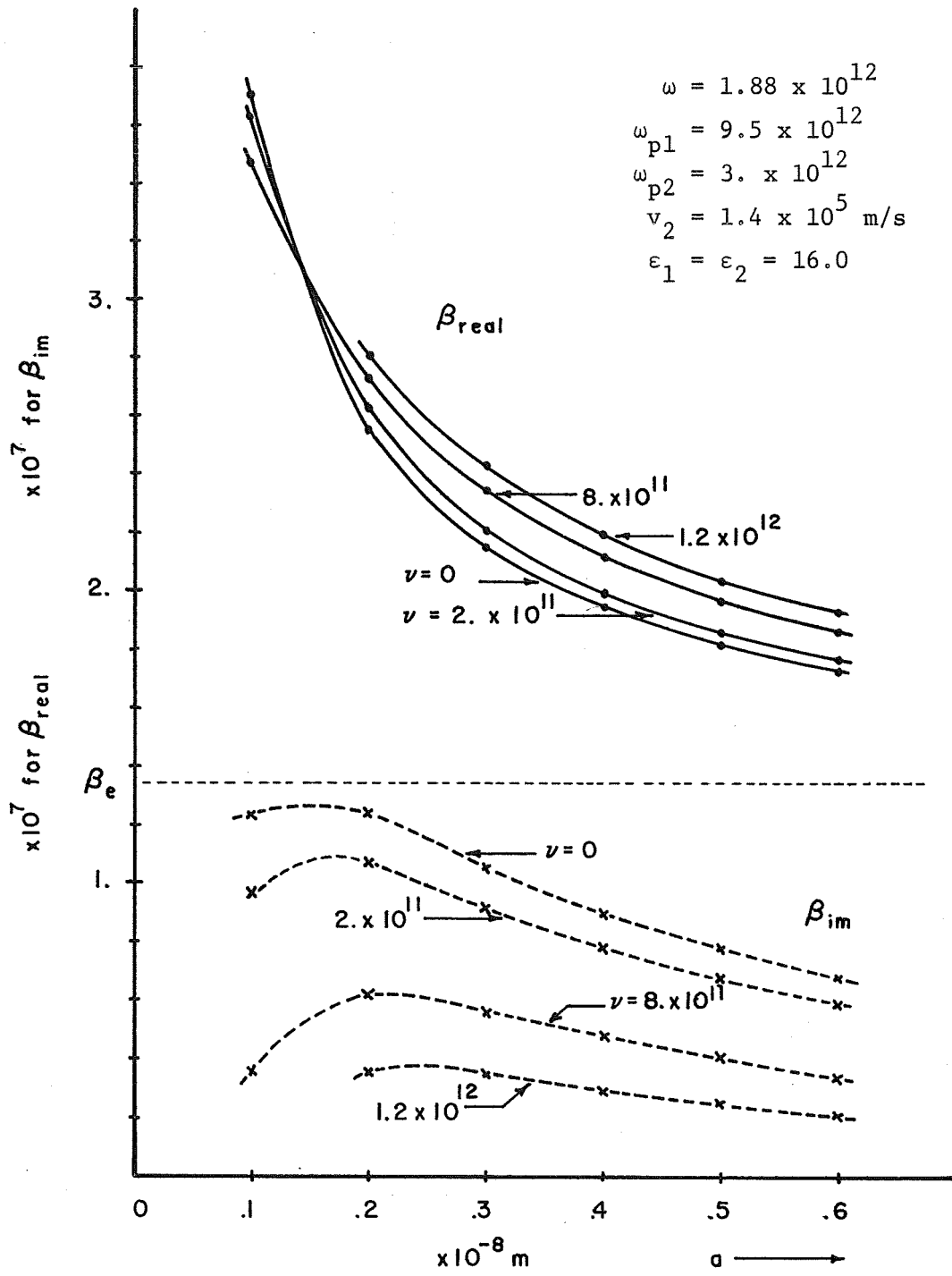
Fig. 24. Complex β as a function of "a" and the collision
frequency ν for optimized parameters at 0°K.
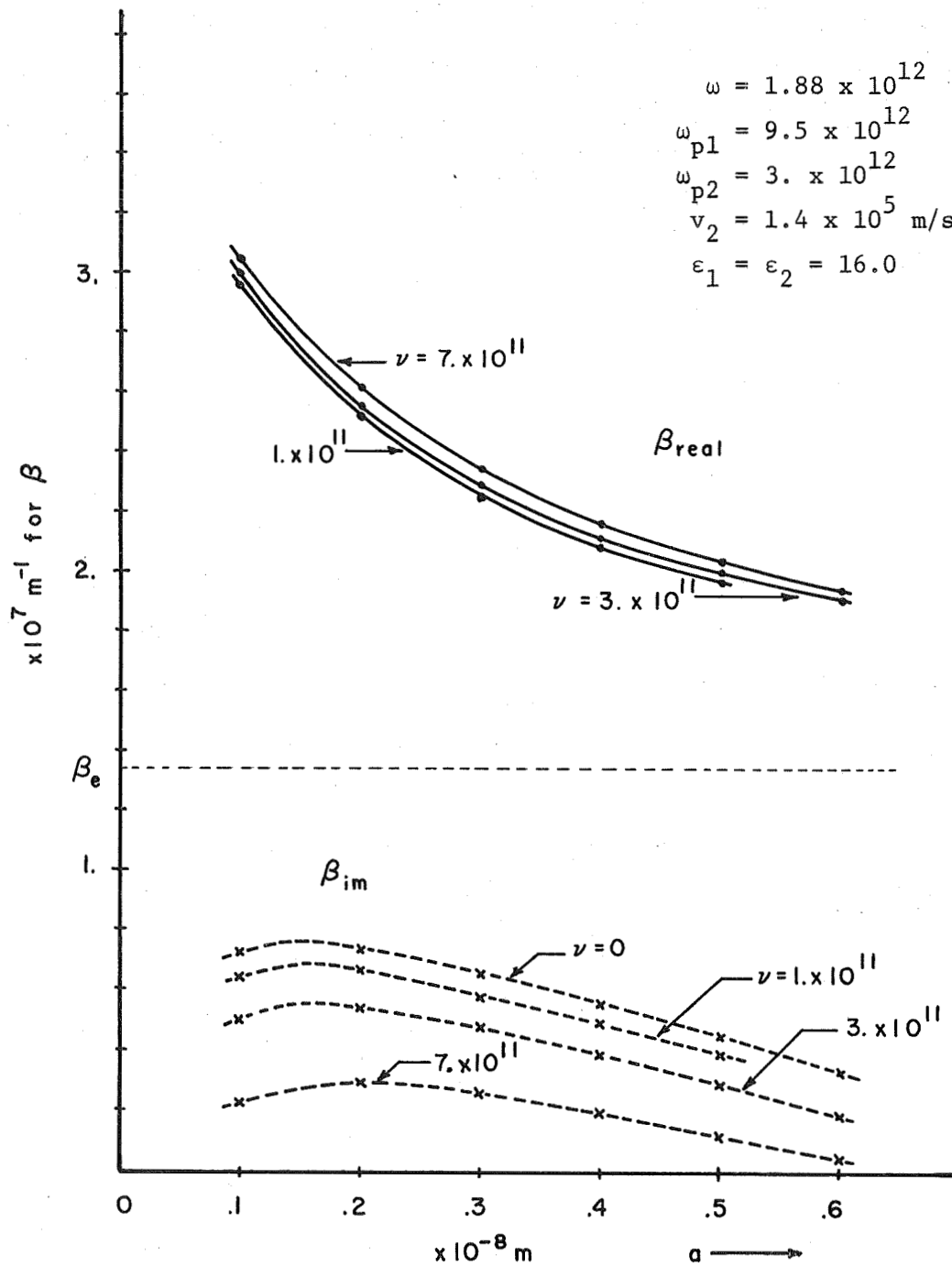
Fig. 25.   Complex β as a function of "a" and "ν" for optimized
parameters with the hydrodynamic model at 33°K.
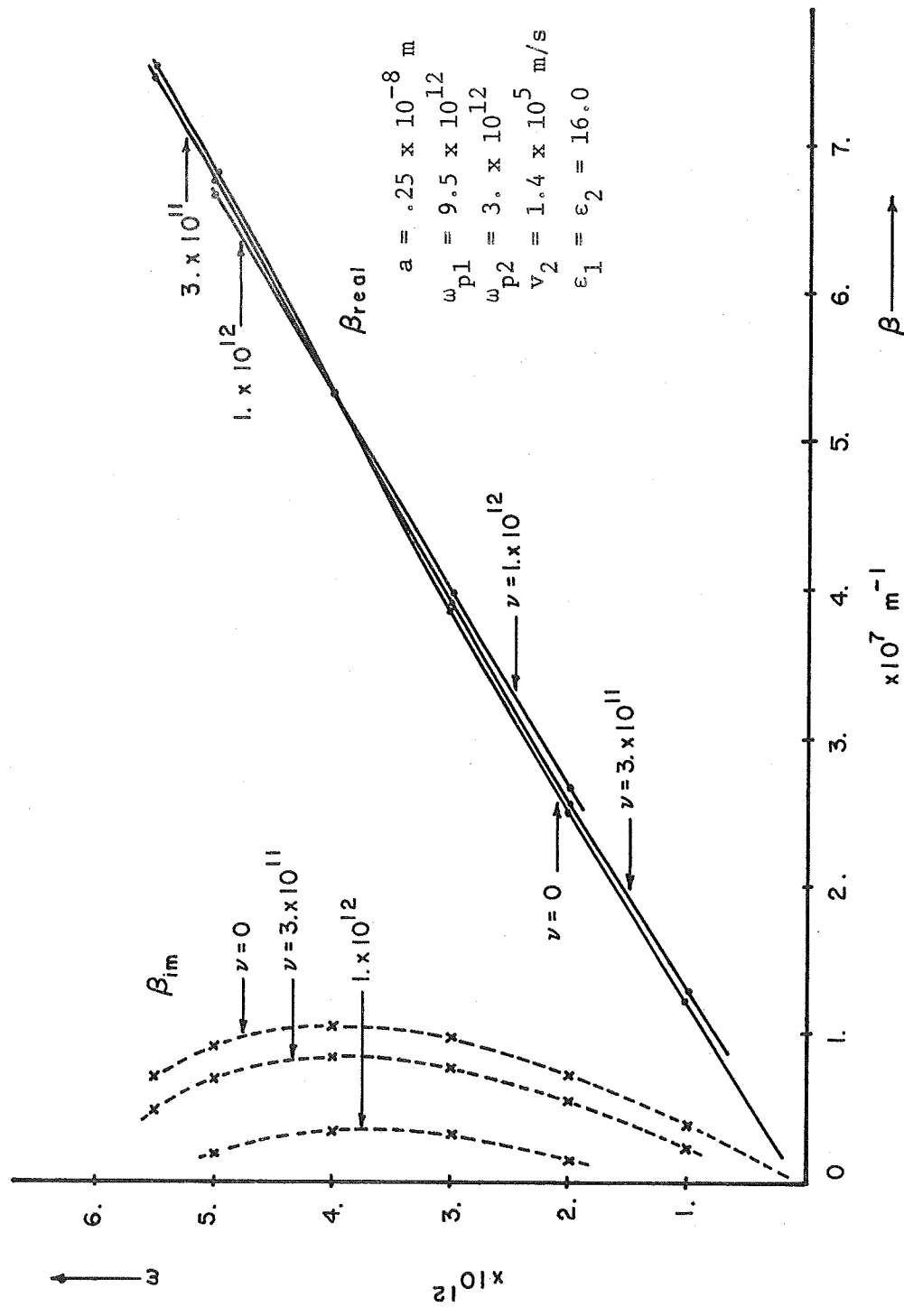
Fig. 26. ω-β diagram for optimized parameters for the hydrodynamic model at 33°K, including particle collisions.

Parameters shown in figure:

$a = .25 \times 10^{-8}$ m

$\omega_{p1} = 9.5 \times 10^{12}$

$\omega_{p2} = 3. \times 10^{12}$

$v_2 = 1.4 \times 10^{5}$ m/s

$\epsilon_1 = \epsilon_2 = 16.0$

Curve labels: β_{real}, β_{im}

$\nu = 0$, $\nu = 3. \times 10^{11}$, $\nu = 1. \times 10^{12}$

Axes: β ($\times 10^{7}$ m^{-1}), ω ($\times 10^{12}$)
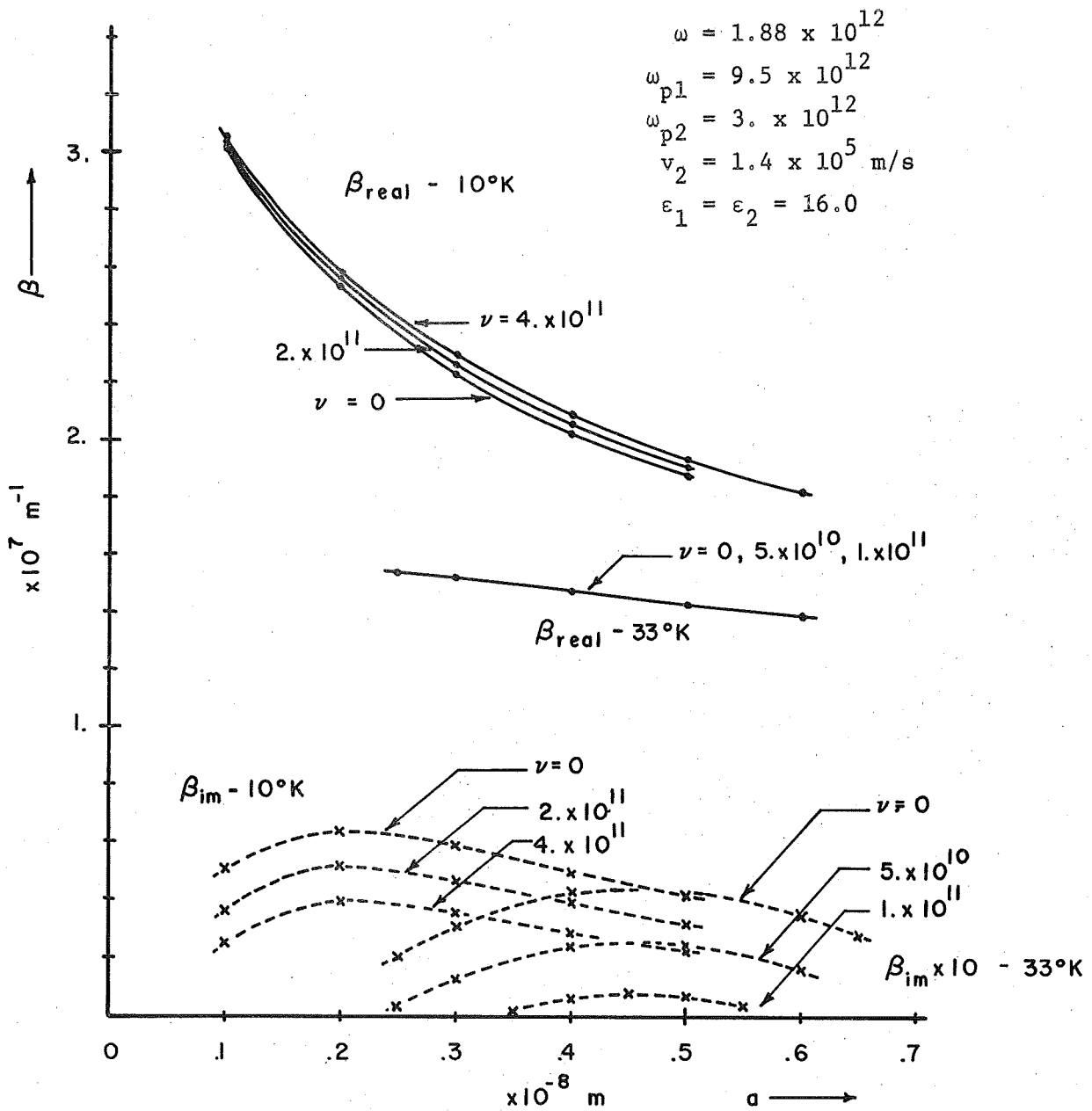
Fig. 27. Complex β as a function of "a" and "ν" for
optimized parameters with the triangle
velocity distribution at 10°K and 33°K.

$\nu = 0$

3×10^{10}

$\nu = 0$
3×10^{10}

1×10^{11}

$\nu = 1 \times 10^{11}$

$a = .45 \times 10^{-8}$ m
$\omega_{p1} = 9.5 \times 10^{12}$
$\omega_{p2} = 3. \times 10^{12}$
$v_2 = 1.4 \times 10^5$ m/s
$\varepsilon_1 = \varepsilon_2 = 16.0$

——— $= \beta_{real}$
--x-- $= \beta_{im}$

$\times 10^7$ for β_{real} $\times 10^5$ for β_{im}

0   1.   2.   3.   4.   5.   6.   7.   8.

ω

$\times 10^{12}$

7.   6.   5.   4.   3.   2.   1.
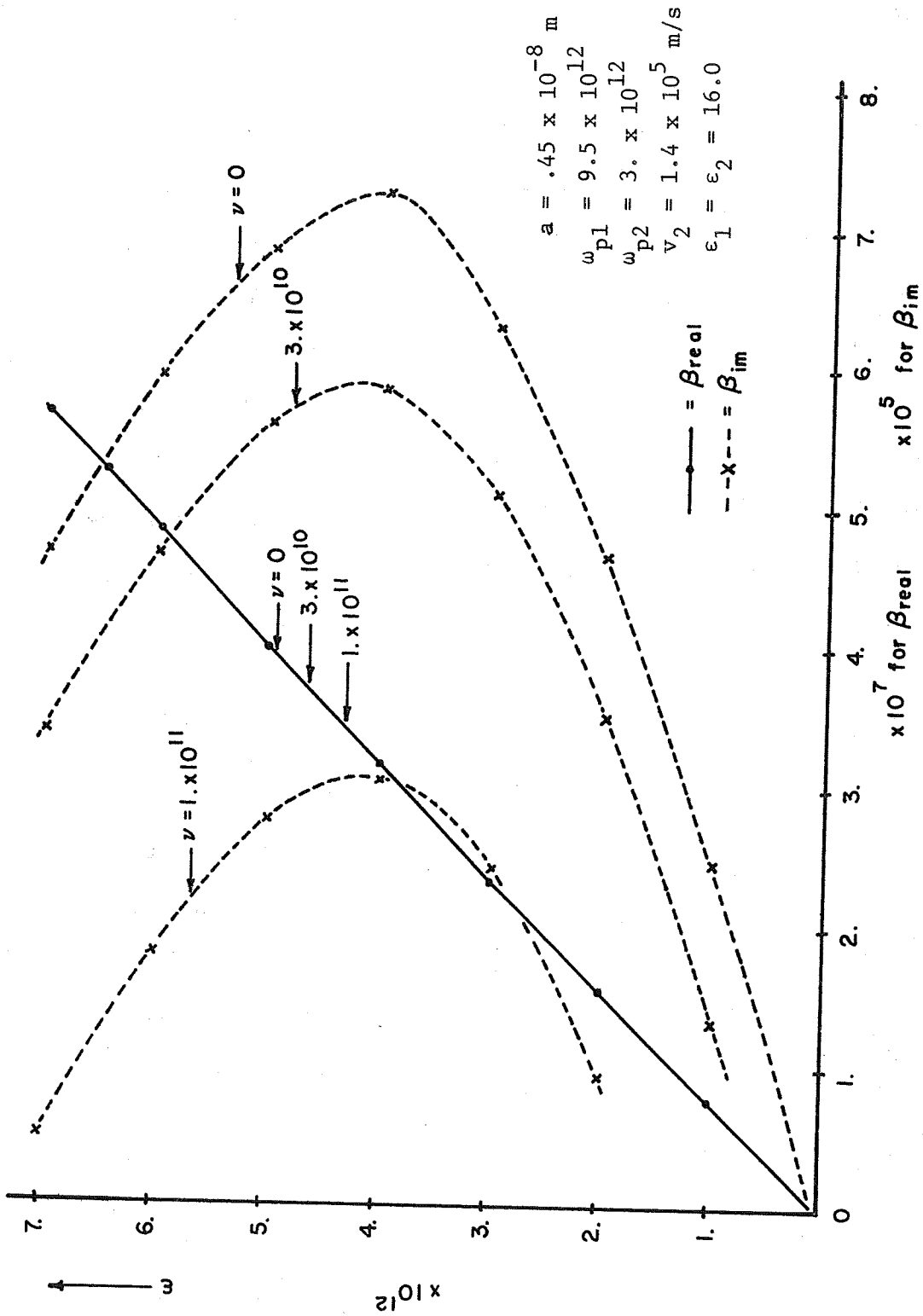
Fig. 28. ω-β diagram for optimized parameters for the triangle
velocity distribution at 33°K including particle collisions.

puter results were obtained for the optimized free-space model that was previously analyzed in Section 5.5 (Figs. 22 and 23). Figure 24 shows the effect of changing the collision frequency but keeping the temperature at 0°K. This shows the effect of only the collisions. Figures 25 and 26 consider the same problem at 33°K. Figure 25 shows the gain and propagation as a function of the thickness and Fig. 26 is the ω-β diagram. It should be noted that with $\nu = 0$, the curves are exactly those of Figs. 22 and 23. Figures 27 and 28 give the corresponding results for the triangle velocity distribution. Figure 27 shows the results for both 10°K and 33°K as a function of the thickness "a." Figure 28 is the corresponding ω-β diagram. The important results from these figures are as follows:

1. The gain is reduced linearly in both the hydrodynamic model and triangle velocity distribution model as the collision frequency is increased.

2. If the gain is already low when ν_c is not included in the theory, then gain will not be possible at all unless the operating frequency is significantly above ν_c.

3. Collision frequencies for semiconductors are in the 200 to 300 GHz range at 77°K. When these values are used in the gain calculations, it shows that device operation at or below the collision frequency is marginal.

4. The highest plasma frequencies possible in semiconductors correspond to about 10 μ in wavelength. It appears possible that the interaction could be useful in the 500 GHz

to 10 μ range, where at present there is a need for gener-
ators and amplifiers. However, the next chapters will show
that other effects, such as transverse velocities and cou-
pling of energy from the sample, add serious problems to the
practical realization of these devices.

VI. TRANSVERSE AC VELOCITIES

In previous chapters, the analysis was developed assuming that it is possible to realize space-charge bunching in the direction of the drifting stream of charges. This is almost always possible in electron beam devices, although the beam border may no longer be uniform and may have a rippling due to the space-charge bunching. The boundaries of a semiconductor, however, are fixed and well defined, so that it may not be possible to apply the electron beam results directly. Most of the solid-state devices that have been proposed as analogues to the familiar electron beam interactions have been analyzed without consideration of this problem. Including transverse velocities increases the complexity of the mathematics tremendously. When they are neglected, it is usually for this reason and not because their existence is unknown.

In this chapter, the double-stream interaction including transverse ac velocities will be analyzed for a simple case of zero temperature and no collisions. The simplification to zero temperature and no collisions is made for two reasons:

1. The analysis is rather complicated mathematically and can be better interpreted if other effects are not included to confuse the result.

2. In most analyses, the problem is usually completely ignored, so it is particularly interesting to illustrate just how important this effect is on the idealized gain mechanism.

6.1. Derivation of the Wave Equations

For this analysis, we will use the familiar small-signal assumption to derive the wave equations. Assuming the usual $e^{j(\omega t - \beta z)}$ wave propagation, Maxwell's curl equations become

$$\nabla \times \vec{E} = -j\omega\mu\vec{H} \tag{103}$$

$$\nabla \times \vec{H} = j\omega\varepsilon\vec{E} + \vec{J} \tag{104}$$

and the force equation may be written as

$$\left(j\omega + \vec{v}_o \cdot \nabla\right)\vec{v} = \eta\left(\vec{E} + \vec{v}_o \times \vec{B}\right) \tag{105}$$

The $\left(\vec{v}_o + \vec{v}\right) \times \vec{B}_o$ and $\vec{v} \times \vec{B}$ terms have been neglected in Eq. 105 because $B_o = 0$, and $\vec{v} \times \vec{B}$ is a second-order term always neglected in small-signal analyses.

The usual small-signal current density and continuity equations are given by Eqs. 106 and 107

$$\vec{J} = \rho_o\vec{v} + \rho\vec{v}_o \tag{106}$$

$$\nabla \cdot \vec{J} = -j\omega\rho \tag{107}$$

These equations can be separated into transverse and longitudinal parts if we assume a dc drift velocity in the z direction, $\vec{v}_o = v_o\hat{z}$; then

$$\vec{J}_t = \rho_o \vec{v}_t \qquad (108)$$

$$J_z = \rho_o v_z + \rho v_o \qquad (109)$$

$$\nabla_t \cdot \vec{J}_t - j\beta J_z = -j\omega\rho \qquad (110)$$

$$j(\omega - \beta v_o)\vec{v}_t = \eta_t(\vec{E}_t + v_o \hat{z} \times \vec{B}_t) \qquad (111)$$

$$j(\omega - \beta v_o)v_z = \eta_z E_z \qquad (112)$$

The "t" and "z" subscripts refer to the transverse and longitudinal components, respectively.

A point of interest in Eqs. 111 and 112 is that η has been written as η_t and η_z. η is usually defined as $\eta = \epsilon/m^*$, where m^* is the effective mass. There are very few known solids that have an isotropic m^*. m^* is usually a strong function of the crystal structure and hence the orientation of the sample. In general, we would have to write m_x^*, m_y^*, and m_z^* and the corresponding η's. This makes the problem very complicated. The basic results can be obtained just as well if we assume only one transverse value. Then it is only necessary to write two sets of equations instead of three.

The preferred orientation for the material is to have the largest η in the direction of the dc electric field. When η is large, m^* is small, and this gives the highest conductivity. In the following analysis, η_z will be assumed to be the "best" value. Furthermore, we

will assume that η_t can be written as

$$\eta_t = \alpha\eta_z \text{ where } 0 \leq \alpha \leq 1 \tag{113}$$

When $\alpha = 0$ in Eq. 113, we get just the one-dimensional model of previous chapters. When $\alpha = 1$, then we have an isotropic material. Now, combining Eqs. 108, 111, and 113

$$\vec{J}_t = \frac{\alpha\rho_o\eta_z}{j(\omega - \beta v_o)} \left[\vec{E}_t + v_o\hat{z} \times \vec{B}_t \right] \tag{114}$$

Similarly, combining Eqs. 109, 110, and 112

$$J_z = \frac{\rho_o\eta_z\omega E_z}{j(\omega - \beta v_o)^2} + \frac{jv_o\nabla_t \cdot \vec{J}_t}{(\omega - \beta v_o)} \tag{115}$$

The curl equations are now separated into transverse and longitudinal components.

$$\nabla_t \times \vec{E}_z + \nabla_z \times \vec{E}_t = -j\omega\mu\vec{H}_t \tag{116}$$

$$\nabla_t \times \vec{E}_t = -j\omega\mu\vec{H}_z \tag{117}$$

$$\nabla_t \times \vec{H}_z + \nabla_z \times \vec{H}_t = j\omega\epsilon\vec{E}_t + \vec{J}_t \tag{118}$$

$$\nabla_t \times \vec{H}_t = j\omega\epsilon\vec{E}_z + \vec{J}_z \tag{119}$$

Substituting Eq. 114 into 118

$$\nabla_t \times \vec{H}_z + \nabla_z \times \vec{H}_t = j\omega\varepsilon \left[\left(1 - \frac{\alpha\omega_p^2}{\omega(\omega - \beta v_o)} \right) \vec{E}_t \right.$$

$$\left. - \frac{\alpha\omega_p^2 v_o}{\omega(\omega - \beta v_o)} \left(\hat{z} \times \vec{B}_t \right) \right]$$

(120)

The plasma frequency ω_p in Eq. 120 has the usual definition

$$\omega_p^2 = \frac{\rho_o \eta_z}{\varepsilon}$$

(121)

Substituting Eq. 114 into Eq. 115 and then putting this result into Eq. 119, we get

$$\left[1 + \frac{\alpha\omega_p^2 v_o^2 \varepsilon\mu}{\left(\omega - \beta v_o\right)^2} \right] \left(\nabla_t \times \vec{H}_t \right) = j\omega\varepsilon \left[1 - \frac{\omega_p^2}{\left(\omega - \beta v_o\right)^2} \right] E_z$$

(122)

$$+ \frac{\alpha v_o \varepsilon\omega_p^2}{\left(\omega - \beta v_o\right)^2} \nabla_t \cdot \vec{E}_t$$

Equations 116, 117, 120 and 122 form a new set of curl equations which no longer contain an explicit current density term. These equations can now be solved to obtain the wave equations for E_z and H_z.

Equations 116 and 120 can be simplified somewhat by observing
that

$$\nabla_z \times \vec{E}_t = -j\beta\hat{z} \times \vec{E}_t$$

and similarly for $\nabla_z \times \vec{H}_t$. Then,

$$\nabla_t \times \vec{E}_z - j\beta\hat{z} \times \vec{E}_t = -j\omega\mu\vec{H}_t \qquad (123)$$

and

$$\nabla_t \times \vec{H}_z - j\beta \left[1 - \frac{\alpha\omega_p^2 v_o \varepsilon\mu}{\beta(\omega - \beta v_o)} \right] \hat{z} \times \vec{H}_t \qquad (124)$$

$$= j\omega\varepsilon \left[1 - \frac{\alpha\omega_p^2}{\omega(\omega - \beta v_o)} \right] \vec{E}_t$$

Solving Eq. 123 for $\vec{H}_t$

$$\vec{H}_t = \frac{j}{\omega\mu} \nabla_t \times \vec{E}_z + \frac{\beta}{\omega\mu} \hat{z} \times \vec{E}_t \qquad (125)$$

Taking the vector cross product of Eq. 125 with $\hat{z}$

$$\hat{z} \times \vec{H}_t = \frac{j}{\omega\mu} \hat{z} \times \left(\nabla_t \times \vec{E}_z \right) + \frac{\beta}{\omega\mu} \hat{z} \times \left(\hat{z} \times \vec{E}_t \right) \qquad (126)$$

But

$$\hat{z} \times \left(\hat{z} \times \vec{E}_t \right) = -\vec{E}_t \qquad (127)$$

and

$$\hat{z} \times \left(\nabla_t \times \vec{E}_z \right) = \nabla_t \vec{E}_z \qquad (128)$$

Vector identities such as Eqs. 127 and 128 will be used throughout this analysis. They have been derived by simple application of the general definitions. No particular purpose would be served by showing these derivations in detail.

Replacing the appropriate terms in Eq. 126 by those of Eqs. 127 and 128

$$\hat{z} \times \vec{H}_t = \frac{j}{\omega\mu} \nabla_t E_z - \frac{\beta}{\omega\mu} \vec{E}_t \qquad (129)$$

Equation 129 can now be used in Eq. 124

$$\vec{\nabla}_t \times \vec{H}_z - j\beta \left[1 - \frac{\alpha\omega_p^2 v_o \epsilon\mu}{\beta\left(\omega - \beta v_o\right)} \right] \left[\frac{j}{\omega\mu} \nabla_t E_z - \frac{\beta}{\omega\mu} \vec{E}_t \right]$$

$$= j\omega\epsilon \left[1 - \frac{\alpha\omega_p^2}{\omega\left(\omega - \beta v_o\right)} \right] \vec{E}_t \qquad (130)$$

By simple algebraic manipulation, Eq. 130 can be solved for $\vec{E}_t$

$$\vec{E}_t = \frac{\nabla_t \times \vec{H}_z + \dfrac{\beta}{\omega\mu}\left[1 - \dfrac{\alpha\omega_p^2 v_o \epsilon\mu}{\beta(\omega - \beta v_o)}\right]\vec{\nabla}_t E_z}{j\omega\epsilon\left[1 - \dfrac{\alpha\omega_p^2}{\omega^2} - \dfrac{\beta^2}{k^2}\right]} \tag{131}$$

Now, putting Eq. 131 back into Eq. 117

$$\frac{\nabla_t \times \left(\nabla_t \times \vec{H}_z\right) + \dfrac{\beta}{\omega\mu}\left[1 - \dfrac{\alpha\omega_p^2 v_o \epsilon\mu}{\beta(\omega - \beta v_o)}\right]\nabla_t \times \nabla_t E_z}{j\omega\epsilon\left[1 - \dfrac{\alpha\omega_p^2}{\omega^2} - \dfrac{\beta^2}{k^2}\right]} = -j\omega\mu H_z \tag{132}$$

But,

$$\nabla_t \times \nabla_t E_z = 0$$

and

$$\nabla_t \times \left(\nabla_t \times H_z\right) = -\nabla_t^2 H_z \hat{z}$$

Then Eq. 132 reduces to Eq. 133

$$\nabla_t^2 H_z + \left[k^2\left(1 - \dfrac{\alpha\omega_p^2}{\omega^2}\right) - \beta^2\right]H_z = 0 \tag{133}$$

Equation 133 is the general wave equation for H_z. It is interesting to note that for wave propagation which satisfies this H_z equation

$$\varepsilon' = \varepsilon \left(1 - \frac{\alpha \omega_p^2}{\omega^2} \right)$$

can be thought of as an effective dielectric constant.

The wave equation for E_z can be obtained in a similar manner by combining Eqs. 116, 120 and 122. From Eq. 122 and Eq. 125, which was derived from Eq. 116,

$$\left[1 + \frac{\alpha \omega_p^2 v_o^2 \varepsilon \mu}{\left(\omega - \beta v_o \right)^2} \right] \left[\frac{j}{\omega \mu} \nabla_t \times \left(\nabla_t \times \vec{E}_z \right) + \frac{\beta}{\omega \mu} \nabla_t \times \left(\hat{z} \times \vec{E}_t \right) \right]$$

(134)

$$= j \omega \varepsilon \left[1 - \frac{\omega_p^2}{\left(\omega - \beta v_o \right)^2} \right] E_z + \frac{\alpha v_o \varepsilon \omega_p^2}{\left(\omega - \beta v_o \right)^2} \nabla_t \cdot \vec{E}_t$$

But

$$\nabla_t \times \left(\hat{z} \times E_t \right) = \nabla_t \cdot \vec{E}_t \hat{z}$$

and

$$\nabla_t \times \left(\nabla_t \times E_z \right) = -\nabla_t^2 E_z \hat{z}$$

which simplifies Eq. 134 as follows:

$$-\frac{j}{\omega\mu}\left[1 + \frac{v_o^2\,\alpha\omega_p^2\,\varepsilon\mu}{\left(\omega - \beta v_o\right)^2}\right]\nabla_t^2 E_z + \left[\frac{\beta}{\omega\mu} - \frac{\alpha v_o\,\varepsilon\omega_p^2}{\omega\left(\omega - \beta v_o\right)}\right]\nabla_t \cdot \vec{E}_t$$

$$\text{(135)}$$

$$= j\omega\varepsilon\left[1 - \frac{\omega_p^2}{\left(\omega - \beta v_o\right)^2}\right]E_z$$

Substituting Eq. 131 for $\vec{E}_t$ into Eq. 135

$$-\frac{j}{\omega\mu}\left[1 + \frac{v_o^2\,\alpha\omega_p^2\,\varepsilon\mu}{\left(\omega - \beta v_o\right)^2}\right]\nabla_t^2 E_z + \left[\frac{\beta}{\omega\mu} - \frac{\alpha v_o\,\varepsilon\omega_p^2}{\omega\left(\omega - \beta v_o\right)}\right]$$

$$\text{(136)}$$

$$\left[\frac{\dfrac{\beta}{\omega\mu}\left(1 - \dfrac{\alpha\omega_p^2\,v_o\,\varepsilon\mu}{\beta\left(\omega - \beta v_o\right)}\right)}{j\omega\varepsilon\left(1 - \dfrac{\alpha\omega_p^2}{\omega^2} - \dfrac{\beta^2}{k^2}\right)}\right]\nabla_t^2 E_z = j\omega\varepsilon\left[1 - \frac{\omega_p^2}{\left(\omega - \beta v_o\right)^2}\right]E_z$$

Equation 136 can be simplified considerably by simple algebraic manipulation. The simplified result is given by Eq. 137, which is the general wave equation for E_z.

$$\nabla_t^2 E_z + \frac{\left[1 - \dfrac{\omega_p^2}{\left(\omega - \beta v_o\right)^2}\right]\left[k^2\left(1 - \dfrac{\alpha\omega_p^2}{\omega^2}\right) - \beta^2\right]}{1 - \dfrac{\alpha\omega_p^2}{\omega^2}\left[\dfrac{\omega^2 - v_o^2 k^2}{\left(\omega - \beta v_o\right)^2}\right]} E_z = 0 \tag{137}$$

This wave equation can be written in the familiar form

$$\nabla_t^2 E_z - T^2 E_z = 0$$

The T^2 term is then defined as in Eq. 138

$$T^2 = \frac{\left[\beta^2 - k^2\left(1 - \dfrac{\alpha\omega_p^2}{\omega^2}\right)\right]\left[1 - \dfrac{\omega_p^2}{\left(\omega - \beta v_o\right)^2}\right]}{1 - \dfrac{\alpha\omega_p^2}{\omega^2}\left[\dfrac{\omega^2 - v_o^2 k^2}{\left(\omega - \beta v_o\right)^2}\right]} \tag{138}$$

when $\alpha = 0$, we get

$$T^2 = \left(\beta^2 - k^2\right)\left[1 - \frac{\omega_p^2}{\left(\omega - \beta v_o\right)^2}\right] \tag{139}$$

which is just the result we derived in Section 4.2 for the one-dimensional model with no temperature or collision effects.

With two wave equations for H_z and E_z, Eqs. 133 and 137, we are now in a position to derive the dispersion relations. The one

additional equation that is required is a relation between $\vec{E}_z$ and $\vec{H}_t$. This is needed to match the boundary conditions as was done in Chapter IV. In general, it would be necessary to know both $\vec{H}_t$ and $\vec{E}_t$. For the configuration of Chapter IV, however, only $\vec{H}_t$ is required. From Eq. 131

$$\vec{E}_t = \frac{\nabla_t \times H_z + \frac{\beta}{\omega\mu}\left[1 - \frac{\alpha\omega_p^2 v_o \varepsilon\mu}{\beta(\omega - \beta v_o)}\right]\nabla_t E_z}{j\omega\varepsilon\left[1 - \frac{\alpha\omega_p^2}{\omega^2} - \frac{\beta^2}{k^2}\right]} \tag{131}$$

Since we will require only $\vec{E}_z$ and $\vec{H}_t$ to match boundary conditions, it is entirely acceptable to the solution to assume that $H_z = 0$. This corresponds to TM modes in wave guide theory. Another way to explain this is to note that we were able to write separate wave equations for E_z and H_z. Then E_z and H_z modes are not coupled and the solutions are expressible in terms of TM or TE modes.

Then assuming $H_z = 0$

$$\vec{E}_t = \frac{-j\beta\left[1 - \frac{\alpha\omega_p^2 v_o \varepsilon\mu}{\beta(\omega - \beta v_o)}\right]\nabla_t E_z}{k^2\left(1 - \frac{\alpha\omega_p^2}{\omega^2}\right) - \beta^2} \tag{140}$$

Equation 140 can now be substituted into Eq. 125 to get a relation between $\vec{H}_t$ and $\vec{E}_z$.

$$\vec{H}_t = \frac{j}{\omega\mu} \nabla_t \times E_z - \frac{\frac{j\beta^2}{\omega\mu}\left[1 - \frac{\alpha\omega_p^2 v_o \varepsilon\mu}{\beta\left(\omega - \beta v_o\right)}\right] \hat{z} \times \nabla_t E_z}{k^2\left(1 - \frac{\alpha\omega_p^2}{\omega^2}\right) - \beta^2} \tag{141}$$

But

$$\hat{z} \times \nabla_t E_z = -\nabla_t \times E_z$$

Therefore,

$$\vec{H}_t = \frac{jk^2}{\omega\mu} \left[\frac{1 - \frac{\alpha\omega_p^2}{\omega\left(\omega - \beta v_o\right)}}{\beta^2 - k^2\left(1 - \frac{\alpha\omega_p^2}{\omega^2}\right)}\right] \hat{z} \times \nabla_t E_z \tag{142}$$

With the general equations derived in this section, it is now possible to analyze many different configurations. The ones of particular interest will be considered in the following sections.

6.2. Effect of Transverse Velocities on the Layered Structure

The limiting case of $\alpha = 0$ was shown (in Section 6.1) to reduce the equations to the one-dimensional analysis of Chapter IV. In this section, we will consider the situation when $0 < \alpha \leq 1$, and apply this case to the layered structure with metal boundaries that was analyzed in Section 4.2. This is mathematically the simplest model

and will be illustrative of what can be expected in other configurations.

To begin, let us rederive the dispersion relation with transverse velocities included. The configuration is that of Fig. 2. For the coordinates used in Fig. 2, $\vec{H}_t \rightarrow H_y$. With only an H_y component,

$$\hat{z} \times \nabla_t E_z = \frac{\partial}{\partial x} E_z \hat{y}$$

Then Eq. 142 becomes

$$H_y = \frac{jk^2}{\omega\mu} \left[\frac{1 - \dfrac{\alpha\omega_p^2}{\omega(\omega - \beta v_o)}}{\beta^2 - k^2\left(1 - \dfrac{\alpha\omega_p^2}{\omega^2}\right)} \right] \frac{\partial}{\partial x} E_z \qquad (143)$$

Following the derivation of Section 4.2, assume the same field dependence in Region 1 and Region 2.

$$E_{z1} = B_1 \sinh T_1 (a - x)$$

$$E_{z2} = B_2 \sinh T_2 (b + x)$$

Match the E_z and H_y fields at $x = 0$

$$E_{z1} = E_{z2}$$

$$B_1 \sinh\left(T_1 a\right) = B_2 \sinh\left(T_2 b\right) \qquad (144)$$

and

$$H_{y1} = H_{y2}$$

$$-k_1^2 \left[\frac{1 - \dfrac{\alpha \omega_{p1}^2}{\omega(\omega - \beta v_{o1})}}{\beta^2 - k_1^2 \left(1 - \dfrac{\alpha \omega_{p1}^2}{\omega^2}\right)} \right] B_1 T_1 \cosh\left(T_1 a\right)$$

$$= k_2^2 \left[\frac{1 - \dfrac{\alpha \omega_{p2}^2}{\omega(\omega - \beta v_{o2})}}{\beta^2 - k_2^2 \left(1 - \dfrac{\alpha \omega_{p2}^2}{\omega^2}\right)} \right] B_2 T_2 \cosh\left(T_2 b\right)$$

(145)

For simplicity, α has been assumed to be the same in Region 1 and
Region 2.

Combining Eqs. 144 and 145 to eliminate B_1 and B_2

$$- \left[\frac{\beta^2 - k_1^2 \left(1 - \dfrac{\alpha \omega_{p1}^2}{\omega^2}\right)}{1 - \dfrac{\alpha \omega_{p1}^2}{\omega(\omega - \beta v_{o1})}} \right] \frac{\tanh\left(T_1 a\right)}{k_1^2 T_1}$$

(146)

$$= \left[\frac{\beta^2 - k_2^2 \left(1 - \dfrac{\alpha \omega_{p2}^2}{\omega^2}\right)}{1 - \dfrac{\alpha \omega_{p2}^2}{\omega(\omega - \beta v_{o2})}} \right] \frac{\tanh\left(T_2 b\right)}{k_2^2 T_2}$$

- 142 -

This is the dispersion relation that must be solved in general to get

the propagation characteristics as a function of α.

To check the result, when $\alpha = 0$, Eq. 146 becomes

$$- \left(\beta^2 - k_1^2\right) \frac{\tanh\left(T_1 a\right)}{k_1^2 T_1} = \left(\beta^2 - k_2^2\right) \frac{\tanh\left(T_2 b\right)}{k_2^2 T_2} \tag{147}$$

where the T's are now given by Eq. 139. As expected, this result is

identical to the one-dimensional analysis of Section 4.2 (Eq. 47).

The investigation of Eq. 146 for $0 < \alpha < 1$ was done using the

computer techniques described in Chapters IV and V. The results of

this investigation are summarized in Figs. 29 and 30. First, the

propagation constant was investigated as a function of "a," the thick-

ness of Region 1. This is necessary so that a value of "a" may be

picked for the ω-β diagram. As can be seen from Fig. 29, the peak of

the gain curve shifts to smaller values of "a" as α is increased. The

shift becomes noticeable at $\alpha \simeq .01$. For larger values of α, the value

of "a" for peak gain begins to shift very rapidly as a function of α.

The gain regions become narrower and harder to find. This effect can

be interpreted by referring back to the effective dielectric constant

derived from Eq. 133. It can be seen that α has the effect of increas-

ing ω_p. In Chapter IV, the relationship of ω_p to "a" was discussed in

detail, and exactly this type of behavior was observed.

The ω-β diagram is shown in Fig. 30. The thickness of Region 1
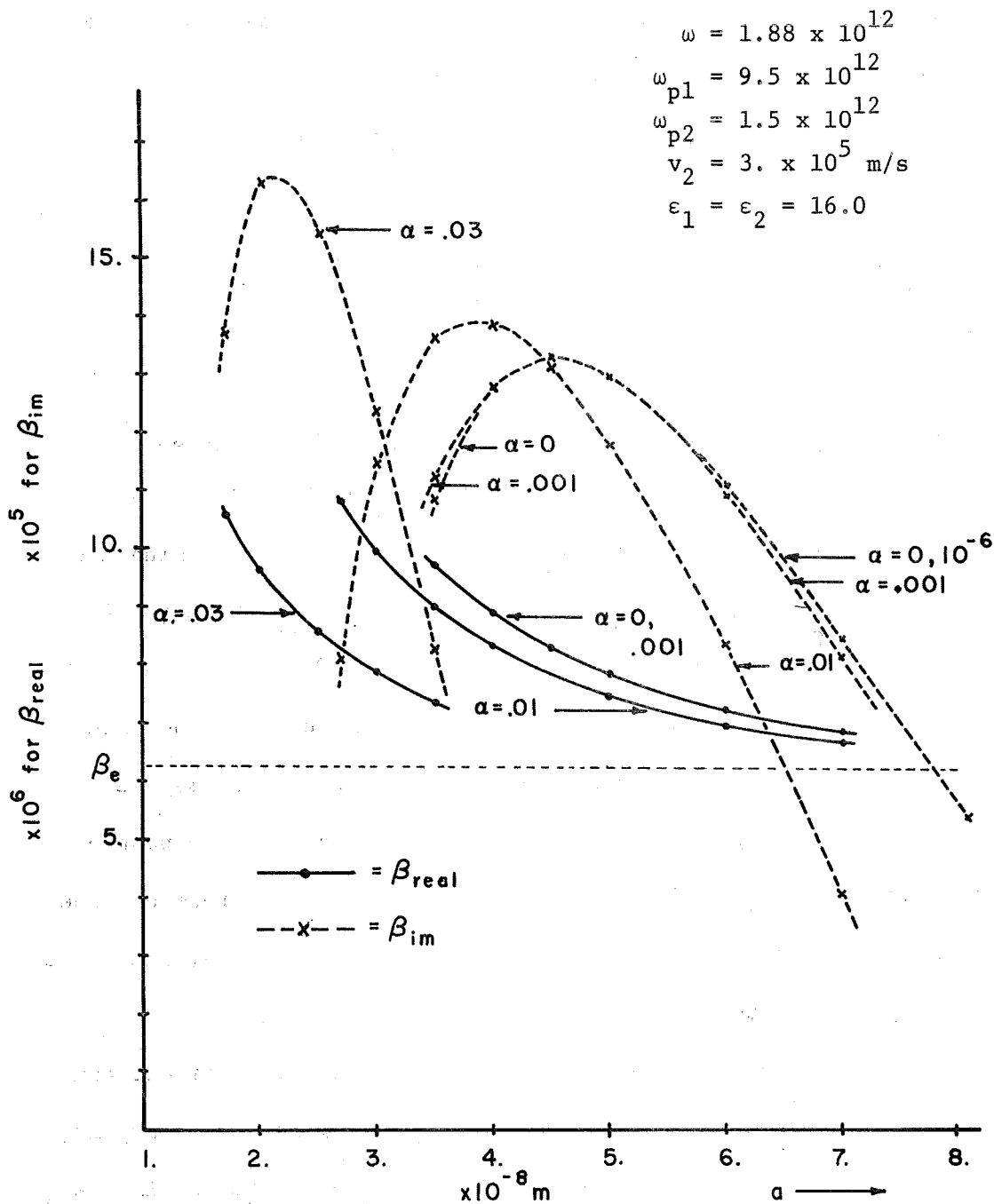
Fig. 29.   Complex β as a function of "a" for anisotropic conductivity, neglecting temperature and particle collision effects.
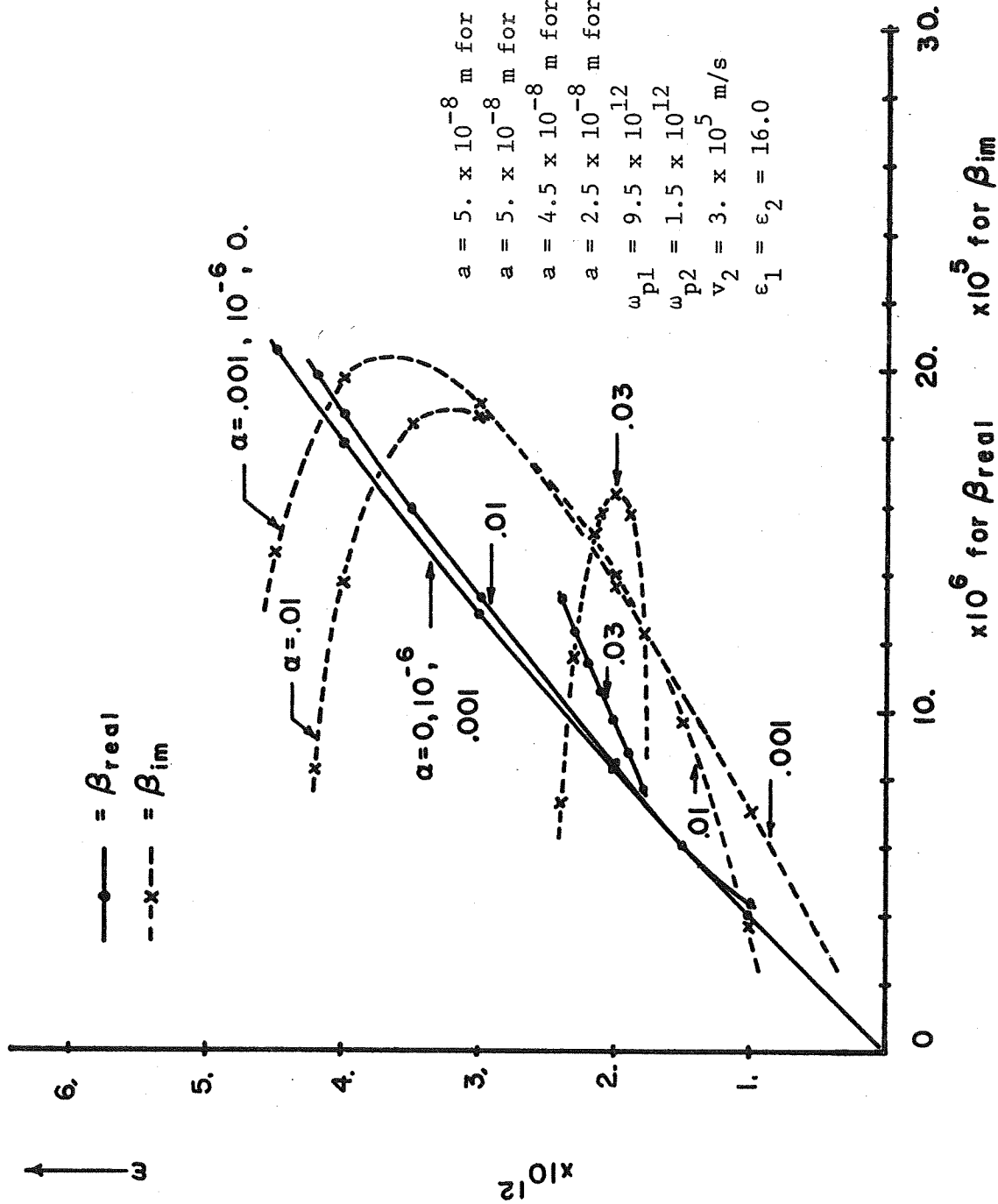
Fig. 30. ω–β diagram for anisotropic conductivity, neglecting temperature and particle collision effects.

$a = 5. \times 10^{-8}$ m for $\alpha = 10^{-6}$
$a = 5. \times 10^{-8}$ m for $\alpha = 10^{-3}$
$a = 4.5 \times 10^{-8}$ m for $\alpha = 10^{-2}$
$a = 2.5 \times 10^{-8}$ m for $\alpha = .03$
$\omega_{p1} = 9.5 \times 10^{12}$
$\omega_{p2} = 1.5 \times 10^{12}$
$v_2 = 3. \times 10^{5}$ m/s
$\varepsilon_1 = \varepsilon_2 = 16.0$

Axis labels: $\times 10^{6}$ for β_{real}, $\times 10^{5}$ for β_{im}

$= \beta_{real}$
$= \beta_{im}$

$\alpha = .001, 10^{-6}, 0.$
$\alpha = .01$
$\alpha = 0, 10^{-6}, .001$

has been adjusted for each value of α to be near the optimum value. The important observation to be made from Fig. 30 is that, as in Fig. 29, α begins to have a noticeable effect for $\alpha \geq .01$. Once the effect becomes noticeable, further increases of α alter the results drastically. The frequency range over which gain is possible becomes very narrow as α increases. In fact, as α gets closer to one, this range becomes so narrow that it cannot be found by numerical techniques. From these computer results, it appears that the conductivity will have to have an anisotropy of more than 100 for the one-dimensional space-charge model to be applicable.

When $\alpha = 1$, a computer search of the ω-β plane does not show any growing waves. The dispersion relation for the layered structure (Eq. 146) can be solved in the slow-wave approximation to check this result. If the slow-wave approximation is made so that $\beta^2 \gg k^2$, then Eq. 146 can be simplified considerably:

$$- \left[\frac{\beta^2}{1 - \dfrac{\omega_{p1}^2}{\omega(\omega - \beta v_{o1})}} \right] \frac{\tanh\left(T_1 a\right)}{k_1^2 T_1} = \left[\frac{\beta^2}{1 - \dfrac{\omega_{p2}^2}{\omega(\omega - \beta v_{o2})}} \right] \frac{\tanh\left(T_2 b\right)}{k_2^2 T_2} \qquad (148)$$

For the slow-wave approximation, T_1 and T_2, as given in general by Eq. 138, reduce to

$$T_1 \simeq T_2 \simeq \beta$$

Furthermore, we will make the simplifying assumptions of Chapter IV

that $k_1 = k_2$ and $v_{o1} = 0$. Then, Eq. 148 reduces to Eq. 149.

$$- \frac{\tanh\,(\beta a)}{1 - \dfrac{\omega_{p1}^2}{\omega^2}} = \frac{\tanh\,(\beta b)}{\left(1 - \dfrac{\omega_{p2}^2}{\omega(\omega - \beta v_{o2})}\right)} \tag{149}$$

Equation 149 can now be investigated to see if instabilities are possible. This can be done by looking for complex β or complex ω. Since the β's are a part of the tanh functions, they are difficult to find. Equation 149, however, can be solved for ω without difficulty. By Sturrock's criterion, as discussed in Section 3.5, it is possible to consider complex ω for real β. If it can be shown that ω is real for all real β, then instabilities are not possible. Equation 149 is solved for ω by expanding all the terms and grouping the like powers of ω in the usual manner. The result of this manipulation is

$$\omega^3 - \left(\beta v_{o2}\right)\omega^2 - \left[\frac{\omega_{p2}^2\,\tanh\,(\beta a) + \omega_{p1}^2\,\tanh\,(\beta b)}{\tanh\,(\beta a) + \tanh\,(\beta b)}\right]\omega$$

$$\tag{150}$$

$$+ \frac{\tanh\,(\beta b)\,\omega_{p1}^2\,\beta v_{o2}}{\tanh\,(\beta a) + \tanh\,(\beta b)} = 0$$

Equation 150 has the general form

$$\omega^3 - a\omega^2 - b\omega + c = 0$$

which can be rearranged as follows

$$1 = \frac{b\left(\omega - \frac{c}{b}\right)}{\omega^2 (\omega - a)}$$ (151)

Equation 151 is in the form of a positive feedback equation for which
a root-locus plot can be made. The loci will depend on the values of
the zero at c/b and the pole at a. The two possibilities are illus-
trated in Fig. 31.
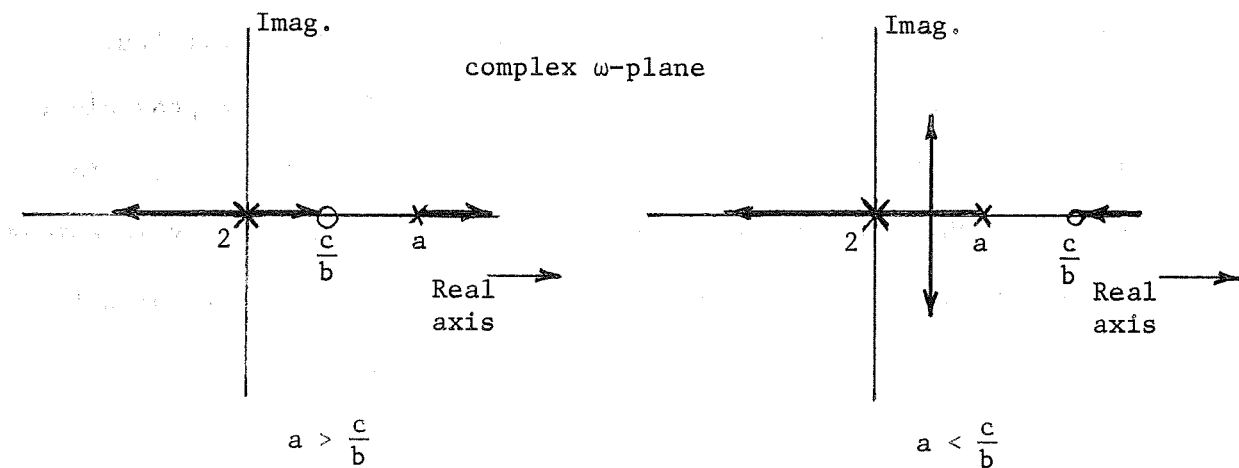
Fig. 31. The two possible root-locus plots of Eq. 151.

It is evident from Fig. 31 that if c/b < a for all values of
real β, then there will be no complex ω and instabilities will not be
possible. The factors in Eq. 150 that correspond to a > c/b are given
as

$$\beta v_{o2} \overset{?}{>} \frac{\tanh(\beta b) \, \omega_{p1}^2 \, \beta v_{o2}}{\omega_{p2}^2 \tanh(\beta a) + \omega_{p1}^2 \tanh(\beta b)}$$

which simplifies to

$$1 \overset{?}{>} \frac{1}{\dfrac{\omega_{p2}^2 \tanh(\beta a)}{\omega_{p1}^2 \tanh(\beta b)} + 1}$$

For real β, the inequality is satisfied and there are no complex solutions for ω.

6.3. Methods for Obtaining Anisotropic Conductivity

Two possible methods of obtaining the necessary anisotropic conductivity are:

1. The material itself is anisotropic with one preferred direction of conduction.

2. A magnetic field is used to "focus" the beam in the solid as is done in electron beam devices.

The prospects for finding a semiconductor with the necessary anisotropy are not promising. Indium antimonide and indium arsenide have nearly spherical energy surfaces and consequently an almost isotropic conductivity. Both germanium and silicon have ratios of about 2 to 5 for effective masses in the longitudinal and transverse directions. To satisfy the theoretically calculated values for the aniso-

tropy, a material should have a ratio of transverse to longitudinal conductivity of .01 or smaller. This would give acceptable results for the gain as calculated in Section 6.2. It is difficult to imagine a semiconducting solid that would have a crystal structure suitable for this large conductivity anisotropy.

The effect of a magnetic field on the conductivity can be derived easily by starting with the force equation used in Chapter III (Eq. 15). Neglecting the temperature term, we have

$$\frac{d\vec{v}}{dt} = \frac{-|e|}{m} (\vec{E} + \vec{v} \times \vec{B}) - \nu_c \vec{v} \tag{152}$$

The current density is defined as

$$\vec{J} = \overline{\overline{\sigma}} \cdot \vec{E} \tag{153}$$

where $\overline{\overline{\sigma}}$ is the conductivity tensor. The ac current density can also be written as

$$\vec{J} = ne\vec{v} \tag{154}$$

The current density due to the dc drift will be neglected in the present analysis. The intent of this treatment is to show what kind of anisotropies can be produced by a magnetic field; the addition of dc drift velocities complicates the analysis considerably.

If Eq. 152 is solved for $\vec{v}$, assuming an $e^{j\omega t}$ dependence and $\vec{B} = B_o \hat{z}$, and substituted into Eq. 154, the conductivity tensor follows immediately.

$$\overline{\overline{\sigma}} = \frac{|e|^2 n}{m} \begin{bmatrix} \dfrac{(\nu_c - j\omega)}{(\nu_c - j\omega)^2 + \omega_b^2} & \dfrac{\omega_b}{(\nu_c - j\omega)^2 + \omega_b^2} & 0 \\[3em] \dfrac{-\omega_b}{(\nu_c - j\omega)^2 + \omega_b^2} & \dfrac{(\nu_c - j\omega)}{(\nu_c - j\omega)^2 + \omega_b^2} & 0 \\[3em] 0 & 0 & \dfrac{1}{(\nu_c - j\omega)} \end{bmatrix} \qquad (155)$$

where

$$\omega_b = \frac{eB_{oz}}{m}$$

Neglecting the collision term in Eq. 155, the conductivity tensor reduces to

$$\overline{\overline{\sigma}} = \frac{|e|^2 n}{m} \begin{bmatrix} \dfrac{-j\omega}{(\omega_b^2 - \omega^2)} & \dfrac{\omega_b}{(\omega_b^2 - \omega^2)} & 0 \\[3em] \dfrac{-\omega_b}{(\omega_b^2 - \omega^2)} & \dfrac{-j\omega}{(\omega_b^2 - \omega^2)} & 0 \\[3em] 0 & 0 & \dfrac{-1}{j\omega} \end{bmatrix} \qquad (156)$$

If ω_b is now made $\gtrsim 10\omega$, then $\omega_b^2 - \omega^2 \simeq \omega_b^2$ and

$$
\overline{\overline{\sigma}} \simeq \frac{|e|^2 n}{m}
\begin{bmatrix}
\dfrac{-j\omega}{\omega_b^2} & \dfrac{1}{\omega_b} & 0 \\[3ex]
\dfrac{-1}{\omega_b} & \dfrac{-j\omega}{\omega_b^2} & 0 \\[3ex]
0 & 0 & \dfrac{-1}{j\omega}
\end{bmatrix}
\tag{157}
$$

It is evident from Eq. 157 that an electric field in the z-direction, the same direction as $\vec{B}$, will result in a current density about 10 times larger than from E fields in either the x- or y-directions

For operation at 300 GHz in germanium, which has an average effective mass of .22 m_e,

$$
B_o = \frac{m^*}{q} \, 10\omega = 2.2 \left(\frac{1.88 \times 10^{12}}{1.75 \times 10^{11}} \right) = 23.6 \ \text{W/m}^2
$$

This field is about ten times larger than practical in most laboratory situations. Either the frequency of operation must be lowered or the conductivity anisotropy cannot be made as large.

There appears to be a rough correlation between this assertion and the observed results in InSb. Broadband emission from InSb has been observed in the 8 to 25 GHz range.[1] The magnetic fields required are usually about 2 kG at the lower threshold for emission. In InSb, a magnetic field of 2 kG corresponds to ω_b of

$$\omega_b = \frac{eB}{m^*} = \frac{\left(1.75 \times 10^{11}\right)(.20)}{.013} = 2.7 \times 10^{12}$$

Then

$$f_b = \frac{\omega_b}{2\pi} = 430 \text{ GHz}$$

The value of f_b is about 20 times larger than the emission frequency. This would give an anisotropy of about the necessary magnitude predicted by the results shown in Fig. 30. It should be noted, however, that collisions were neglected for this calculation, and in the actual material they will be important. It may even be more meaningful to compare ω_b to ν_c instead of to the emission frequency.

Devices may be possible at lower frequencies, but our main interest is in the higher frequency range and for no dc magnetic field. The results of Chapters IV and V indicated that the submillimeter-to-

---

[1] B. Ancker-Johnson, "Microwave Emission from Nonequilibrium Plasmas in InSb Subject to Magnetic Fields," *Journal of Applied Physics*, Vol. 39, June 1968, pp. 3365-3378.

infrared region of the frequency spectrum is particularly suited for the semiconducting materials. Yet, the results of the transverse conductivity analysis indicate that operation in this region is not practical. We are forced to conclude that an adequate solution cannot be given at this time.

Unless the transverse conductivity problem can be resolved, bulk space-charge interactions in the submillimeter-to-infrared region of the frequency spectrum without very large dc magnetic fields do not appear possible.

VII. COUPLING ENERGY FROM SPACE-CHARGE WAVES

A problem common to all interactions involving plasma waves is how to couple the energy out of the electron stream. The difficulty is due to the very short wavelength inside the material compared to the free-space wavelength. To illustrate the problem more specifically, consider a simple situation of a material with a planar surface in the y-z plane and an ac current density J near this surface in the z-direction. This will correspond to the general configuration that has been investigated throughout this report. The current density J can be written as

$$\vec{J} = J_o e^{j(\omega t - \beta z)} \hat{z} \tag{158}$$

This assumes the usual plane wave propagating in the z-direction and with space-charge bunching in the z-direction only. For the general case, the fields and vector potential are related to the current density by Eqs. 159 to 161.

$$\vec{A}(\vec{r}, t) = \int_{V'} \frac{\mu \vec{J}(\vec{r}')}{4\pi R} e^{j(\omega t - kR)} dV' \tag{159}$$

$$\vec{B} = \vec{\nabla} \times \vec{A} \tag{160}$$

$$\vec{E} = -j\omega \left[\vec{A} + \frac{\vec{\nabla}(\vec{\nabla} \cdot \vec{A})}{k^2} \right] \tag{161}$$

where $R = |\vec{r} - \vec{r}'|$; and $\vec{r}'$ refers to the source point, $\vec{r}$ to the field point.

It is appropriate to assume that $r' \ll \lambda$, because the wavelength inside the material will be on the order of the electronic wavelength $\lambda_e = \frac{v}{c} \lambda$. This assumption will restrict the results to small samples. A more general discussion would be very much more complicated, and even in that case the results are only of order-of-magnitude accuracy, because there is no method for calculating the total ac current in the sample from the small-signal theory used in this report.

Furthermore, it is also possible to assume that $r \gg r'$ so that $R \approx r$. This is simply the far-field approximation. This approximation simplifies the calculations considerably. It should predict accurate results for all experiments where wave guides do not enclose the sample. Whenever the experiments are performed inside a wave guide, then the analysis should be done for the particular configuration used. The present analysis will be adequate for making order-of-magnitude estimates of the radiated energy.

For these two approximations, Eq. 159 can be written in a considerably simpler form:

$$\vec{A}(\vec{r}, t) = \frac{\mu e^{j(\omega t - kr)}}{4\pi r} \int_{V'} \vec{J}(\vec{r}') \, dV' \tag{162}$$

The integral of Eq. 162 can be easily evaluated for the current density of Eq. 158

$$\int_{V'} \vec{J}(\vec{r}')dV' = J_o e^{j\omega t} \hat{z}' \int_{V'} e^{-j\beta z'}dV'$$

The integration over the x' and y' coordinates will just result in some constant area determined by the size of the current carrying region. Let this value be denoted by S'.

Then,

$$\int_{V'} \vec{J}(\vec{r}')dV' = J_o S' e^{j\omega t} \hat{z}' \int e^{-j\beta z'}dz' \qquad (163)$$

It is immediately obvious from Eq. 163 that if the limits of the integral are an integer number of space-charge wavelengths, then the integral is equal to zero. Therefore, $\vec{A}$ will take its value only from the last fraction of a wavelength.

The time-averaged radiated power will be given by the real part of the complex Poynting vector.

$$\vec{P} = \frac{1}{2} \text{Re}(\vec{E} \times \vec{H}^*)$$

Equation 163 can be combined with Eq. 162 to get the vector potential, and then this result can be substituted into Eqs. 160 and 161 to write the Poynting vector in terms of the vector potential $\vec{A}$. If the vector potential is zero, we can immediately conclude that there will be no radiated power. Any contribution to the total radiated power will be

from the fractional portion of a wavelength near the end of the sample.

This is a very inefficient method of coupling and has led to other pro-

posed schemes for getting the energy out of the sample. However, be-

fore discussing the more complicated proposals let us derive an approx-

imate equation for the power radiated from a narrow slot, as shown in

Fig. 32. This should give the same result as assuming that the radia-
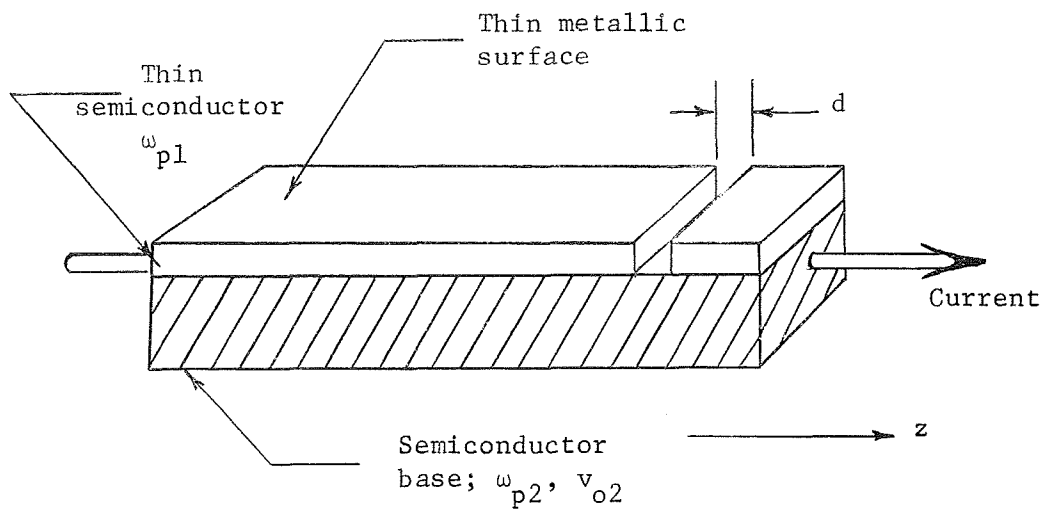
Fig. 32. Layered-semiconductor configuration with a narrow slot.

tion cancels everywhere except at the last fraction of a wavelength. In

Fig. 32, the ac current will be assumed to be near the boundary between

the semiconductors, and the metallic surface will eliminate radiation

everywhere except in the region of the slot.

To evaluate the integral in Eq. 162, the simplest case is to as-

sume a sinusoidal current and then to assume that d, the width of the gap,

is one half of a space-charge wavelength. Then,

$$\vec{A} = \frac{\mu e^{j(\omega t - kr)}}{4\pi r} \left(2 I_1 d\right) \hat{z} \tag{164}$$

where I_1 is the ac current producing the radiated power. Once again, the time-averaged radiated power will be given by the real part of the complex Poynting vector.

$$\vec{P} = \frac{1}{2} \, \text{Re}(\vec{E} \times \vec{H}^*) \tag{165}$$

Equation 164 for the vector potential can now be substituted into Eqs. 160 and 161. When the result of that substitution is used in Eq. 165, the following expression for the Poynting vector is obtained,

$$\vec{P} = \frac{1}{2} \sqrt{\frac{\mu}{\epsilon}} \left(\frac{2 I_1 kd}{4\pi r}\right)^2 \, |\hat{z} \times \hat{n}|^2 \, \hat{n} \tag{166}$$

where $\hat{n}$ is the unit vector normal to the radiating surface.

The total radiated power is found by integrating Eq. 166 over a very large hemispherical surface in order to satisfy the far-field approximation, and since radiation will be seen only from one side of the sample. To do the integration, we must assume that the width of the sample does not affect the radiated fields. This may or may not be a good assumption for all cases, but should be accurate in the region where radiated power is highest.

$$P = \frac{\pi}{2} \sqrt{\frac{\mu}{\epsilon}} \left(\frac{I_1 kd}{2\pi}\right)^2 \int_0^\pi \sin^3\theta \; d\theta = 80 \left(\frac{\pi I_1 d}{\lambda}\right)^2 \qquad (167)$$

Equation 167 for the total radiated power has been derived with some very crude approximations and will probably not give very accurate results. However, this does not eliminate its usefulness. The purpose of this discussion is to get some estimate of the magnitude of the power that can be expected for typical operating parameters that have been specified throughout this report. Equation 167 should be adequate for this purpose.

The most familiar situation to which Eq. 167 can be applied is the configuration investigated in Chapters IV and V, where germanium was used as the semiconductor. All the necessary data are already available for this case and it is easy to do the calculations. The similarity between Fig. 32 and Fig. 2 for the configuration with metallic boundaries is obvious. The growing wave is still assumed to be present at the surface between the two semiconductors.

To evaluate Eq. 167, we need to have numerical values for I_1, d, and λ. I_1 is the ac current which contributes to the radiated power. There is no way that we can get an exact value for I_1 from small-signal theory. I_1 will be determined by the length of the gain region, the amount of gain possible, or the natural saturation level that is encountered in all amplifiers. An approximate upper limit can be set for I_1 by letting the ac current equal the dc current. This would mean

that there is 100 percent bunching in the stream. In a practical device, the bunching will probably be less because of the randomizing effects of temperature and collisions. To make the calculations, it will be convenient to derive the dc current for the radiating region and then assume some fraction of this value as the ac current.

$$I_1 = \vec{J} \cdot \vec{S}$$

$$= nevS$$

S is the effective area of the radiating current and will be given by the width of the sample and a depth of about one electronic wavelength into the sample.

The slot width d was assumed to be one-half of an electronic wavelength,

$$d = \frac{1}{2} \lambda_e = \frac{1}{2} \frac{v}{c} \lambda$$

where λ is the free space wavelength determined by the frequency selected for the interaction.

In Chapter V, the operating frequency was typically chosen around 300 GHz. For a plasma frequency in this range, $n \simeq 3 \times 10^{15}$ cm^{-3} for germanium. To evaluate S, we need the sample width, and this is typically two to three millimeters. The maximum drift velocity v varies from 1.0 to 1.5 x 10^5 m/s. We will choose a value of 1.5 x 10^5 m/s.

Putting all these values into Eq. 167, we can now calculate the total radiated power.

$$P = 80 \left[(3.14)\left(3 \times 10^{15}\right)\left(10^{6}\right)\left(1.6 \times 10^{-19}\right)\left(1.5 \times 10^{5}\right) \right.$$

$$\left. \left(2.5 \times 10^{-3}\right)\left(.5\lambda \times 10^{-3}\right)\left(.25\lambda \times 10^{-3}\right)/\lambda \right]^{2}$$

$$P = .4 \ \mu\text{watts}$$

Assuming a 50 percent bunching of the beam instead of 100 percent, we would get $P = .1$ μwatts and so on for other values of beam bunching.

This calculation can be done for any frequency and for other materials. For example, InSb can be used in the far infrared at about 10μ. For this wavelength the power output is about 600 μwatts for 50 percent bunching.

One may observe that as the plasma frequency increases, the ac power output also shows a corresponding increase. For example, compare the 300 GHz to the 10μ calculations. However, the conductivity also increases and more dc power is required to obtain the necessary electric fields. This problem will be discussed further in Chapter IX.

It is apparent from these calculations that even for strong beam bunching, the output powers are very low. Power outputs of a few microwatts are difficult to detect experimentally. Devices with these

output levels certainly would not serve as useful oscillators or amplifiers.

The observed microwave emission from InSb with various sample configurations, usually large compared to λ_e, has been at very low power levels -- on the order of a few microwatts. This would agree with the approximate results obtained in this chapter.

A few attempts have been made to improve the coupling to obtain increased output power. G. A. Swartz and B. B. Robinson[1] have cut very narrow slots into samples of InSb and obtained somewhat improved power output and also coherent emission. R. D. Larrabee and W. A. Hicinbothem[2] have proposed a periodic laminar array to block out alternate half-wavelengths over the entire sample length and hence to realize much higher powers. They did not observe the expected increase in power, and concluded that the oscillations may be due to other than space-charge effects.

For a space-charge wave interaction, the periodic structure as proposed by Larrabee and Hicinbothem should work very well. The problem is one of constructing such a structure. At 300 GHz the electronic wavelength is about one micron. The slots would have to be of about this dimension. Even the well-developed thin-film vacuum deposition technology is only able to approach these dimensions. For effective coupling

---

[1] G. A. Swartz and B. B. Robinson, *Coherent Microwave Instabilities in a Thin Layer Solid-State Plasma.* Princeton, New Jersey, RCA Laboratories, 1968.

[2] R. D. Larrabee and W. A. Hicinbothem, "A Laminar Slow-Wave Coupler and its Application to Indium Antimonide," *IEEE Transaction on MTT*, Vol. MTT-15, June 1967, pp. 382-383.

there would have to be perhaps one hundred or more of these slots. Even if the slots could be made to the required dimensions, the entire array must have an accuracy to within $\lambda_e/4$. For a structure of many slots this becomes a formidable undertaking.

In conclusion, it appears that even though the gain may be high inside the material, the energy cannot be effectively coupled out of the sample with the techniques proposed in this chapter. The dimensions of coupling structures become so small at the higher microwave frequencies that with present technology they cannot be constructed.

VIII. MATERIAL PROPERTIES

The accuracy of the computer results described in Chapter V relies heavily on accurate values for the various material properties that need to be included, such as the plasma frequency, dc drift velocity, and electron temperature. In addition, any proposed experiments to verify space-charge waves, or to investigate gain mechanisms, should be performed on the basis of accurate information on the materials that are selected. Therefore, the purpose of this chapter will be to discuss and tabulate some of the important properties of semiconducting solids which are necessary to a theoretical or experimental investigation of space-charge wave interactions.

In this chapter, we will first briefly discuss the general requirements for the plasma frequency, drift velocity, electron temperature, and collision frequency. Numerical values for these parameters were used in the computer results of Chapter V. Then a brief discussion will be presented on absorption properties and dielectric constants of the materials. This problem has not been included in the analysis to this point. The assumption has been made that the background lattice does not affect the interaction except through collisions and temperature. There are other mechanisms which sometimes cause high losses for a wave propagating through a crystal lattice. Although a detailed knowledge of how the absorption arises is not necessary to the present discussion, the absorption of the material should be known and compared to the gain obtainable from the interaction mechanism. The permittivity

(or dielectric constant) has been assumed to be independent of frequency. The validity of this assumption will be discussed briefly.

A table of the important material properties summarizes the information discussed in the chapter.

8.1. Plasma Frequencies

The plasma frequency is defined as

$$\omega_p = \sqrt{\frac{ne^2}{m^* \varepsilon}}$$

It is determined by the permittivity, effective mass, and charge density. The effective mass and permittivity can be assumed approximately constant. Then the plasma frequency is proportional to the square root of the carrier concentration. The carrier concentration is determined by the impurity doping of the semiconducting material and can vary over many orders of magnitude. In InSb, for example, n can be varied in a commercial process from 1.1×10^{13} cm^{-3} to 2.28×10^{18} cm^{-3}. This corresponds to plasma frequencies, ω_p, from 4.0×10^{11} to 1.88×10^{14} or from 64 GHz to a wavelength of 10μ. Similarly, germanium can be varied from about 30 GHz to about 50μ. Other semiconductors have frequency ranges that are larger or smaller. The values for typical materials are given in Table II at the conclusion of this chapter.

The important result is that the plasma frequency will deter-

mine the upper limit of the gain region. In Chapter V, we found that gain was not possible at frequencies higher than about $\omega_{pl}/2$. From Table II, we can then conclude that InSb will give gain up to about 20μ in the far infrared. Shorter wavelengths will not be possible with this kind of an interaction. Most of the other materials will be limited to wavelengths longer than about 100μ or 3000 GHz in frequency. Other space-charge interactions may have a different dependence on the plasma frequency, but clearly it is one of the important properties of a plasma model.

8.2. Drift Velocity and Electron Temperature

The drift velocity of the carriers determines the propagation of the space-charge waves. The electron temperature adds a velocity spread which decreases the gain. For low loss, the drift velocity should be high compared to the width of the thermal velocity spread. This is a difficult condition to meet experimentally. Applying high electric fields to achieve the high drift velocities also causes heating of the electrons, thereby raising their temperature and thermal velocity. Furthermore, at high electric fields, the simple linear relationship of velocity vs. E field is no longer valid. Impact ionization and other quantum effects come into play and effectively limit the highest attainable velocity. Before the saturation region is reached, there is a region of nonlinear behavior which should be avoided, if possible, in an experiment. Figure 33 shows the result for velocity as a
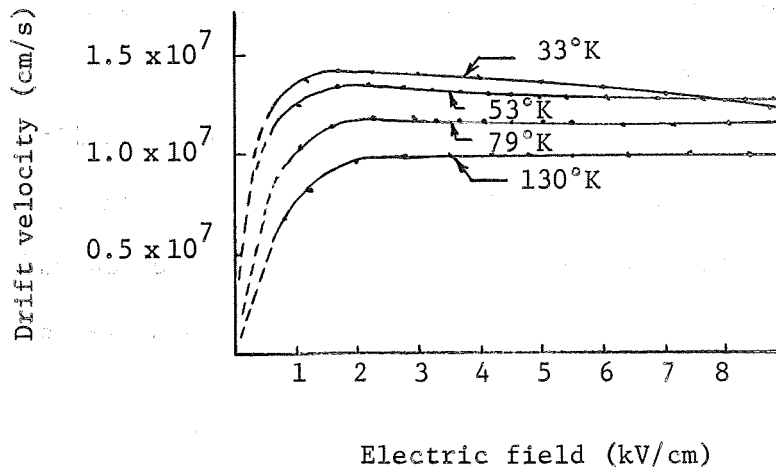
Fig. 33.   Velocity field characteristic of electrons in germanium.[1]

function of electric field for Ge. As can be seen from Fig. 33, a

velocity of about 10^7 cm/s is possible in Ge at low temperatures. In

InSb, velocities of the order of 5 x 10^7 cm/s appear to be practical.[2]

M. Glicksman and W. A. Hicinbothem[3] have calculated electron tempera-

ture as a function of electric field for InSb. Their results indicate

that at a 77°K sample temperature the electron temperature is on the

---

[1] D. M. Chang and J. G. Ruch, "Measurement of the Velocity Field
    Characteristic of Electrons in Germanium," *Applied Physics Letters*,
    Vol. 12, February 1968, p. 112.

[2] M. Glicksman and W. A. Hicinbothem, "Hot Electrons in Indium Anti-
    monide," *Physical Review*, Vol. 129, February 1963, pp. 1572-1577.

[3] *Ibid.*, p. 1576.

order of 150°K at a drift velocity of about 5 x 10^7 cm/s, which corresponds to a field of about 200 volts/cm. Additional results are shown in Table II at the end of the chapter. In performing an experiment, any observed output can be optimized by changing the dc voltage across the sample. From the discussion above we can see that there will have to be a compromise between highest possible drift velocity and a reasonably low electron temperature.

8.3. Collision Frequencies

As discussed in Section 5.6, a rough estimate of collision effects is possible by assuming a single effective collision frequency. The computer investigation showed a significant decrease in the gain when the collision frequency ν_c became on the order of the operating frequency. In Table II, the collision frequencies, based on the simple model, have been calculated for some of the materials. Most of the collision frequencies are in the 150 to 300 GHz range at 77°K. This will limit the lower frequencies for which most space-charge interactions may be used. The collision frequency range is about ten times higher than the usual microwave frequencies. If an interaction is to be investigated in the 10 to 50 GHz frequency range, then the theory must be developed assuming that collisions will dominate the interaction mechanism. Some of the work with InSb has been done on the basis of this kind of an assumption, e.g., B. B. Robinson and G. A. Swartz.[4]

---

[4] B. B. Robinson and G. A. Swartz, "Two-Stream Instability in Semiconductor Plasmas," *Journal of Applied Physics*, Vol. 38, May 1967, pp. 2461-2465.

8.4. Absorption Coefficients and Permittivities

The computer analysis of Chapter V was based on an electron stream model which ignored the losses due to lattice excitation. Any losses due to the crystal lattice will reduce the gain coefficient. Fortunately in the microwave and far infrared frequencies, semiconductors have comparatively low losses.

Figures 34 to 39 show the experimental results of the absorption of some typical materials as found in the literature. The gain coefficients obtained from the computer work of Chapter V were 10^3 cm^{-1} or larger. A loss coefficient α of 100 cm^{-1} would, therefore, not be troublesome. This compares well with the experimental results shown in the figures. The only troublesome frequencies are the occasional lattice absorption peaks as shown explicitly for germanium in Fig. 38. The InSb curves of Fig. 39 also show a high-absorption region around 60 μ. These regions should be avoided in choosing the operating frequency. Some of the more important regions have been noted in Table II.

Figure 34 gives the transmission for some common semiconductors in the infrared. The sharp drop in transmission near 1 μ is known as the absorption edge and is due to bound electron excitation. The transmission properties shown usually continue down into the microwave region, except for the occasional peaks mentioned above. Figure 35 gives the corresponding results for the III-V semiconducting compounds. Figure 36 gives the absorption on InSb as a function of temperature for a sample of a carrier concentration that could be used in the far infrared with the type of interaction proposed in Chapter IV. The absorption coeffi-

Material	Thickness (mm)
Ge	0.82
Si	1.00
Se	1.69
Te	1.50
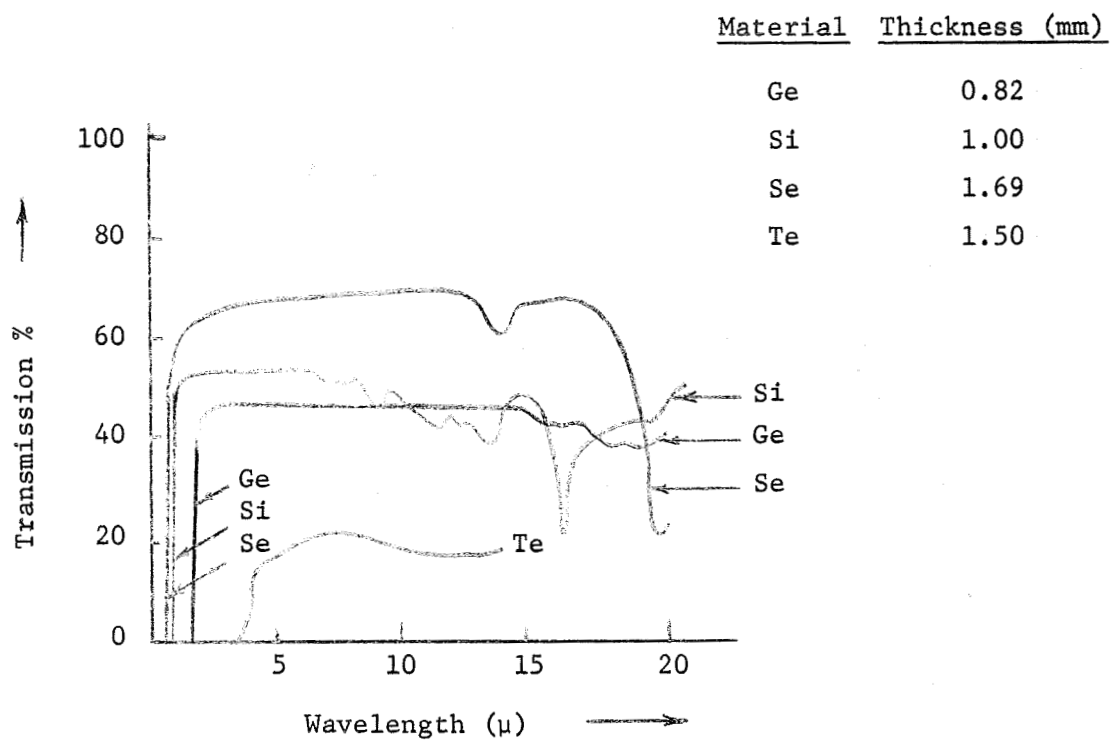
Fig. 34. Transmission of Si, Ge, Se, and Te.[5]

---

[5] G. K. T. Conn and D. G. Avery, *Infrared Methods*, New York, Academic Press, 1960, p. 44.

Thickness — 0.1 mm
for InSb and AlSb,
1 mm for other compounds
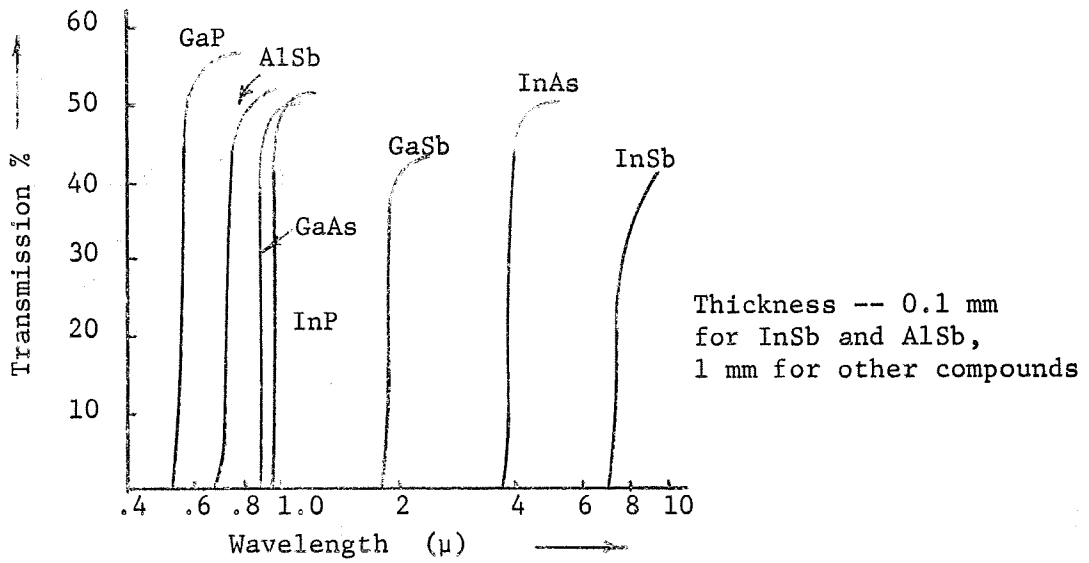
Fig. 35. Transmission of III - V compounds.[6]

n-type sample

$$\left(n = 10^{17} \text{ cm}^{-3}\right)$$
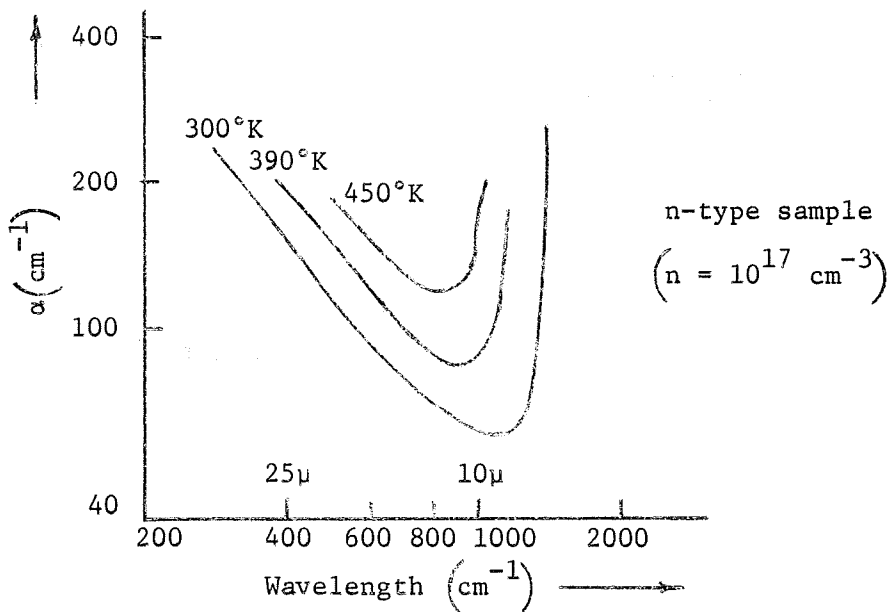
Fig. 36. Absorption coefficients for InSb.[7]

---

[6] C. Hilsum and A. C. Rose-Innes, *Semiconducting III-V Compounds*, New York, Pergamon Press, 1961, p. 226.

[7] W. Kaiser and H. Y. Fan, "Infrared Absorption in Indium Antimonide," *Physical Review*, Vol. 98, May 1955, p. 966-968.
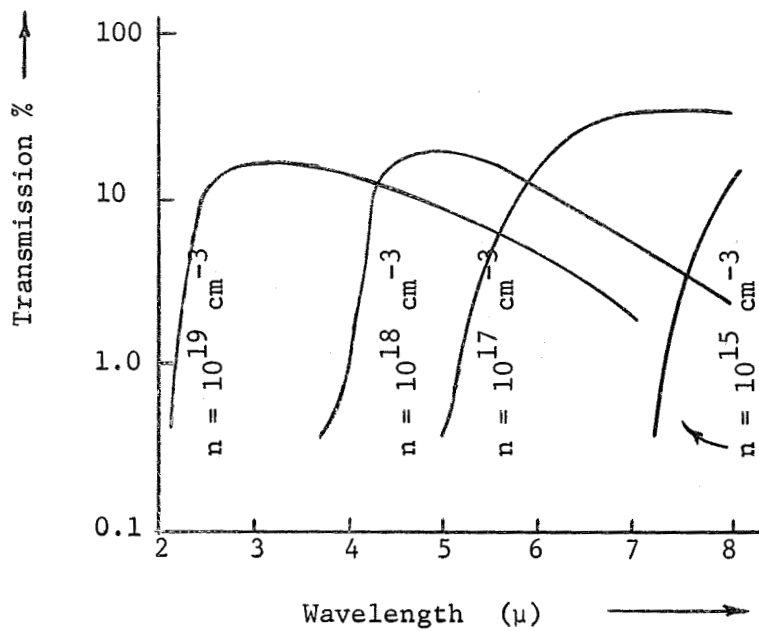
Fig. 37. Infrared properties of InSb.[8]
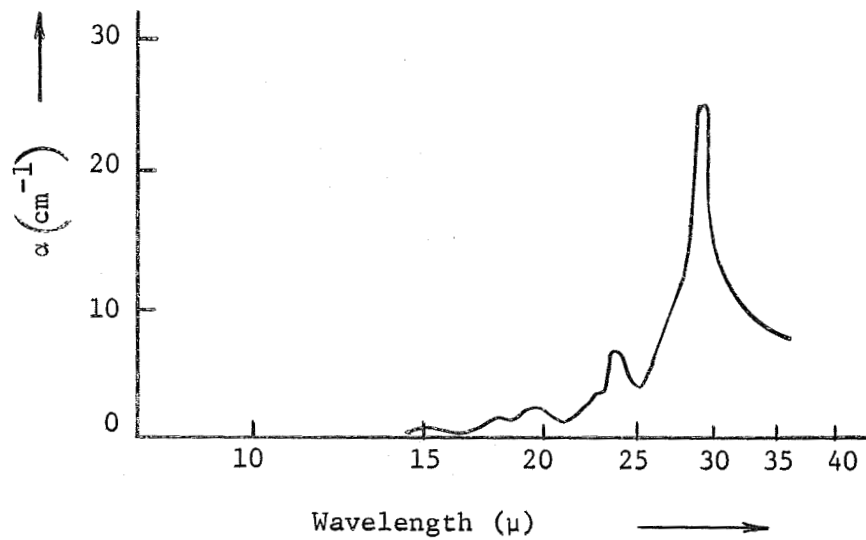
Fig. 38. Infrared absorption spectrum of germanium
due to lattice vibrations.[9]

---

[8] C. Hilsum, *op. cit.*, p. 228.

[9] T. S. Moss, *Optical Properties of Semi-Conductors*, London, Butterworth
Scientific Publications, 1959, p. 141.

- 173 -
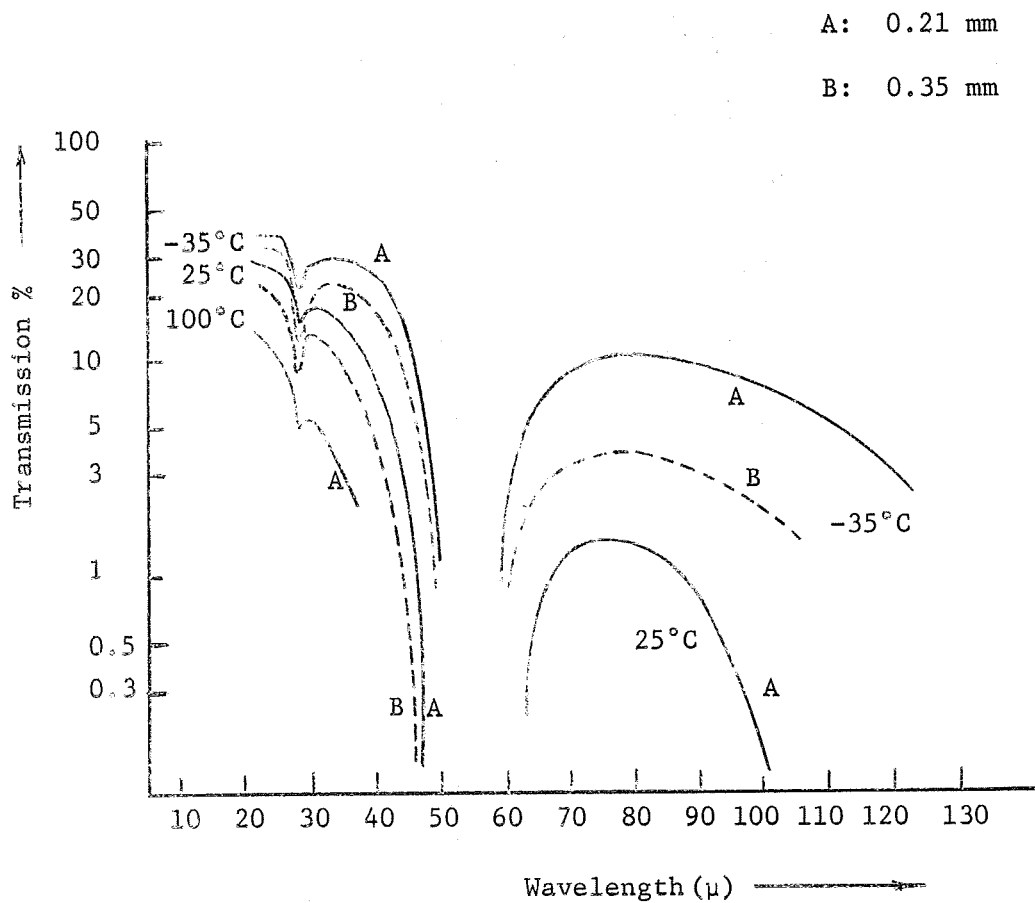
A: 0.21 mm

B: 0.35 mm

Fig. 39. Transmission of InSb crystals of 0.21 mm
and 0.35 mm thickness at -35°C, 25°C and 100°C.[10]

_____

[10] H. Yoshinaga and R. A. Oetjen, "Optical Properties of Indium Anti-
monide in the Region from 20 to 200 Microns," *Physical Review*,
Vol. 101, January 1956, pp. 526-531.

cient would be low compared to the expected gain, provided other conditions could be met. Figure 37 illustrates the effect of carrier concentration on the absorption edge. An interesting result here is that the peak transmission is not significantly affected by the different carrier concentrations. Figure 38 gives the absorption of the germanium lattice excluding the free electron absorption. Since the electrons are producing the gain, their absorption is not important. Only the losses due to the lattice will be detrimental. Figure 39 shows the transmission of InSb over a wide frequency range in the far infrared.

The relative dielectric constant, ε, for germanium was taken as 16.0, for the computer work of Chapter V, at all frequencies. The dielectric constant is not strongly frequency dependent in the low absorption region for any of the materials investigated. There is usually only about a 10 percent change in the dielectric constant from infrared to microwave frequencies. The only precaution is to avoid the occasional absorption peaks due to lattice excitation. Temperature will also affect the dielectric constant, but here again the effect is rather small and can probably be neglected. As an example, the dielectric constant of GaAs at 70.2 GHz changes only by 1.5 percent from 100°K to 300°K. Relative dielectric constants for typical materials are given in Table II.

TABLE II

PROPERTIES OF SOME USEFUL SEMICONDUCTORS

Material	1. Available carrier concentrations for n-type materials. 2. Plasma frequency ω_p corresponding to these concentrations. 3. ω_p converted to GHz or μ for more convenient reference.	Dielectric Constants for Several Pertinent Frequencies[11,12]	Important Absorption Bands[11]
InSb	$n = 1.1 \times 10^{13}$ cm^{-3} to 2.28×10^{18} cm^{-3} $\omega_p = 4 \times 10^{11}$ to 1.88×10^{14} (64 GHz) (10 μ)	$\varepsilon = 16.0$ at 8 μm. $\varepsilon = 15.7$ (due to lattice only in i-r). $\varepsilon_0 = 17.5$ (estimate of dc dielectric const.)	Strong band at 52 μm. Weaker bands at multiples of 52 μm.
Ge	4×10^{13} cm^{-3} to 1×10^{18} cm^{-3} $\omega_p = 1.9 \times 10^{11}$ to 3×10^{13} (30 GHz) ($\sim$50 μ)	$\varepsilon = 16.0$ over a wide frequency range from dc to infrared.	Dispersion region at 32 GHz. Free carrier dispersion around 24 μm.
Si	3×10^{10} cm^{-3} to 1×10^{18} cm^{-3} $\omega_p = 5.5 \times 10^9$ to 3.2×10^{13} (.88 GHz) ($\sim$50 μ)	$\varepsilon = 11.7$ in infrared. $\varepsilon = 13.7$ at 24 GHz.	Fairly strong band at 9.1 μm.
GaAs	5×10^{16} cm^{-3} to 1×10^{18} $\omega_p = 1.4 \times 10^{13}$ to 6.4×10^{13} ($\sim$120 μ) ($\sim$30 μ)	$\varepsilon = 11.0$ at 2.5 - 10 GHz. $\varepsilon = 13.0$ at 70.0 GHz. $\varepsilon = 13.05$ in infrared.	
InAs	1.8×10^{16} cm^{-3} to 1.5×10^{17} cm^{-3} $\omega_p = 1.42 \times 10^{13}$ to 4.1×10^{13} ($\sim$120 μ) ($\sim$40 μ)	$\varepsilon = 14.0$ (probably in infrared).	
PbS	3×10^{16} cm^{-3} to 1×10^{20} $\omega_p = 6 \times 10^{12}$ to 3.5×10^{14} ($\sim$300 μ) ($\sim$6 μ)	$\varepsilon = 17.5 - 18.0$ for 1 to 4 μm. Little change at longer wavelengths.	Weak absorption due to free carriers in infrared. Strong lattice absorption near 100 μm.
GaSb	1×10^{17} cm^{-3} to 1×10^{18} cm^{-3} $\omega_p = 2.1 \times 10^{13}$ to 6.7×10^{13} ($\sim$90 μ) ($\sim$30 μ)	$\varepsilon = 14.0$ (probably in infrared).	

[11] C. A. Hogarth, *Materials Used in Semiconductor Devices*, Interscience Publishers, New York, 1965.

[12] T. S. Moss, *Optical Properties of Semiconductors*, Butterworth Scientific Publications, London, 1959.

TABLE II - CONTINUED

PROPERTIES OF SOME USEFUL SEMICONDUCTORS

Drift velocities vs. E field (near saturation)	Collision frequencies $$f_\nu = \frac{e}{\mu_e m_e^*}$$ $$= 1.759 \times 10^{11}/\mu_e m^*$$	Electron temperatures vs. drift velocity.
Saturation velocity at $E = 300$ v/cm.[13] $v_d \simeq 5 \times 10^7$ cm/sec. in region just below saturation (at 77°K)	$\mu \simeq 50 \frac{vm^2}{sec}$ at 77°K $\mu \propto T^{-1.7}$ $f_\nu \simeq 300$ GHz at 77°K	$E = 300$ v/cm[13], electron temp $\simeq$ 230°K; $E = 150$ v/cm, electron temp $\simeq$ 130°K
Velocity saturation begins $\simeq 1000$ v/cm at 300°K[14] $\simeq 100$ v/cm at 77°K $v \simeq 1.0 \times 10^7$ cm/sec. near saturation (at 77°K)	$\mu \simeq 3.8 \frac{vm^2}{sec}$ at 77°K $f_\nu = 200$ GHz at 77°K	
Drift velocity saturation at $v_d \simeq 10^7$ cm/sec. at 300°K This corresponds to E field $\simeq 10^4$ v/cm.	$\mu \propto T^{-2.6}$ $\mu \simeq 4.1 \frac{vm^2}{sec}$ at 77°K $f_\nu \simeq 165$ GHz at 77°K	
	$\omega_{p\ min} \gg f_\nu$ f_ν not needed	
	$\omega_{p\ min} \gg f_\nu$ f_ν not needed	
	$\omega_{p\ min} \gg f_\nu$ f_ν not needed	
	$\omega_{p\ min} \gg f_\nu$ f_ν not needed	

[13] M. Glicksman and W. A. Hicinbothem, *op. cit.*

[14] D. M. Chang and J. G. Ruch, *op. cit.*

IX. EXPERIMENTAL INVESTIGATION

A limited experimental program was pursued during the theoretical investigation described in this report. A brief description will be given of some of the techniques available as an aid to future work. It is possible that the thermal and transverse velocity problems, described in Chapters V and VI, can be overcome with a different configuration and the use of a magnetic field. In that case, it would be desirable to try experimentally to verify the interaction. The following sections will very briefly describe some of the problems to be expected and what can be done to overcome some of them.

9.1. DC Energy and Heat Dissipation

The first experimental problem is that of heat dissipation and the practicality of getting the higher drift velocities. For example, assume that the semiconductor is germanium as in the computer work of Chapter V. For a drift velocity of about 1 to 1.5 x 10^7 cm/s the electric field is about 700 volts/cm. The power dissipated would be

$$P = \int \vec{J} \cdot \vec{E} \, dV = \sigma E^2 V$$

where σ is the conductivity and V is the volume of the solid. A typical value for the conductivity σ would be $10^2 (\Omega \text{ cm})^{-1}$. The volume of a typical thin sample would be about 10^{-3} cm^3. Putting these values into the above equation gives a power of 5000 watts! Thicker samples will require

correspondingly greater amounts of power. Unless a very exotic heat sink is developed, these power levels will restrict operation to short pulses at a low duty cycle. Not only is it important to keep the sample under test from melting, but any significant temperature increase will raise the thermal velocity and reduce any expected amplification. The samples in the experiments that were performed in this laboratory usually had impedances of one to fifty ohms. At the higher impedances, commercial pulse generators are readily available and no particular problems are encountered. At the lower impedances of a few ohms, a suitable commercial unit could not be found. The required currents and voltages were obtained in pulses of 4 to 5 μsec duration by using a lumped parameter delay line triggered by a very fast rise time silicon controlled rectifier.[1] The design and construction of this pulser, in addition to the units available commercially, permitted the testing of a wide range of materials and sample dimensions.

9.2. Sample Preparation

The theoretical work discussed in the previous chapters assumed that samples of the required dimensions and surface uniformity could be made in the laboratory. In this section, a few of the possible techniques and their limitations will be discussed.

---

[1] A. Silzars, C. H. Durney, and R. W. Grow, "Theoretical and Experimental Investigation of Solid-State Mechanisms for Generating Coherent Radiation in the Ultraviolet and X-Ray Regions," Technical Report UTEC MD 67-033, Microwave Device and Physical Electronics Laboratory, University of Utah, Salt Lake City, Utah, June 1967.

The minimum thickness of a semiconductor sample that can be made in the laboratory is usually determined by the mechanical strength required to have a self-supporting structure. For application of contacts and for propagation measurements, it is usually necessary to have samples of at least a few millimeters in width and length. Samples of this size can be cut with a wire saw using silicon carbide as an abrasive. The thickness can be as desired down to about .005 inches. These samples can then be bonded to a glass plate with a thermoplastic resin and mechanically polished to produce a more uniform surface and to further decrease the thickness. In practice, it was found that the limit of mechanical polishing is a sample about .001 inches in thickness. This can be accomplished by using a semiconductor grade diamond paste for the final polish. These pastes are available with a grain size as small as 1/2 to 1 micron. A surface polished in this manner appears shiny under a microscope with 30 x magnification. The grain size of the polishing paste would indicate that the surface nonuniformity is on the order of a micron with some damage to the crystal structure extending somewhat deeper into the sample.

Another method of preparing the surfaces is to use a chemical etch subsequent to a rough mechanical polish. Many such solutions are available and have been tabulated in the literature, e.g., Biondi, *Transistor Technology*, Vol. III.[2] Both germanium and indium antimonide can

---

[2] F. J. Biondi, *Transistor Technology*, Vol. III, D. Van Nostrand, Inc., Princeton, New Jersey, 1958, pp. 117-151.

be polished using the well known CP4 etch. Using this etch will also

reduce the thickness of the samples. The chemical etching method has

the advantage that surface strains and fractures are not introduced.

The disadvantage is that the etch does not act uniformly over large

areas. The sample, after etching, appears shiny but with some undula-

tions or waviness. This would make it difficult to get intimate con-

tact between two samples if a layered structure is desired. A micro-

scopic examination reveals that the etching process leaves a surface

that has small "craters" of about 5 microns in diameter covering the

entire extent of the sample. The chemical etch is very sensitive to

the precleaning process and it may be possible to get more uniform sur-

faces with special precautions during the cleaning operations.

Although these results appear to be very good when compared to

the free-space wavelength, which is 1 mm at 300 GHz, we must remember that

the slow-wave space-charge interactions have wavelengths of $\sim 10^{-3} \lambda$.

This means that the space-charge wavelength at 300 GHz is only about 1

micron. This is now of the same order as the surface nonuniformity,

and large losses will result for the surface wave at the boundary. Un-

less considerable improvement can be realized in the surface preparation,

successful experimental results cannot be expected.

Vacuum deposition offers yet another promising method for making

thin and uniform samples in the laboratory. The only drawback is that

the samples produced are usually of very low mobility. The layered

structure proposed in Chapter IV could be made experimentally from a

thick substrate with a very good surface on which a thin layer of low

mobility material has been vacuum deposited.

In conclusion, it appears that if a space-charge interaction in the 300 GHz or higher region is to be investigated, then a very careful study should first be made of the optimum surface conditions that can be achieved experimentally.

9.3. Ohmic Contacts

The high electric fields which are needed for the high drift velocities require good electrical contacts. Low resistance ohmic contacts can be made to n-type germanium by alloying antimony-doped gold to the contact area and then using ordinary tin-lead solder or a gold fillet. For very small contact areas the antimony-gold can be vacuum deposited onto the germanium through a mask which shields the rest of the sample. Alloying of the deposited material is done by heating in a hydrogen atmosphere while observing the sample through a low-power microscope. A characteristic color change occurs when the utechtic temperature is reached. Indium antimonide can be treated similarly or it may also be used with a flux and indium solder to provide the contacts.

The contacts were tested in pulsed operation by plotting the current vs. voltage curves. The resistances measured corresponded to those calculated from the resistivities of the samples, indicating very low resistance contacts. The current-voltage curves were approximately linear so that the contacts were not rectifying. Some nonlinearity was observed at high currents, but this could easily be explained by considering the heating of the samples due to these same large currents.

A rise in temperature will naturally increase the carrier concentration
and thereby lower the resistance.

The high voltages and currents that were applied also served as
a test for any defects in the contact area. Cracks or poor solder joints
resulted in arcing and eventual destruction of the sample.

9.4. Detectors and Sources

The interaction investigated in this paper is especially inter-
esting because it is suitable for frequencies from 300 GHz to the far
infrared. This is a range where good sources and detectors are pres-
ently lacking. Unfortunately, the lack of sources and detectors makes
experimentation difficult. At the microwave frequencies, wave guides
and klystrons are readily available up to about 100 GHz. Then doubler
crystals can be used to raise the frequency up to about 200 GHz. Crys-
tal detectors are available for frequencies up to about 250 GHz. Beyond
this the detection and source problem becomes very difficult. The wave-
length becomes so short that wave guides must be so small that they can
no longer be easily manufactured. At present, 150 to 200 GHz seems to
be the upper limit for practical microwave experiments. This frequency
is about a factor of two lower than would be desirable for experiments
on the proposed space-charge interactions. In the infrared region, use-
ful devices could possibly be built down to free-space wavelengths of
about 10 microns. Because very short dc pulses are required, the detec-
tor in this wavelength region must have a response time of about 1 μsec.
The only detectors which fulfill this criterion are the doped germanium

detectors. Gold-doped germanium has a useful response from about 1 μ to 9 μ. Copper-doped germanium will respond up to about 25 μ, but requires liquid helium for cooling.

At present there appears to be no available method for investigating the frequency range where the space-charge interactions have the best chance for success. If the theoretical results were more encouraging, then it might be worthwhile to try an experiment near the low-frequency or high-frequency limits of the interaction. Unfortunately, this is not the case. Further experimental work is not warranted at this time.

X. SUMMARY AND CONCLUSIONS

In the previous chapters, space-charge interactions in solid-
state plasmas have been considered from several different viewpoints.
Some particular cases have been analyzed and quantitative results have
been presented. It is now appropriate to summarize some of the more
important results and to draw some conclusions from this work.

The double-stream interaction with one stream stationary was
analyzed for a configuration where the two streams are in adjacent
materials. The analysis predicted high gain for this configuration
when temperature and particle collisions were not included, and only
one dimension was considered. Properties of semiconductors indicated
that useful devices could be made for operation over a broad frequency
range. Frequencies from $1. \times 10^9$ Hz to 3×10^{13} Hz satisfy the neces-
sary conditions for gain in the idealized model. For this configura-
tion, the material with the drifting stream could be taken of arbitrary
thickness. The thickness of the stationary stream material was then
adjusted to optimize the gain. Typical values of gain are about 10
percent per space-charge wavelength. This value is comparable to a
similar analysis for electron beams. Since the space-charge wavelength
in a solid is about 10^{-3} of the free-space wavelength, this results in
very large values of gain per cm.

The idealized model was then reconciled with the physical world
by including finite temperatures and particle collisions. The tempera-
ture problem was investigated in detail and several methods were com-

pared. The hydrodynamic model, Boltzmann transport equation, and velocity superposition techniques were all considered. The hydrodynamic model, which assumes an averaged thermal velocity, was found to give values of gain that are too optimistic. The distribution function approach, i.e., velocity superposition, was investigated in some detail because the physically expected distribution function of the Maxwell-Boltzmann type cannot be integrated explicity. Other distribution functions were tried to find a good approximate technique for evaluating the integral. The best results were obtained from straight-line approximations which resulted in a triangular-shaped distribution function. This distribution gave results to within ± 20 percent of the Maxwell-Boltzmann distribution function as numerically integrated on a digital computer. The trial of other distributions led to the conclusion that both the width and the slope of the distribution function chosen are very important. It is felt that the use of a triangular-shaped distribution provides a very good approximate technique for investigating temperature effects.

The numerical analysis of a germanium sample using physically attainable velocities and plasma frequencies showed a sharp drop in the gain as temperature was increased, even for very low temperatures. Useful gain is possible only up to about 30° to 35°K. This means that liquid nitrogen temperatures will not be sufficient for a laboratory experiment.

A simple collision theory, assuming a single collision frequency, was then included to get some indication of the lower frequency limit for useful gain. The computer results show that, for typical values of gain

coefficients, the operating frequency must be above the collision fre-
quency to avoid severe collision damping. Collision frequencies in
semiconductors are in the 200 to 300 GHz range at 77°K. This will limit
operation to the submillimeter or shorter wavelengths, unless strong dc
magnetic fields are applied. If the collisionless gain is already low,
then operation will have to be at even higher frequencies.

The overall effect of temperature and particle collisions is to
impose severe restrictions on the operating conditions for the proposed
device. The sample must be cooled to very low temperatures and the op-
erating frequency must be in the submillimeter region.

Transverse ac velocities add another serious restriction to the
construction of a practical device. In electron beams, transverse
velocities are usually not considered because magnetic fields are used
to contain the beam. A solid, presumably, has well-defined boundaries
so that a magnetic field is not needed to keep the electrons in the
sample; however, inside the sample the electrons may move in all direc-
tions. Computer calculations showed that an anisotropic conductivity
is necessary for useful gain to result from the double-stream inter-
action. Furthermore, these calculations showed that the anisotropy
must be large. For the layered configuration, a ratio of longitudinal
to transverse conductivity as large as 10^3 begins to reduce the gain
as obtained from the one-dimensional analysis. Longitudinal-to-trans-
verse conductivity ratios of less than 10 are too low for useful gain.
A magnetic field can be used to produce an anisotropy artificially, but
the fields required are too large at the frequencies of interest.

In addition to the theoretically predicted obstacles, there are some problems of a more practical nature. Even if the interaction works as intended, there is still the problem of how to get enough of the energy out of the sample to realize a useful device. The mismatch between the space-charge wavelength and the free-space wavelength is so great that only a small fraction of the total dc energy can be converted to useful output. Typical power levels that can be expected from narrow slots, that act like dipole antennas, are in the microwatt range.

Presently available semiconductors will satisfy the theoretical requirements for plasma frequency, drift velocity, etc. However, the space-charge wavelength is so short, about 1 micron for an operating frequency of 300 GHz, that very uniform and undamaged surfaces are necessary at the boundary between the two layers.

Based on this study, we conclude that space-charge interactions in solids without an applied dc magnetic field hold little promise for development into useful devices for the following reasons:

1. Idealized one-dimensional space-charge models which neglect temperature and collision effects always give results that are far too optimistic.

2. The randomizing effect of finite temperature on the particle velocities causes severe damping of the interaction gain. Any practical device configuration will probably require operation at temperatures below 77°K. The layered double-stream structure investigated in this report must be operated at 35°K or below for useful gain to result.

3. Particle collisions further add to the damping of the idealized gain. Operation must be above 300 GHz if severe collision damping is to be avoided. A strong dc magnetic field may be used to reduce the effects of collisions for operation at lower frequencies.

4. Transverse ac velocities must be included in any analysis. Their effect is to eliminate useful gain unless a sizable conductivity anisotropy can be realized. Dc magnetic fields for producing this anisotropy become impractically large for submillimeter or shorter wavelengths.

5. The space-charge wavelength is so small at the submillimeter or shorter wavelengths that there is presently no available technology for producing efficient coupling structures or semiconductors with the required surface uniformity.

The research described in this report has resulted in better understanding of the potential of space-charge interactions in solids. The more detailed consideration of the problem has shown that simple models are not adequate for making proposals for interaction mechanisms. In particular, it is now reasonable to conclude that the possibility of ultraviolet or X-ray devices based on space-charge interactions is not very promising. Even if the basic difficulties of temperature, collisions, etc., can be overcome, a major problem at X-rays would be the coupling of energy from the material. The space-charge wavelength is so short that coupling structures would have to approach the dimension of the atomic spacing in the material.

Thus the analysis of interactions of drifting charges in solids based on the plasma model indicates that these interactions, particularly double-stream interactions, will probably not be useful at X-ray frequencies. Because of the complexity of the problem, however, we feel that a quantum mechanical analysis involving electron waves should be made to explore adequately the possibility of interaction of drifting charges in solids at X-ray frequencies.

BIBLIOGRAPHY

1. B. Ancker-Johnson, "Microwave Emission from Nonequilibrium Plasmas in InSb Subject to Magnetic Fields," *Journal of Applied Physics*, Vol. 39, June 1968, pp. 3365-3378.

2. B. Ancker-Johnson and J. E. Drummond, "Thermal Pinching in Electron-Hole Plasma," *Physical Review*, Vol. 131, September 1963, pp. 1961-1965.

3. F. J. Biondi, *Transistor Technology*, Vol. III, Princeton, New Jersey, D. Van Nostrand, Inc., 1958.

4. C. K. Birdsall and J. R. Whinnery, "Waves in an Electron Stream with General Admittance Walls," *Journal of Applied Physics*, Vol. 24, March 1953, pp. 314-323.

5. R. Bowers and M. C. Steele, "Plasma Effects in Solids," *Proceedings IEEE*, Vol. 52, October 1964, pp. 1105-1112.

6. D. M. Chang and J. G. Ruch, "Measurements of the Velocity Field Characteristic of Electrons in Germanium," *Applied Physics Letters*, Vol. 12, February 1968, pp. 111-112.

7. G. K. T. Conn and D. G. Avery, *Infrared Methods*, New York, Academic Press, 1960.

8. H. Ehrenreich, "The Optical Properties of Metals," *IEEE Spectrum*, Vol. 2, March 1965, pp. 162-170.

9. M. Ettenberg and J. Nadan, "Gain in Solid-State Traveling-Wave Amplifiers," *IEEE Proceedings*, Vol. 56, April 1968, pp. 741-742.

10. B. D. Fried and S. D. Conte, *The Plasma Dispersion Function*, New York, Academic Press, 1961.

11. M. Glicksman and W. A. Hicinbothem, "Hot Electrons in Indium Antimonide," *Physical Review*, Vol. 129, February 1963, pp. 1572-1577.

12. H. Heinrich and D. K. Ferry, "Hot Carrier Current Oscillations in n-Type Germanium," *Applied Physics Letters*, Vol. 11, August 1967, pp. 126-128.

13. C. Hilsum and A. C. Rose-Innes, *Semiconducting III-V Compounds*, New York, Pergamon Press, 1961.

14. C. A. Hogarth, *Materials Used in Semiconductor Devices*, New York, Interscience Publishers, 1965.

15. C. C. Johnson, *Field and Wave Electrodynamics*, New York, McGraw-Hill, 1965.

16. W. Kaiser and H. Y. Fan, "Infrared Absorption in Indium Antimonide," *Physical Review*, Vol. 98, May 1955, pp. 966-968.

17. C. Kittel, *Introduction to Solid State Physics*, New York, John Wiley & Sons, 1966.

18. R. D. Larrabee and W. A. Hicinbothem, "Observation of Microwave Emission from InSb," *Symposium on Plasma Effects in Solids*, Paris, 1964; Dunod, publisher, 1965.

19. R. D. Larrabee and W. A. Hicinbothem, "A Laminar Slow-Wave Coupler and its Application to Indium Antimonide," *IEEE Transactions on MTT*, Vol. MTT-15, June 1967, pp. 382-383.

20. K. F. Lee, "Higher-Order Modes of the Two-Stream Instability in Bounded and/or Inhomogeneous Plasmas," *Journal of Applied Physics*, Vol. 38, April 1967, pp. 2172-2178.

21. A. Libchaber and R. Veilex, "Wave Propagation in a Gyromagnetic Solid Conductor: Helicon Waves," *Physical Review*, Vol. 127, August 1962, pp. 774-776.

22. T. S. Moss, *Optical Properties of Semiconductors*, London, Butterworth Scientific Publications, 1959.

23. D. Pines, "Coherent Excitation of Plasma Oscillations in Solids," *IRE Transactions on MTT*, Vol. 9, January 1961, pp. 89-92.

24. D. Pines and J. R. Schrieffer, "Collective Behavior in Solid-State Plasmas," *Physical Review*, Vol. 124, December 1961, pp. 1387-1400.

25. B. B. Robinson and G. A. Swartz, "Two-Stream Instability in Semiconductor Plasmas," *Journal of Applied Physics*, Vol. 38, May 1967, pp. 2461-2465.

26. B. B. Robinson and B. Vural, "Double-Stream Interaction in a Thin Semiconductor Layer," *RCA Review*, Vol. 29, June 1968, pp. 270-280.

27. L. Solymar and E. A. Ash, "Some Traveling-Wave Interactions in Semiconductors: Theory and Design Considerations," *International Journal of Electronics*, Vol. 20, February 1966, pp. 127-148.

28. M. C. Steele, "Microwave Generation from Photoconductive Mixing of Amplified Spontaneous Radiation," *RCA Review*, Vol. 27, June 1966, pp. 263-271.

29. T. H. Stix, *The Theory of Plasma Waves*, New York, McGraw-Hill, 1962.

30. P. A. Sturrock, "Kinematics of Growing Waves," *Physical Review*, Vol. 112, December 1958, pp. 1488-1503.

31. M. Sumi, "Traveling-Wave Amplification by Drifting Carriers in Semiconductors," *Applied Physics Letters*, Vol. 9, September 1966, pp. 251-253.

32. R. N. Sudan, "Classification of Instabilities from their Dispersion Relations," *Physics of Fluids*, Vol. 8, October 1965, pp. 1899-1904.

33. G. A. Swartz and B. B. Robinson, *Coherent Microwave Instabilities in a Thin Layer Solid-State Plasma*, Princeton, New Jersey, RCA Laboratories, 1968.

34. M. A. Uman, *Introduction to Plasma Physics*, New York, McGraw-Hill, 1964.

35. B. Vural and M. C. Steele, "Possible Two-Stream Instabilities of Drifted Electron-Hole Plasmas in Longitudinal Magnetic Fields," *Physical Review*, Vol. 139, July 1965, pp. A300-A304.

36. G. A. Williams, *Bulletin of the American Physical Society*, Vol. 7, 1962, p. 409.

37. H. Yoshinaga and R. A. Oetjen, "Optical Properties of Indium Antimonide in the Region from 20 to 200 Microns," *Physical Review*, Vol. 101, January 1956, pp. 526-531.

38. A. Silzars, C. H. Durney, and R. W. Grow, "Theoretical and Experimental Investigation of Solid-State Mechanisms for Generating Coherent Radiation in the Ultraviolet and X-Ray Regions," Technical Report UTEC MD 67-033, Microwave Device and Physical Electronics Laboratory, University of Utah, Salt Lake City, Utah, June 1967.

DISTRIBUTION LIST

ACTIVITIES AT WPAFB	No. of Copies
AVN	1
AVTL	1
AVWW	1
AVTA	3

OTHER DEPARTMENT OF DEFENSE ACTIVITIES

Air Force

Air University Library
Maxwell AFB, Alabama 36112   1

AFCRL (CRR-CSA)
Attn: Mr. Charles Ellis, Jr.
L. G. Hanscom Field
Bedford, Massachusetts 01731   1

RADC (RALTP)
Attn: Mr. H. Chiosa
Techniques Laboratory
Griffiss AFB, New York 13442   1

BSD (BSYDF)
Attn: Captain Hyslop
Norton AFB, California 92409   1

Navy

Chief, Bureau of Ships
Attn: Mr. C. C. Walker
Room 3337, Department of the Navy
Washington, D. C. 20360   1

Director, Naval Research Laboratory
Attn: Mr. H. D. Arnett, Code 5244
Washington, D. C. 20360   1

Commanding Officer and Director
USNASL, Mr. P. J. Giardano
U. S. Naval Base
Brooklyn, New York 10001   1

Office of Naval Research
Department of the Navy
Attn: Dr. E. H. Hurlburt, Code 427
Washington, D. C. 20360   1

Director
U. S. Naval Electronics Laboratory
San Diego, California 92152   1

Chief, Bureau of Ordnance
Department of the Navy
Code RE-9
Washington, D. C.   1

Chief, Bureau of Aeronautics
Department of the Navy
Code EL-412.1
Washington, D. C. 20025   1

Mr. Jay Froman
Scientific Department
Department of the Navy
Office of Naval Research
1076 Mission Street
San Francisco, California 94103   1

Army

Commanding Officer, USAECOM
Attn: AMSEL-KL-SS
       Dr. H. Jacobs
Fort Monmouth, New Jersey 07703   1

Commander, U. S. Army Material Command
Harry Diamond Laboratories
Attn: H. W. A. Gerlach
Connecticut and Van Ness Street, N. W.
Washington, D. C. 20025   1

Commander, U. S. Army Missile Command
Attn: Mr. W. D. McKnight
       ORDXR-RBE
Redstone Arsenal, Alabama 35809   1

Commanding Officer
U. S. Army Mob. Equip. Rsch. & Dev. Cen.
Attn: Technical Documents Center
       Building 315, Vault
Fort. Belvoir, Virginia 22060   1

LSI/Laser Systems Center
Attn: Technical Library
313 N. First St.
Ann Arbor, Michigan 48103   1

Dr. Arthur Lewis / CTR
National Aeronautics and Space
   Administration, ERC
575 Technology Square
Cambridge, Massachusetts 02139   1

DDC (TISIA)
Cameron Station
Alexandria, Virginia 22314   10

National Science Foundation
Washington, D. C. 20550   1

Dr. Royal E. Rostenbach
Acting Program Director
Engineering Energetics, Engineering Division
National Science Foundation
Washington, D. C. 20550   1

Advisory Group on Electron Devices
Attn: Mr. H. N. Serig
201 Varick Street, 9th Floor
New York, New York 10014   4

National Bureau of Standards
Attn: Librarian
Department of Commerce
Washington, D. C. 20025   1

Library
U. S. Department of Commerce
Environmental Science Services Administration
Boulder Laboratories
Boulder, Colorado 80302   1

NONGOVERNMENT INDIVIDUALS AND ORGANIZATIONS

Aerospace Corporation
Attn: V. Bevc
Box 95085
Los Angeles, California 90045   1

Amperex Electronic Corporation
230 Duffy Avenue
Hicksville, L. I., New York   1

Dr. Lawrence Bowman
Brigham Young University, ELB 174
Provo, Utah 84601   1

Dr. C. Kent Bullock
Naval Weapons Center
Code 3522
China Lake, California 93555   1

California Institute of Technology
Attn: Professor Roy W. Gould
Pasadena, California   1

Dr. W. Charles Carr
EIMAC
Division of Varian
301 Industrial Way
San Carlos, California   1

Dr. Douglas A. Christensen
662 Rossmore Road
Goleta, California 93017   1

Dr. Su-Min Chou
2445 Lyttonsville Road, No. 803
Silver Spring, Maryland 20910   1

Mr. John C. Clark
8389 Vereda del Padre
Goleta, California 93017   1

Cornell University
Electrical Engineering Department
Attn: Professor Lester F. Eastman
316 Phillips Hall
Ithaca, New York 14850   1

Cornell University
School of Electrical Engineering
Attn: Dr. Joseph M. Ballantyne
Ithaca, New York 14850   1

Dr. Maylin Dittmore
697 Meadowlark Street
Livermore, California 94550   1

EIMAC, A Division of Varian Associates
Attn: Technical Library
301 Industrial Way
San Carlos, California   1

EIMAC, A Division of Varian Associates
Attn: Dr. George Caryotakis
301 Industrial Way
San Carlos, California   1

Eitel McCullough Inc.
Attn: Larry Hansen, Manager
1678 Pioneer Road
Salt Lake City, Utah   1

General Electric Company
Research Laboratories
Attn: Dr. T. G. Mihran
P. O. Box 1088
Schenectady, New York 12305   1

General Telephone and Electronics Physical
    Electronics Laboratory
Attn: Dr. Louis R. Bloom   1
       Miss M. Franc, Documents Custodian   1
208-20 Willets Point Blvd.
Bayside, L. I., New York

Hughes Aircraft Company
Attn: Dr. Donald C. Forster
3011 Malibu Canyon Toad
Malibu, California   1

Dr. John H. Keller
7 Duchess Court
Newburgh, New York 12550   1

Litton Industries
Electron Tube Division
Attn: Dr. A. J. Prommer
960 Industrial Road
San Carlos, California   1

Dr. C. H. Ma
P. O. Box 3894
University, Mississippi 38677   1

Microwave Associates Inc.
Attn: Dr. Paul Chorney
South Avenue
Burlington, Massachusetts   1

Microwave Electronics Corporation
Attn: Dr. William E. Waters
4061 Transport Street
Palo Alto, California   1

Alpheus Smith Laboratory
Physics Library
Ohio State University
174 West 18th Ave.
Columbus, Ohio 43210   1

Raytheon Company
Attn: Dr. W. C. Brown
Wayside Road
Burlington, Massachusetts   1

RCA Laboratories
Attn: Dr. Stanley Bloom
Member, Technical Staff
Princeton, New Jersey   1

S. F. D. Laboratories
Attn: Dr. Farney
800 Rahway Avenue
Union, New Jersey   1

Dr. Richard L. Schriever
1018 Lisbon Avenue
Livermore, California 94550   1

Sperry Rand Corporation
Electron Tube Division
Attn: Dr. Sutherland
Gainesville, Florida   1

Stanford Research Institute
Attn: Dr. M. Pease
Menlo Park, California 94025   1

Stanford University
Electron Devices Laboratory
Stanford Electronics Laboratory
Attn: Dr. D. A. Dunn, Director
Stanford, California   1

Stanford University
Plasma Physics Library
Institute for Plasma Research
Attn: Librarian
Via Crespi, Stanford, California 94305   1

Tulane University
Electrical Engineering Department
Attn: James A. Cronvich
New Orleans, Louisiana   1

University of California
Electronics Research Laboratory
Attn: Professor J. R. Whinnery
Berkeley, California 94704   1

University of California Lawrence Radiation Laboratory
Attn: Verle Gilson
Bldg. 170C, Room 2597
Box 808
Livermore, California 94551   1

University of California
Attn: Professor Glen Wade
Santa Barbara, California   1

University of Colorado
Department of Electrical Engineering
Attn: Professor Russell E. Hayes
Boulder, Colorado 80304   1

University of Illinois
Department of Electrical Engineering
Attn: Professor Paul D. Coleman
Urbana, Illinois   1

University of Michigan
Office of Research Administration
Attn: Professor Joe Rowe
3505 East Engineering Building
Ann Arbor, Michigan 48107   1

Varian Associates, Inc.
Attn: Technical Library
611 Hansen Way
Palo Alto, California 94303   1

Watkins-Johnson Company
Attn: Dr. Rolf Peter
190 Southwood Drive
Palo Alto, California 94301   1

Dr. David C. Watson
Electromagnetic Systems Laboratory
495 Java Drive
Sunnyvale, California 94086   1

Westinghouse Electric Corporation
Air Arm Electronics Division
Attn: Mr. G. Klein
Friendship International Airport
Baltimore, Maryland 21203   1

Zenith Radio Corporation
Attn: Dr. Robert Adler, Director of Research
6001 West Dickens Avenue
Chicago, Illinois 60639   1

Dr. Aris Silzars
290 Wheeler Avenue
Redwood City, California 94016   1